

6-30-2016


The Degradation of Pharmaceutical Pollutants in Wastewater Catalyzed by Chloroperoxidase and the Construction of Chloroperoxidase H105R Mutant

Qinghao He

Florida International University, qhe001@fiu.edu

DOI: 10.25148/etd.FIDC000780

Follow this and additional works at: <https://digitalcommons.fiu.edu/etd>

 Part of the [Biochemistry Commons](#), [Enzymes and Coenzymes Commons](#), [Genetics Commons](#), [Medical Biochemistry Commons](#), [Medicinal Chemistry and Pharmaceutics Commons](#), [Other Chemicals and Drugs Commons](#), and the [Other Pharmacology, Toxicology and Environmental Health Commons](#)

Recommended Citation

He, Qinghao, "The Degradation of Pharmaceutical Pollutants in Wastewater Catalyzed by Chloroperoxidase and the Construction of Chloroperoxidase H105R Mutant" (2016). *FIU Electronic Theses and Dissertations*. 2540.
<https://digitalcommons.fiu.edu/etd/2540>

This work is brought to you for free and open access by the University Graduate School at FIU Digital Commons. It has been accepted for inclusion in FIU Electronic Theses and Dissertations by an authorized administrator of FIU Digital Commons. For more information, please contact dcc@fiu.edu.

FLORIDA INTERNATIONAL UNIVERSITY

Miami, Florida

THE DEGRADATION OF PHARMACEUTICAL POLLUTANTS IN
WASTEWATER CATALYZED BY CHLOROPEROXIDASE AND THE
CONSTRUCTION OF CHLOROPEROXIDASE H105R MUTANT

A dissertation submitted in partial fulfillment of

the requirements for the degree of

DOCTOR OF PHILOSOPHY

in

CHEMISTRY

by

Qinghao He

2016

To: Dean Michael R. Heithaus
College of Arts, Sciences and Education

This dissertation, written by Qinghao He, and entitled The Degradation of Pharmaceutical Pollutants in Wastewater Catalyzed by Chloroperoxidase and the Construction of Chloroperoxidase H105R Mutant, having been approved in respect to style and intellectual content, is referred to you for judgment.

We have read this dissertation and recommend that it be approved.

John T. Landrum

Lou W. Kim

Watson J. Lees

Yuan Liu

Xiaotang Wang, Major Professor

Date of Defense: June 30, 2016

The dissertation of Qinghao He is approved.

Dean Michael R. Heithaus
College of Arts, Sciences and Education

Andrés G. Gil
Vice President for Research and Economic Development
and Dean of the University Graduate School

Florida International University, 2016

© Copyright 2016 by Qinghao He

All rights reserved.

DEDICATION

I dedicate this dissertation to my father Wenlong He and my mother Ronghua Wan. Without their support and encouragement, the completion of this work would not have been possible.

ACKNOWLEDGMENTS

The completion of this work is the outcome of many people's contribution. During my five years' graduate study at Florida International University. Most importantly, I would like to express my sincerest gratitude to my major professor, Dr. Xiaotang Wang, for his continuous encouragement, understanding and support. He was always there to guide me in becoming a good researcher by keeping passion and ambition in my project, developing independent thinking and never to give up. He also taught me how to be a responsible individual to benefit others and society with his excellent patience. Without his consistent help and guidance, the completion of this project would not have been possible.

I am immensely grateful to all my committee members, Dr. John T. Landrum, Dr. Lou Kim, Dr. Watson Lees and Dr. Yuan Liu, for their professional assistance and many intelligent and helpful suggestions during the years. I also want to acknowledge my labmates and friends, Lin Jiang, Elwood Kwong, Elena Shersher, and Yongjian Guo for their inspiring discussion and kindly assistance. We helped and encouraged each other like brothers and sisters. It has been an unforgettable experience in my whole life to work in such a warm and kindly lab.

I would like to express my appreciation to Dr. Kevin O'Shea and Dr. Stanislaw F. Wnuk for giving me extraordinary professional suggestions in organic chemistry related to my work. I also would like to thank Dr. Luis E. Arroyo-Mora from Dr. Anthony P. Decaprio's lab for teaching me LC-Q-TOF mass spectrometry, from the very basic knowledge such as sample preparation to troubleshooting the machine, and Vanessa Linero from the same lab for guiding

me to use Triple-Quadrupole mass spectrometer. Also, I would like to thank Dr. Palmer Graves and Dr. Uma Swamy for guiding me to be a good teaching assistance. In addition, I would like to thank all my family and friends for their understanding, support and encouragement. Finally, I would like to acknowledge the Department of Chemistry and Biochemistry, Florida International University.

ABSTRACT OF THE DISSERTATION
THE DEGRADATION OF PHARMACEUTICAL POLLUTANTS IN
WASTEWATER CATALYZED BY CHLOROPEROXIDASE AND THE
CONSTRUCTION OF CHLOROPEROXIDASE H105R MUTANT

by

Qinghao He

Florida International University, 2016

Miami, Florida

Professor Xiaotang Wang, Major Professor

Trace amounts of pharmaceuticals have been detected in water, from nanograms per liter to micrograms per liter, and have a negatively effect in the aquatic environment and an increased potential risk of drug poisoning for human and animals. In order to address the problem, drug degradation catalyzed by chloroperoxidase (CPO) has been investigated. CPO is a heme-containing glycoprotein secreted by the fungus, *Caldariomyces fumago*, it catalyzes two major types of oxidations, two one-electron oxidations as catalyzed by most peroxidases and two-electron oxidations which are rare for conventional peroxidases.

Five common drugs from a variety of classes (acetaminophen, carbamazepine, sulfamethazine, diclofenac and naproxen) which were persistent in the environment have been studied. The metabolites of each drug were identified and the pathways of degradation were proposed. All of them were found to be 100% degradation efficiency in the CPO-H₂O₂-Cl⁻ system which the

catalyzation only required low concentration of CPO (normally nanomolar level) as well as relatively low concentration of H₂O₂ as cofactor. This degradation method is economic and highly efficient, the results of my experiment extensively support the hypothesis that CPO has a great potential in the environmental application.

A new mutant of CPO has been constructed to investigate the role of histidine 105 in the active site of distal pocket. Histidine 105 was suggested to play an essential role in modulating the chlorination activity by forming hydrogen bond with glutamic acid 183, histidine has been replaced by arginine to generate CPO H105R mutant. The construction and transformation were a success but the protein was expressed as apoenzyme, suggesting the mutagenesis to a larger arginine residue at position105 disturbed the heme incorporation.

TABLE OF CONTENTS

CHAPTER	PAGE
I. INTRODUCTION.....	1
1.1 The occurrence of pharmaceutical pollutants in water	1
1.2 The treatment for removal of pharmaceuticals in water	3
1.3 The structure of CPO	6
1.4 The mechanism of CPO catalyzed reactions	10
1.5 CPO catalyzed reactions	11
1.5.1 One-electron oxidations	11
1.5.2 Two-electron oxidations	14
II. CPO-CATALYZED CHLORINATION AND POLYMERIZATION OF ACETAMINOPHEN.....	18
2.1. Background.....	18
2.2 Experimental Procedure	18
2.2.1 Material.....	18
2.2.2 UV-Visible spectrophotometry	19
2.2.3 Liquid chromatography and mass spectrometry.....	19
2.3 Result and discussion	22
2.3.1 UV-Vis study of CPO-catalyzed degradation of APAP	22
2.3.2 LC-Q-TOF- MS	23
2.3.3 Triple-quadruple LC/MS/MS.....	25
2.4 Discussion.....	33
III. CPO-CATALYZED DEGRADATION OF CARBAMAZEPINE	35
3.1 Background.....	35
3.2 Experimental Procedure	36
3.2.1 Material.....	36
3.2.2 UV-Visible spectrophotometry	36
3.2.3 Liquid chromatography and mass spectroscopy	38
3.3 Result and discussion	40
3.3.1 UV-Vis study of CP O-catalyzed degradation of carbamazepine	40
3.3.2 The effect of chloride on the degradation of CBZ.....	41
3.3.3 The effect of pH on the degradation of CBZ.....	43
3.3.4 The effect of H ₂ O ₂ concentration	43
3.3.5 The kinetic parameters of CBZ degradation catalyzed by CPO	44
3.3.6 LC-Q-TOF- MS.....	45
3.3.7 Triple-Quadruple LC/MS/MS.....	52
3.4 Discussion.....	58
IV. CPO-CATALYZED DEGRADTION OF SULFAMETHAZINE	61
4.1 Background	61
4.2 Experimental Procedure	61

4.2.1 Material	61
4.2.2 UV-Visible spectrophotometry	61
4.2.3 Liquid chromatography and mass spectrometry	62
4.3 Result and discussion	64
4.3.1 UV-Vis study of CPO-catalyzed degradation of carbamazepine	64
4.3.2 LC-Q-TOF- MS	65
4.4 Discussion	78
V. ENGINEERING THE HYDROGEN BOND OF CPO BY MUTANT H105R	81
5.1 Introduction	81
5.2 Experimental Procedure	82
5.2.1 Materials	82
5.2.2 Construction of H105R mutant and plasmid propagation	83
5.2.3 Transformation into <i>A. niger</i> and selection for expression	85
5.2.4 Expression of the H105R mutant protein	86
5.2.5 Purification of the mutant protein	87
5.3 Result and discussion	88
5.3.1 Mutant DNA sequencing	88
5.3.2 Transformaiton and expression result	88
5.3.3 Purification	89
5.4 Discussion	90
VI. DEGRADATION OF NON-STEROIDAL ANTI-INFLAMMATORY DRUGS DICLOFENAC AND NAPROXEN BY CHLOROPEROXIDASE	92
REFERENCE	137
APPENDIX	147
VITA	165

LIST OF TABLES

TABLE	PAGE
Table 1.1 Conventional and advanced wastewater treatment and their removal range efficiency of pharmaceuticals.	5
Table 2.1 Accurate-Mass LC-Q-TOF-MS data for the identification of APAP and its metabolites.	24
Table 2.2 Information of the proposed isomers.....	29
Table 3.1 The kinetic parameters of CBZ degradation catalyzed CPO.	45
Table 3.2 Accurate-Mass LC-Q-TOF-MS data for the identification of CBZ and its metabolites.	46
Table 3.3 The optimizer data of CM4, CM5 and CM7.....	55
Table 4.1 Accurate-Mass QTOF-LC/MS data for the identification of SMZ and its metabolites catalyzed in CPO-H ₂ O ₂ -Cl ⁻ system.	66
Table 4.2 Possible identities of C ₁₂ H ₁₄ N ₄ (SM1).....	71
Table 4.3 Accurate-Mass LC-Q-TOF-MS data for the identification of SMZ and its metabolites catalyzed in CPO-H ₂ O ₂ -Br ⁻ system.....	76

LIST OF FIGURES

FIGURE	PAGE
Figure 1.1 Fate of human and veterinary pharmaceuticals in the environment.	2
Figure 1.2 Crystal structure of CPO was presented by Pymol software	7
Figure 1.3 Slice of CPO crystal structure with surface presentation.....	8
Figure 1.4 CPO active site presented by Pymol software (PDB entry 1CPO) with important amino acids in the distal pocket	9
Figure 1.5 The general mechanism of CPO catalyzed reaction	12
Figure 1.6 The oxidation of ABTS catalyzed by CPO	13
Figure 1.7 The dehalogenation of trihalophenol catalyzed by CPO	13
Figure 1.8 The mechanism of CPO catalyzed one electron oxidation of fluorophenol.....	14
Figure 1.9 Reactions catalyzed by CPO in phosphate buffer with chloride ions .	16
Figure 1.10 The chlorination of aromatic substrates catalyzed by CPO in phosphate buffer with chloride ions	17
Figure 2.1 UV-Vis Spectra of APAP , APAP with H ₂ O ₂ and its metabolites at 1min, 2.5min, and 4min	22
Figure 2.2 The targeted MS/MS spectra of APAP and its metabolites	27
Figure 2.3 The relative area of each metabolite	28
Figure 2.4 The proposed mechanism of the degradation of APAP catalyzed by CPO present by primary structure of each metabolites	30
Figure 2.5 Extracted chromatogram of APAP and its metabolites detected by Triple-Quadrupole LC/MS/MS.	31
Figure 2.5 (Cont.) Extracted chromatogram of APAP and its metabolites detected by Triple-Quadrupole LC/MS/MS.	32
Figure 3.1 UV-Vis Spectra of CBZ with H ₂ O ₂ and its metabolites at 1min, 2.5min and 4min	40

Figure 3.2. The effect of chloride on the degradation of CBZ.....	42
Figure 3.3 The effect of pH on CBZ degradation	43
Figure 3.4 The effect of H ₂ O ₂ concentration	44
Figure 3.5 The effect of CBZ concentration.....	44
Figure 3.6 The targeted MS/MS spectra of CBZ and its metabolites .	48
Figure 3.6 (Cont.).The targeted MS/MS spectra of CBZ and its metabolites	49
Figure 3.7. The percentage of each metabolites measured by compound area	50
Figure 3.8 The area of metabolites with limited H ₂ O ₂ at 1 min, 3 min and 5 min detected by Accurate-Mass LC-Q-TOF-MS.....	51
Figure 3.9 The chromatograms of CBZ and its metabolites	53
Figure 3.9 (Cont.) The chromatograms of CBZ and its metabolites	54
Figure 3.10 The proposed mechanism of the degradation of CBZ catalyzed by CPO.....	57
Figure 4.1 UV spectrum of SMZ degradation catalyzed by CPO	65
Figure 4.2 (cont.) The targeted MS/MS spectra of APAP and its metabolites	69
Figure 4.3 The percentage of each metabolites measured by compound area ..	69
Figure 4.4 The area of metabolites with limited H ₂ O ₂ at 1 minute, 3 minutes and 5 minutes detected by Accurate-Mass LC-Q-TOF-MS.....	71
Figure 4.5. The chromatograms of CBZ and its metabolites	73
Figure 4.5. (cont.) The chromatograms of CBZ and its metabolites	74
Figure 4.6. The proposed mechanism of the degradation of SMZ catalyzed by CPO-H ₂ O ₂ -Cl- system presented by primary structure of each metabolite ..	75
Figure 4.7 The percentage of the three metabolites measured by compound area.....	76
Figure 4.9.The mechanism of SMZ bromination catalyzed by CPO	78

Figure 5.1 The Proposed mechanism of His 105 in the cleavage of the peroxide O-O bond.....	81
Figure 5.2 The CPO expression vector pCPO3.1-AmdS.....	84
Figure 5.3 DNA sequence of H105R mutant	88
Figure 5.4 H105R mutant grown on 1.2 sorbitol selective agar plate	88
Figure 5.5 The ABTS activity of H105R cultures since the second day of inoculation. Samples were run in triplicate.....	89
Figure 5.6 SDS-PAGE of mutated protein	90
Figure 5.7 UV-Vis spectra of H105R mutant	90

LIST OF ABBREVIATIONS AND ACRONYMS

ABBREVIATION	FULL NAME
A	Alanine
ABTS	2,2'-azino-bis(3-ethylbenzothiazoline-6-sulfonic acid)
AMDOPH	1-acetyl-1-methyl-2-phenylhydrazide
<i>Amds</i>	<i>A.nidulans</i> acetamidase gene
<i>A. niger</i>	<i>Aspergillus niger</i>
<i>A. nidulans</i>	<i>Aspergillus nidulans</i>
APAP	N-acetyl-p-aminophenol/Acetaminophen
Asp	Aspartic acid
CBZ	Carbamazepine
CE	Collision energy
COSY	Correlation spectroscopy
CPO	Chloroperoxidase
DEAE	Diethylaminoethanol
DNA	Deoxyribonucleic acid
dNTP	Deoxyribonucleotide
E	Extinction coefficient
E/Glu	Glutamic acid
ee	Enantiomeric excess

EE2	Estrogen 17 α -ethinylestradiol
FbF	Find by Formula
FIA	Flow injection analysis
His/H	Histidine
HPLC	High performance liquid chromatography
LC-Q-TOF-MS	Liquid chromatography Quadrupole Time-of-Flight mass spectrometry
LC-QQQ-MS	Liquid chromatography Triple-Quadrupole-mass spectrometry
LDH	Lactate dehydrogenase
MCD	Monochlorodimedone
MRM	Multiply reaction monitoring
m/z	Mass-to-charge ratio
NAPQI	N-acetyl-p-benzoquinone imine
NMR	Nuclear magnetic resonance spectroscopy
NOE	Nuclear overhauser effect
NOESY	Nuclear overhauser enhancement Spectroscopy
OTC	Over-the-counter
R	Arginine
P450	Cytochrome P450 mono-oxygenase

PCR	Polymerase chain reaction
<i>PglaA</i>	<i>A. niger</i> glucoamylase promoter
Phe	Phenylalanine
ppm	Parts per million
RRHD	Rapid Resolution High Definition
Rz value	Reinheitzahl value
RT	Retention time
SDS-PAGE	Sodium dodecyl sulfate polyacrylamide gel electrophoresis
SMZ	Sulfamethazine
STP	Sewage treatment plant
TCC	Thermostatted column compartment
<i>TtrpC</i>	<i>A. nidulans</i> anthranilate synthetase terminator
UV	Ultraviolet
UV-Vis	Ultraviolet-Visible

CHAPTER I.

INTRODUCTION

1.1 The occurrence of pharmaceutical pollutants in water

Trace amounts of pharmaceuticals have been detected in water from nanograms per liter to micrograms per liter. Pharmaceuticals are chemicals that arise from natural sources or through artificial synthesis with the purpose to treat disease with highly specific biological targets. Even with lower concentration than regular contaminants, pharmaceuticals could still target biological organisms efficiently due to their properties. Pharmaceutical overdose or prolong exposure increase the potential risk of drug poisoning for both human and animals. Also, the hazards of pharmaceutical in the aquatic environment have been widely discussed in recent years. [1, 3]

The annual consumption of prescribed drugs is about 100 tons in Germany, not including over-the-counter (OTC) drugs, so the actual total should be much more than the prescribed amounts. The pharmaceutical compounds that enter in the aquatic environment are mainly from human and veterinary medicines. The urine and feces from humans and animals affect the environment by different pathways. Human pharmaceuticals arise from their excreted and passed into sewage and are partially removed through the sewage treatment plant (STP) before entering the surface water that will go through a series of processes forming the drinking water we intake. Veterinary pharmaceuticals enter the environment similar to the human route where the animal's excreted form contaminate manure which affect the soil and ground water by soil fertilization.

Rainfall makes liquid manure and digested sludge flows into surface water. Soil and ground water may get contaminants from digest sludge applied in STP treatment. Another contaminated source is the disposal of pharmaceuticals in domestic waste without any previous treatment, leachates flow from the waste to landfill site, and continue to ground water and surface water. Finally, these detectable amount of pharmaceuticals reaches the drinking water sources. (Fig. 1.1).[3, 4]

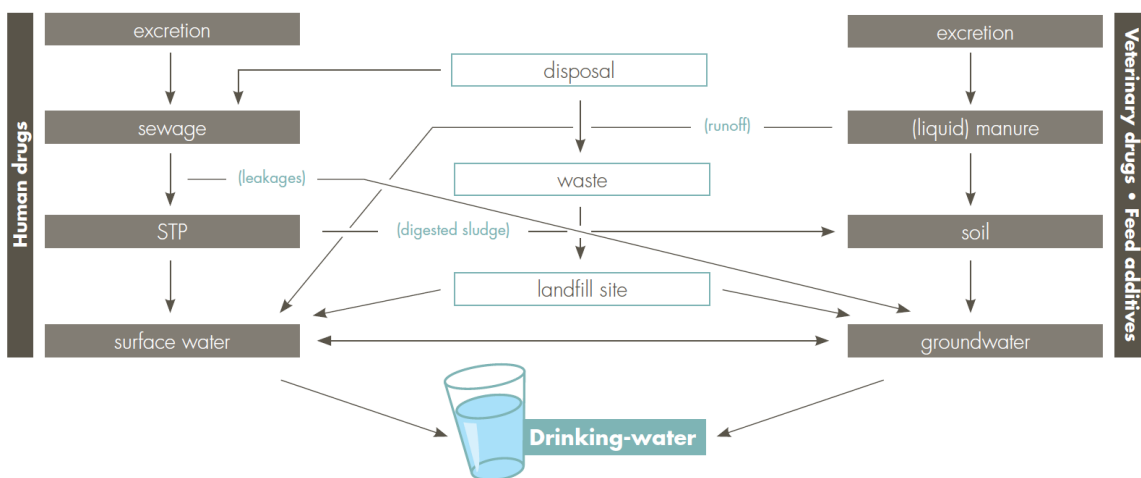


Figure 1.1 Fate of human and veterinary pharmaceuticals in the environment. [1, 4]

The trace amounts of pharmaceuticals are not likely to have acute toxicity but have showed chronic ecotoxicity effects in animals. The lowest observed effect concentration (LOEC) of diclofenac on organ level for rainbow trout (*Oncorhynchus mykiss*) was in the same range as the detected concentration of the drug in wastewater.[5] The endocrine disrupter drugs have dramatically negative effects on aquatic animal such as fathead minnows, with environmentally relevant concentrations (less than 1 ng/L) of estrogen 17 α -ethinylestradiol (EE2),

showed adverse effects on fertilization and sex ratio and even secondary sex characteristics.[6, 7]

The impact of trace amount drugs in environment cannot be regardless, antibiotics resistant bacteria were detected in the surface water with highest average concentration of 78.31 ng/L.[8] Even in low concentration, antibiotics can affect microorganism as signaling hormones, potentially threaten aquatic ecosystems and the public health[9]

In drinking water, more than 10 drugs were detected frequently, the concentration of drug could achieve concentration as high as 270 ng/L (clofibrac acid), and the concentration of drug metabolites could reach 0.9 ug/L (AMDOPH deriving from dimethylaminophenazone). Currently, there is no routine test for monitoring the concentration of drug in drinking water. The risk of low concentrations of pharmaceuticals maybe minor, but with scarce information about the effects of chronic drug exposure, it still has the potential to affect human health negatively. The risk assessment of pharmaceutical in aquatic environment still needs to be evaluated in the future.[10-12]

After 2006, the new compounds approved in Europe have to complete the assessment of environmental toxicity and fate datasets, the older medicine are still need to consider of their persistence and hazards.[13]

1.2 The treatment for removal of pharmaceuticals in water

There are two types of wastewater treatment, conventional treatment and advanced treatment (Table 1.1).

Active sludge is the typical treatment of conventional treatment process, the removal efficiencies were varying regarding different factors such as temperature of degradation, and hydraulic retention time.[14] The biological filtration including the STP treatment, a process to remove contaminants in municipal wastewater, and produce environmental friendly metabolites, has been found to be insufficient to eliminate all persistent pharmaceutical residues. [15] The removal rates are inconstant due to the diversity of drug properties, for example, carbamazepine is resistant in STP but have different removal rate in active sludge.[16]

Advanced treatments are widely investigated in the removing drugs in wastewater. Ozonation, microfiltration and ultrasound can achieve up to 100% degradation.

Table 1.1 Conventional and advanced wastewater treatment and their removal range efficiency of pharmaceuticals.

Wastewater treatment	Removal range (%)
Conventional wastewater treatment	
Activated sludge	-193-100 ^a
Biological filtration	6-71
Primary settling	3-45
Coagulation, filtration and settling	5-36
Sand filtration	0-99
Advanced wastewater treatment	
Ozonation	1-100
Ozonation/ultrasound and sonocatalysis	23-45
Ozonation and catalytic ozonation	>9-100
UV irradiation	29
Photolysis (UV/hydrogen peroxide)	52-100
Dark and light Fenton	80-100
UV/TiO ₂	>95
Biomembrane	23-99
Microfiltration and reverse osmosis	91-100
Reverse osmosis	62-97
Ultrasound	24-100

^a The removal efficiency is negative due to the calculation method, the hydraulic retention time is considered. The influent sample and effluent sample are not absolutely related. And carbamazepine, the negative removal efficiency is consistent, it is suggested the metabolite carbamazepine can be converted to parent compound by enzyme activity in STP. [1]

The application of ozonation with H₂O₂ is used in wastewater recycling for indirect potable reuse to degrade persistent organic pollutant. [1] However, the advanced treatments are needed to be further investigated considering the application possibility to individual pharmaceuticals, for instance, ozonation the high efficiency normally is activated by relatively high concentration of O₃. The

oxidized products might be resistant to the ozonation and contain high acute toxicity. [17] Different economic and efficient wastewater treatments are required to be developed considering the complexity of pharmaceutical pollutions.

1.3 The structure of CPO

Chloroperoxidase (CPO) is a heme-containing glycoprotein secreted by the fungus *Caldariomyces fumago*. The molecular weight of CPO is approximately 42,000 Daltons. Ferriprotoporphyrin IX is found to be its prosthetic group.[18] CPO consists of 299 amino acids, the tertiary structure of CPO mainly consists of eight alpha helical segments and a small beta pair (Fig. 1.2).[19] It has an active site similar to that of P450s and peroxidase. In comparison with P450s and peroxidase, the cysteine 29 is the heme ligand of CPO in the proximal pocket resembling P450s. The polar distal side is similar to peroxidase, whereas the acid-base catalyst in the active site of CPO responsible for the cleavage of the peroxide O-O bond is glutamic acid 183, instead of histidine which is typical in other peroxidase. [20] [21]

There is a narrow channel connected the protein surface to the heme center, halogen ions are found to bind in the narrow channel, the halogen ion binding sites found suggested the pathway of halides from the protein surface to heme active center. In addition, there is a wide channel which suggest to be the binding site of bulky molecules, reaction such as oxidation, epoxidation might happen here (Fig 1.3).[21]

In conventional heme peroxidases, histidine residue is the acid-base catalyst, whereas glutamic acid 108 (Glu 183) is the acid-base catalyst of CPO. Generally

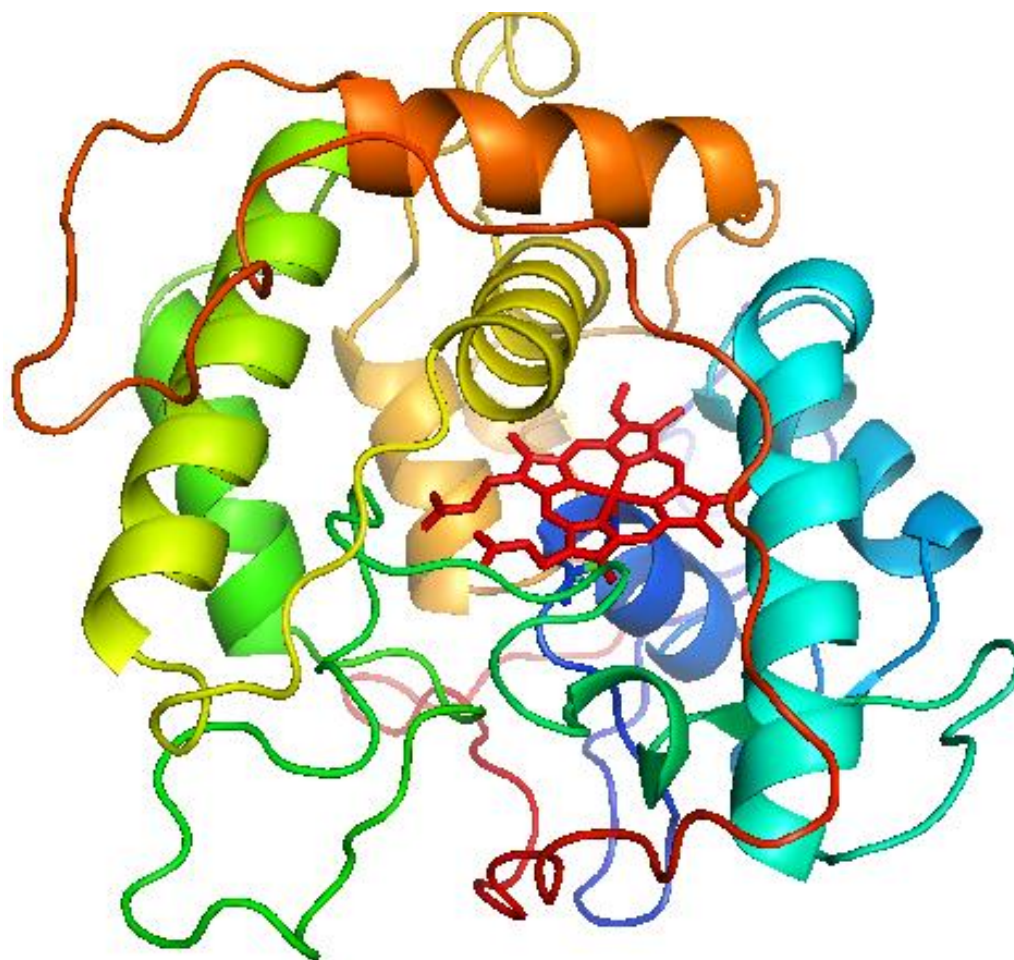


Figure 1.2 Crystal structure of CPO was presented by Pymol software, the protein data bank (PDB; <http://www.pdb.org>) entry 1CPO was used. Heme propyrin was depicted as red color, located in the center of protein. [20]

for heme peroxidase, the catalyst residue interact with another amino acid to cleave the peroxide bond. In CPO, the residue suggested to interact with Glu183 assisting in the formation of compound I is His105.

In conventional heme peroxidases, histidine residue is the acid-base catalyst, whereas glutamic acid 108 (Glu 183) is the acid-base catalyst of CPO. Generally

for heme peroxidase, the catalyst residue interact with another amino acid to cleave the peroxide bond. In CPO, the residue suggested to interact with Glu183 assisting in the formation of compound I is histidine105.

His 105 is hydrogen bonded to Glu 183 and Asp 106, the hydrogen bondings facilitates the cleavage of peroxide bond and positioning Glu 183 properly with relation to heme center during the catalyzation. [20, 21, 23] Two phenylalanine residues (Phe 103 and Phe 186) are close to the heme iron and thought to interact with hydrophobic substrate and control the substrate to access the heme center (Fig 1.4). [21] There is also other result that occurs because of the

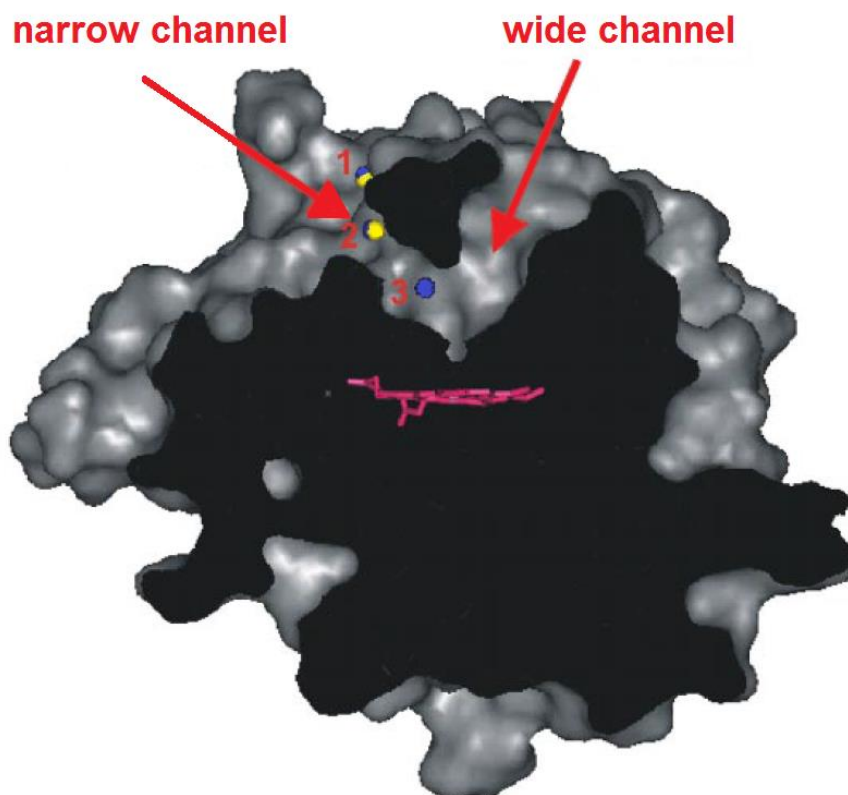


Figure 1.3 Slice of CPO crystal structure with surface presentation. Heme is depicted in magenta, narrow channel and wide channel are marked by arrow. Yellow sphere presents bromide and blue sphere presents iodide. The binding sites of halide are labeled by numbers (1-3) in red color. [22]

modification of histidine residues, suggested His 105 affected epoxidation and peroxide dismutations but not decreased peroxidation rate.[24] CPO might have multiply reactive sites regarding the same reaction, and the role of H105 still needs to be further investigated by other techniques to unravel the mechanism of CPO.

His 105 is hydrogen bonded to Glu 183 and Asp 106, the hydrogen bondings facilitates the cleavage of peroxide bond and positioning Glu 183 properly within heme center during the catalyzation. [20, 21, 23] Two pheylalanine residues (Phe 103 and Phe 186) are close to the heme iron and thought to interact with hydrophobic substrate and control the substrate to access the heme center (Fig 1.4). [21] There is also other result based on the modification of histidine residues, suggested His 105 affected epoxidation and peroxide dismutations but not decreased peroxidation rate.[24] CPO might have multiply reactive sites for

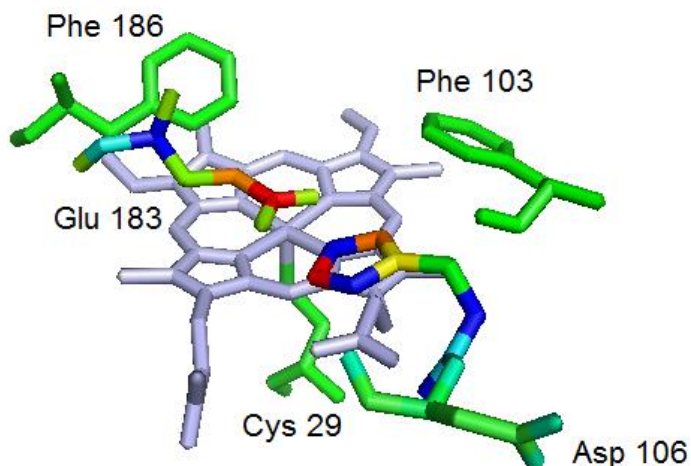


Figure 1.4 CPO active site presented by Pymol software (PDB entry 1CPO) with important amino acids in the distal pocket. Heme is depicted in grey. His 105 was proposed to form hydrogen bonds with Glu 183 and Asp 106, conferring the proper position of Glu183 and the orientation to form compound I. Phe 103 and Phe 186 were observed to be close to heme center, might control the access of substrate by polarity. [21]

the same reaction, and the role of H105 still needs to be further investigated by other techniques to unravel the mechanism of CPO.

1.4 The mechanism of CPO catalyzed reactions

The complex structure of the CPO active site associates with the multiple functions of CPO. The general catalytic cycle of CPO starts from the resting state of the enzyme, the native ferric center binds by H_2O_2 at the heme iron and to form the oxo-ferryl cation radical intermediate called compound I, during the reaction, two electrons from the heme center are transferred to H_2O_2 and cleaved the O-O bond, producing H_2O . Compound I is involved in different types of chemical reactions. In the dismutation pathway, compound I will continue to react with H_2O_2 to generate O_2 and H_2O , and be reduced back to its resting state. In the P450 pathway, the organic substrate (RH) is hydroxylated and compound I is reduced back to ferric resting state.

Another pathway is peroxidation by forming another reactive intermediate compound II, the oxo-ferryl intermediate. During the process, one electron from compound I is transferred to an organic molecule (AH), converting AH to the radical molecule (A^\cdot). [25, 26] Electron is transferred to the organic substrate from compound II, and CPO returns to the resting state.[27] In general, another major pathway of compound I is halogenation by interacting with halide (X) to form compound X, a ferric intermediate. Compound X will halogenate organic substrate (AH) and generate hydroxyl ion (OH^-), returns back to its resting state (Fig. 1.5).

Compound I with strong oxidizing ability is also proposed to generate hypochlorous acid / hypobromous acid, or Cl_2 / Br_2 as the active intermediates in the oxidative chlorination. They are presumed to diffuse into the medium and to oxidize the substrate externally or react with substrates within the active sites. [28-32] The chlorination mechanism of CPO will be further discussed and confirmed in my research.

1.5 CPO catalyzed reactions

CPO catalyzes two major types of oxidations; they are two one-electron oxidations as catalyzed by most peroxidases and two-electron oxidations which are rare for conventional peroxidases.

1.5.1 One-electron oxidations

The one electron oxidations of CPO include peroxidation and dehalogenation and polymeration driven by radical. [33, 34] The typical peroxidation of CPO is the oxidation of 2,2'-azinobis-3-ethylbenzothiazoline-6-sulfonic acid (ABTS), it is used as ABTS assay to measure the peroxidase activity of CPO / mutant CPO (Fig 1.6). [35]

Dehalogenation was found in trihalophenols and fluorophenols (Fig 1.7) According to the general mechanism, fluoride is not involved in halogenation catalyzed by CPO, whereas in dehalogenation, fluoride of substrate is reacted. Both reactions show the potential application of CPO in environmental pollutant treatment. In the defluorination of fluorophenols, dimers and trimers were generated in one electron oxidation. [33, 34] The function of polymerization showed in some other peroxidase is also found in CPO catalyzed reaction. [34, 35]

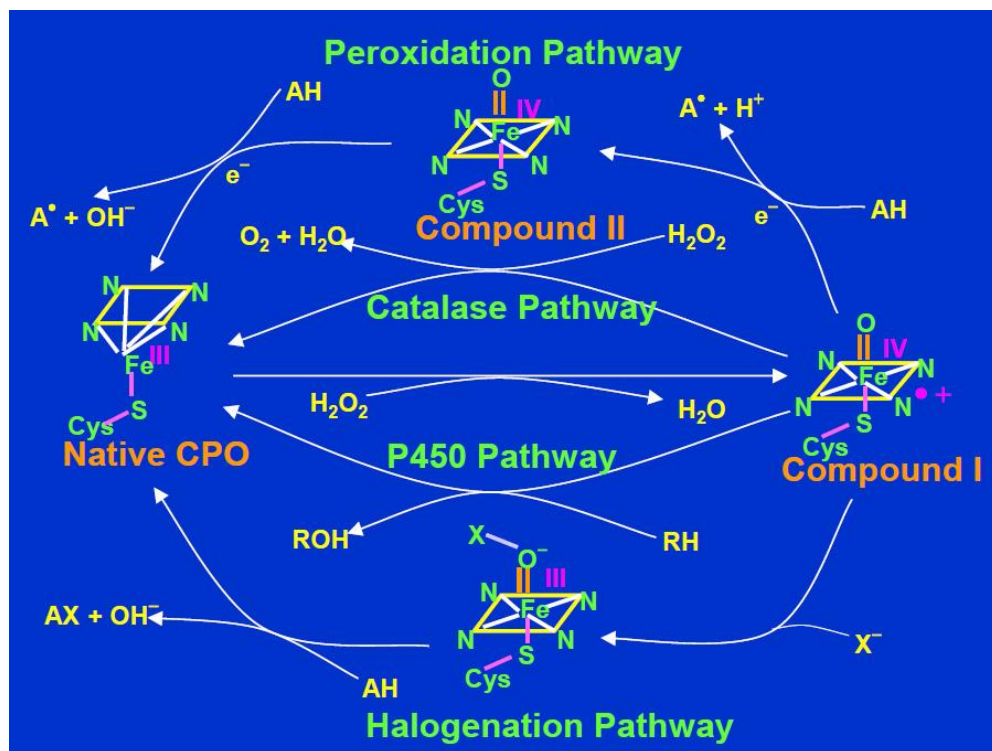


Figure 1.5 The general mechanism of CPO catalyzed reaction. AH presents the substrate, the oval presents the heme; compound I and II present the ferryl intermediates; X presents halogen atom (except F⁻).[29]

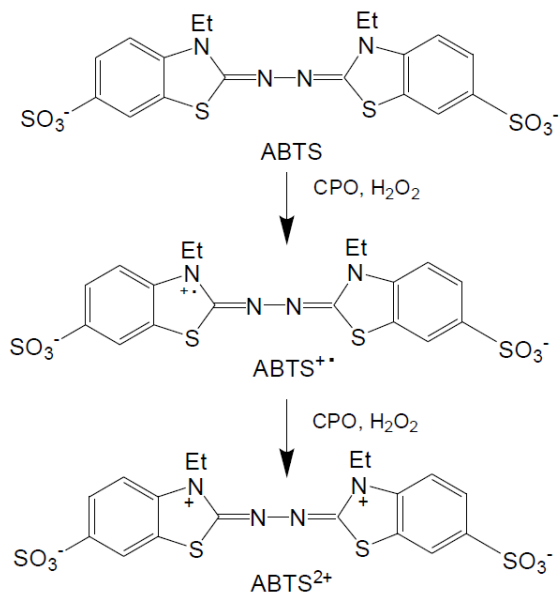


Figure 1.6 The oxidation of ABTS catalyzed by CPO.[36]

Dehalogenation was found in trihalophenols (Fig. 1.7) and fluorophenols (Fig. 1.8). According to the general mechanism, fluoride is not involved in halogenation catalyzed by CPO, whereas in dehalogenation fluoride of substrate reacted. Both reactions show the potential application of CPO in environmental pollutant treatment. In the defluorination of fluorophenols, dimers and trimers were generated in one electron oxidation. [33, 34] The function of polymerization showed in some other peroxidase is also found in CPO catalyzed reaction. [34, 35]

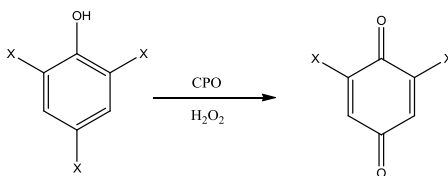


Figure 1.7 The dehalogenation of trihalophenol catalyzed by CPO.[33]

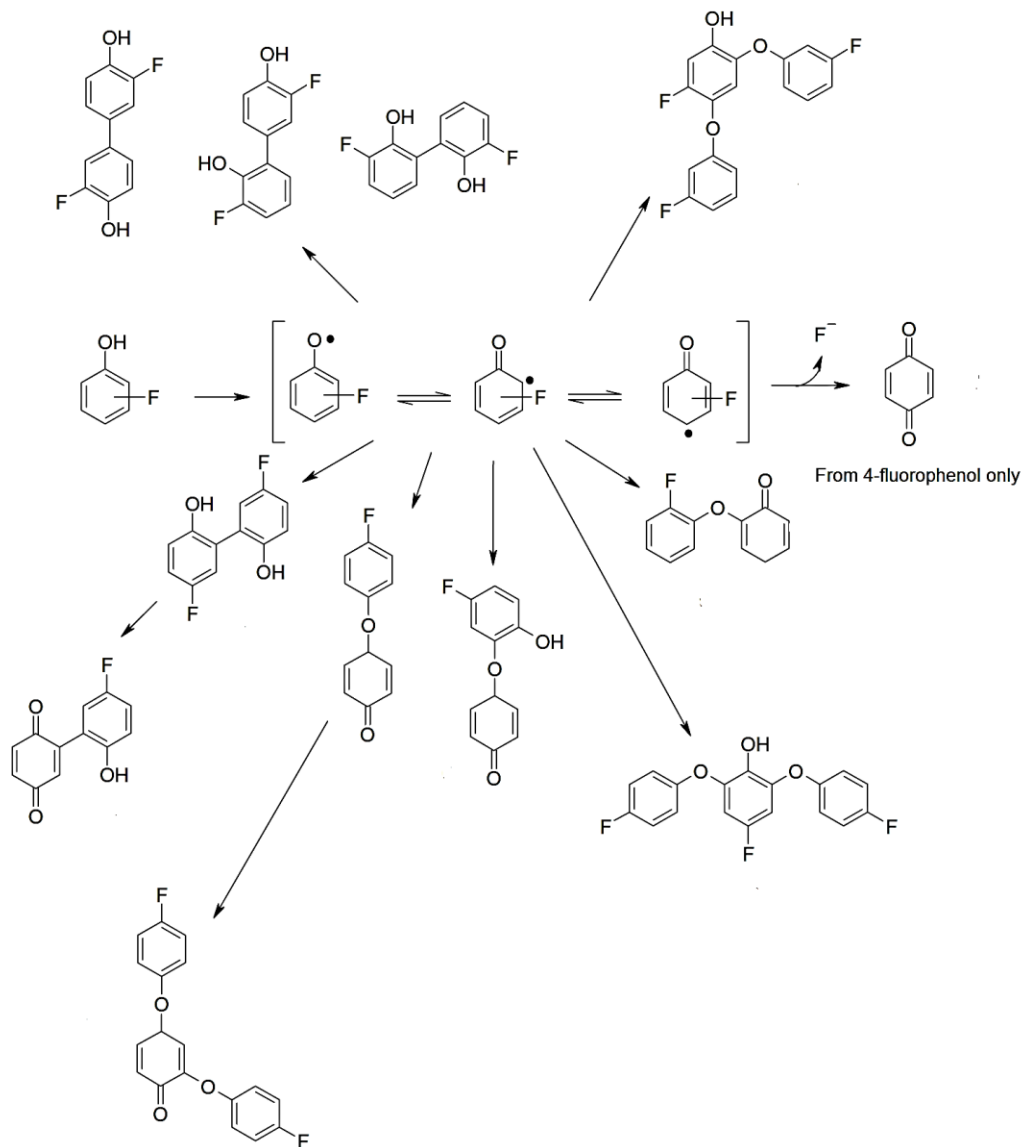


Figure 1.8 The mechanism of CPO catalyzed one electron oxidation of fluorophenol.[34]

1.5.2 Two-electron oxidations

The two-electron oxidations includes halogenation and oxygen transfer as the major reactions. The significant function of CPO was found as the chlorination of monochlorodimedone (MCD), this reaction is routinely used as MCD assay to measure the chlorination activity of CPO /mutant CPO (Fig 1.8a). Other halogenation can also be carried out by bromide or iodide ions.[37] There are other substrates catalyzed by CPO

in the halogenation, such as phenol. (Fig .1.9), 1,3-cyclopentanedione and alkenes (Fig 1.8b) [37-39] The oxidative chlorination catalyzed by CPO for halogenated phenols or phenols typically generated different isomers, which will be discussed in my research.

The other important two-electron oxidation consists of epoxidation with enantioselectivity, hydroxylation examples are showed in figure 1.8c [40]

1.6 The application tendency of CPO

The structural and functional features of CPO are suggested its potential as industrial and environmental biocatalysts, the catalyzation only needs relatively low concentration H_2O_2 as cofactor which is economic and safe in application.

To synthesize biological or pharmaceutical chemicals, CPO is an ideal candidate. The enantioselectivity of oxidation catalyzed by CPO was relatively high regarding the reaction of oxidizing primary alcohols to the corresponding aldehydes, and result could be improved with lowered temperature and at fixed pH to achieve a higher enantiomeric purities (ee). In addition, tert-butyl hydroperoxide was used instead of hydrogen peroxide.[41]

The fate and mechanism of azo dye degradation catalyzed by CPO was investigated and the high efficiency of the reaction implied the possibility of CPO application in the large scale wastewater treatment.[28, 42]

Recently, the degradation of sulfamethoxazole was investigated by utilizing CPO with active sludge to increase the drug degradation efficiency. [43] The potential of CPO application in degrading different pharmaceuticals will be analyzed in my dissertation.

To stabilize CPO and increase the recyclability of the enzyme the catalyst was conjugated to poly (hydroxypropyl methacrylate-co-polyethyleneglycole methacrylate) membranes, which enhanced the storage and thermal stability compared to the free CPO. Immobilization of CPO will be one tendency of CPO application, a research will be

done to introduce CPO to the large scale application.

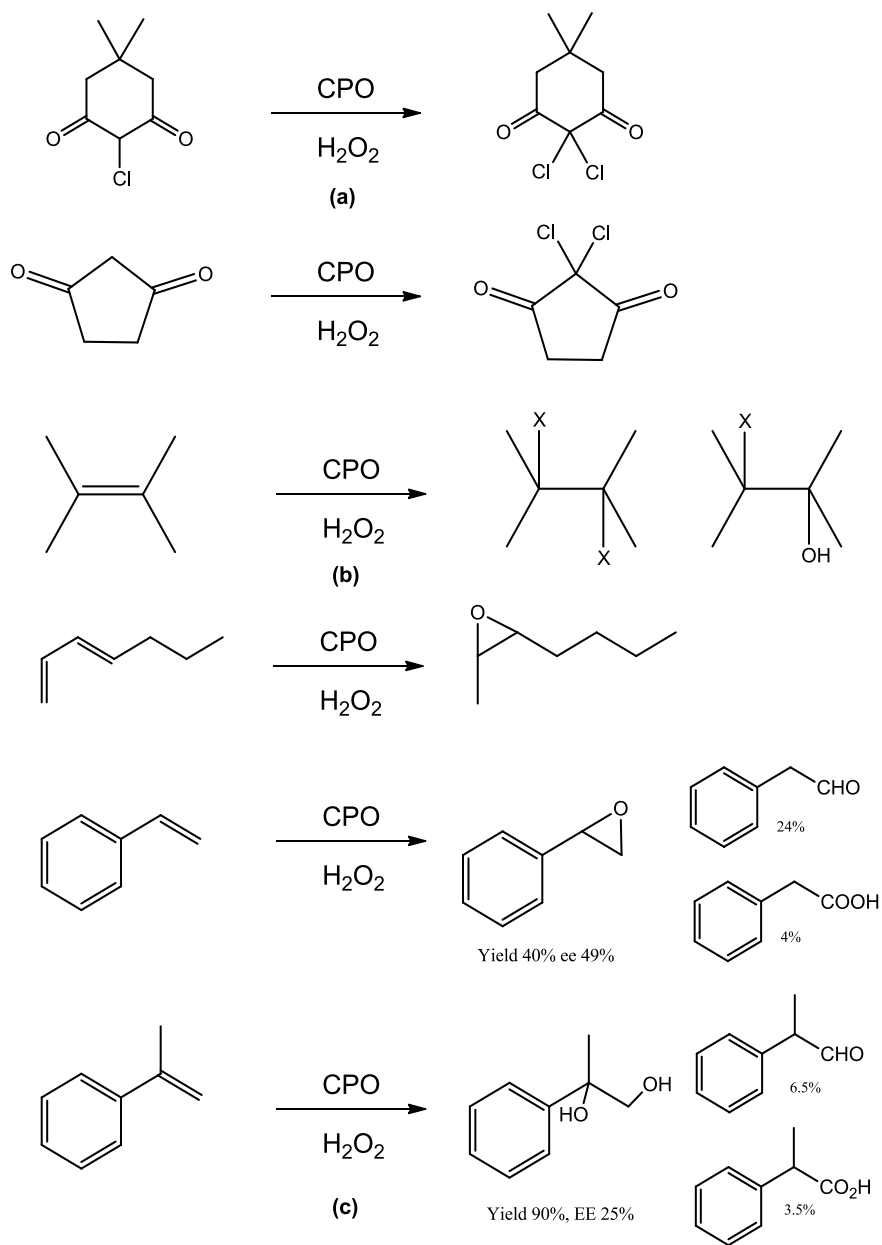


Figure 1.9 Reactions catalyzed by CPO in phosphate buffer with chloride ions. (a) The chlorination of MCD catalyzed by CPO.[38] (b) The examples of halogenation by 3-cyclopentanone and alkenes.[38, 39] (c) The typical examples of epoxidation and hydroxylation catalyzed by CPO with the yields and enantiomeric purities (ee).[41]

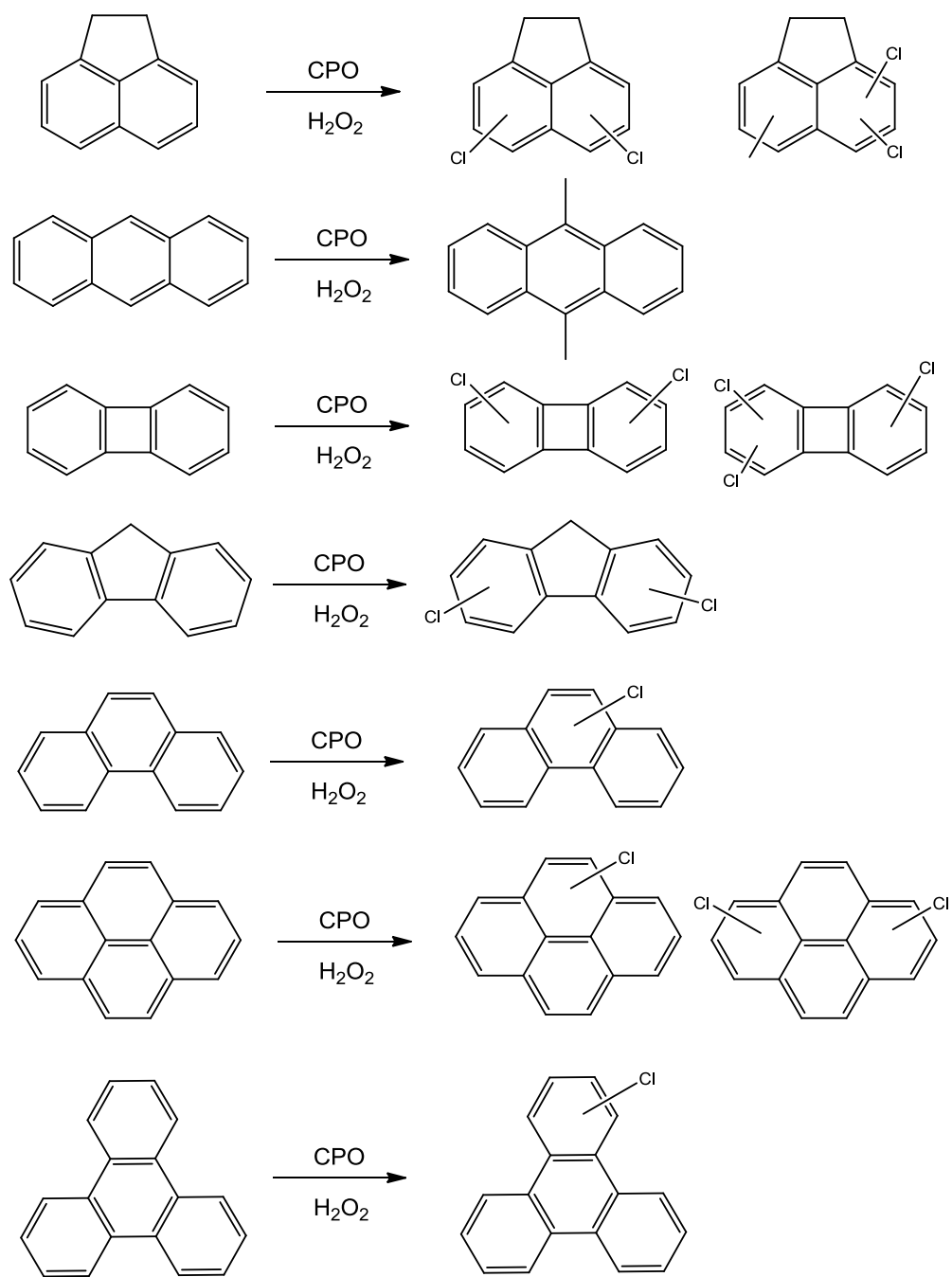


Figure 1.10 The chlorination of aromatic substrates catalyzed by CPO in phosphate buffer with chloride ions.[39]

CHAPTER II.

CPO-CATALYZED CHLORINATION AND POLYMERIZATION OF ACETAMINOPHEN

2.1. Background

Acetaminophen (N-acetyl-p-aminophenol, APAP), also known as paracetamol, is an active ingredient in over-the counter medicines and widely used for relieving fever and pain. The production of APAP was estimated to be in the kiloton level in the USA per year.[44] Overdose causes serious liver damage because of the formation of N-acetyl-p-benzoquinone imine (NAPQI).[45] APAP is ubiquitous in the natural environment, detected as 1.89 µg/L in ground water in the U.S.A[46] Occurrence of APAP as a contaminant in wastewater and drinking water increased the risk of human health and investigations of biodegradation of APAP.[47, 48]

Bioremediation catalyzed by CPO is a potential treatment as a consequence of its environmental friendliness and low cost investment. The efficiency of APAP degradation catalyzed by CPO would be investigated, the metabolites and pathway would be proposed in this experiment.

2.2 Experimental Procedure

2.2.1 Material

Chloroperoxidase (CPO) is a heme-containing glycoprotein secreted by the marine fungus *Caldariomyces fumago*. The isolation of CPO proposed in this study was a modification of the protocol reported by Morris and Hager[18] where acetone was used as precipitating agent instead of ethanol as the fractionation

solvent. CPO with $R_z = 1.45$ (R_z is purity standard defined as $A_{398}/A_{280} = 1.44$ for pure enzyme) was applied in all reactions. All solvents were HPLC grade or Optima[®] LC/MS grade, purchased from Thermo Fisher Scientific Inc. (Waltham, MA, USA). Water was produced by using a Milli-Q[®] Biocel™ Ultra-Pure water purification system equipped with 0.22 μM membrane filter cartridge (EMD Millipore, Billerica, MA, USA), and an organic removal cartridge (Evoqua Water Technologies, Lowell, MA, USA).

2.2.2 UV-Visible spectrophotometry

A VARIAN UV-Vis spectrophotometer (Cary 200 Bio) was used to collect the UV spectra of the degradation products. The drug solution was scanned by dissolving 0.11 mM APAP in 100 mM KH_2PO_4 buffer with 20 mM KCl at pH 2.75. The same solution was monitored after mixed with 0.55mM H_2O_2 . The reaction was initiated with the addition of 5 nM CPO and UV-Vis spectrum was recorded for the reaction time: 1 minute, 2.5 minutes, and 4 minutes.

2.2.3 Liquid chromatography and mass spectrometry

2.2.3.1 Sample preparation

To investigate the degradation efficiency, 62.56 μM APAP was reacted with 321.56 μM H_2O_2 and 0.43 nM CPO for 1 hour at room temperature. Mixture was centrifuged at 3,000 g in Centriprep[®] centrifugal filter unit with a 30,000 Dalton cut-off membrane (EMD Millipore, Billerica, MA, USA). The yielded products was collected after centrifuged for 1min. Ethyl acetate was used to extract the filtrate while shaking vigorously, and the supernatant was evaporated to dryness by using nitrogen gas. The dried metabolites were dissolved in H_2O /methanol (95:5

v/v) to make the final concentration 1 mg/L (ppm). Sample was stored at -20 °C in a freezer or immediately run in the LC-Q-TOF-MS mass spectrometer system.

A low concentration of CPO and H₂O₂ reaction sample was prepared as follows: 6.86 μM H₂O₂ was added directly to Centriprep[®] centrifugal filter unit with the same membrane size as described above. Then 66.20 μM APAP were added, catalyzed by the addition of 1.28 nM CPO in the 100 mM phosphate buffer with 20 mM KCl for 3 minutes and 5 minutes. The experiments were run in triplicate. The dried metabolites were dissolved in H₂O/methanol (95:5 v/v) to make an approximate concentration of 1 mg/L (ppm), and detected by LC-Q-TOF-MS system immediately.

The high concentration of APAP sample was prepared by mixing 413 μM APAP with 2 mM H₂O₂, catalyzed by 2 nM CPO for 35 minutes at room temperature. The extraction was carried out by ethyl acetate, and the organic layer was dried by nitrogen gas. Metabolites were dissolved in 1.5 mL H₂O/methanol (95:5 v/v) to make an approximate final concentration of 5 mg/L (ppm). The sample was filtrated through 0.22 μM polyethersulfone syringe filter. The sample was stored in a freezer at -20°C, detected both in Q-TOF-LC-MS system and Triple-quadrupole LC-MS/MS system.

2.2.3.2 Instrumentation and chromatographic separation

The Agilent 1290 Infinity UPLC system coupled with Agilent 6530 Q-TOF mass spectrometer was used for the chromatographic separation and identification of the metabolites. The Agilent MassHunter Data Acquisition Software (rev. B0.06.00) was used to control the UPLC and the mass

spectrometer. Mass Hunter Qualitative Data Analysis Software (Rev. B.07.00) was used for data mining and identification. An Agilent ZORBAX Eclipse plus C₁₈ Rapid Resolution High Definition (RRHD) column (100 mm×1.8 µm) was applied, the column temperature was set at 30 °C via a thermostatted column compartment (TCC). An infinity 1290 automatic injector was used to inject 1 µL (microliter) of the sample to the column. A flow rate of 0.4 mL/min was used and an aqueous mobile phase A consisting of water with 5 mM ammonium formate with 0.1% formic acid and the organic mobile phase B consisting of acetonitrile with 0.1% formic acid. The optimized chromatographic gradient was at 0 minute, 95% A and 5% B and B increased linearly to 95% over 8 minutes, this gradient was maintained for 1 minute. The positive ionization mode was applied during all experiments.

In full scan MS mode, the accurate mass data of the molecular ions were processed through the Agilent MassHunter Qualitative Analysis software. The collected retention times and confirmed formulas of every metabolite were applied in targeted MS/MS mode to identify metabolite information.

Additionally an Agilent 6460 Triple-Quadrupole LC/MS/MS mass spectrometer was used to increase the detection sensitivity of the isolated metabolites that were initially identified by the LC-QTOF mass spectrometer. The same column and elution program previously used in the LC-QTOF was employed in the LC-MS system.

2.2.3.3. Data Mining and Database development.

To create a database of all metabolites with optimized parameters, several

search algorithms were used in Mass Hunter Qualitative Data Analysis Software. One of this algorithms was Find by Formula (FbF) which allow the search of a compound using its molecular formula. The search could include not only the formation of the molecular ion $[M+H]^+$ but also the formation of adducts (like ammonium or sodium adducts) typically observed under the ionization conditions in electrospray. The samples were initially infused into the system by flow injection analysis (FIA) and later subjected to chromatography. Additional work was performed by LC-QQQ-MS detection for those metabolites present at low levels of concentration.

2.3 Result and discussion

2.3.1 UV-Vis study of CPO-catalyzed degradation of APAP

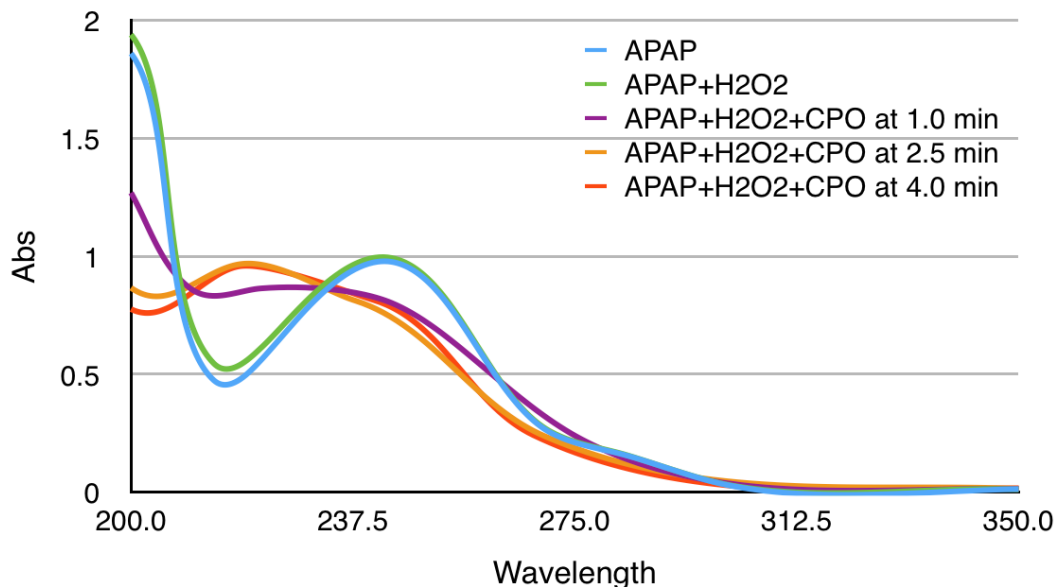


Figure 2.1 UV-Vis Spectra of APAP , APAP with H_2O_2 and its metabolites at 1min, 2.5min, and 4min.

The UV-Vis Spectrum of APAP (0.11 mM) were scanned in 100 mM KH_2PO_4

buffer with 20 mM KCl at pH 2.75. The Spectrum of APAP showed a strong absorption at 242 nm. After mixed with 0.55 mM H₂O₂, the absorption curve increased slightly due to absorbance of H₂O₂. 1 minute after addition of 5 nM CPO, the 477 nm absorption decreased, and increased at 4 min. The absorption at 218 increased after 1 min, and stopped increasing at 2.5 min (Fig. 2.1). The absorption of metabolites covered the absorption of original drug, which made the detection of kinetic parameter of APAP degradation catalyzed by CPO impossible.

The same reaction was carried out under the same condition except for the absence of chloride ion (KCl) in phosphate buffer. Without KCl, the absorbance did not change after the addition of CPO. Chlorine ion is necessary in the degradation of APAP in CPO-H₂O₂-Cl⁻ system.

2.3.2 LC-Q-TOF- MS

To investigate the degradation efficiency of APAP in CPO-H₂O₂-Cl⁻ system, 62.56 μM APAP was reacted with H₂O₂ (321.56 μM) and CPO (0.43 nM) for 1 hour, the sample was analyzed by LC-Q-TOF-MS, APAP was not observed, the degradation efficiency by low concentration of CPO could achieved 100%, suggesting the potential of the application of CPO in large-scale waste water treatment.

There were 7 APAP metabolites (coded from AM1 to AM7) confirmed by different retention times and accurate mass-to-charge ratios (m/z). The elemental formula, retention time, the relative mass difference between the observed mass and the mass of the target compound (in parts per million), and the difference

between the observed mass and the mass of target compound (in milliDaltons) were collected (Table 2.1).

Table 2.1 Accurate-Mass LC-Q-TOF-MS data for the identification of APAP and its metabolites.

Code	Formula	Retention time (min)	Experimental mass (m/z)	Theoretical mass (m/z)	Diff (ppm)	Diff (mDa)
APAP	C ₈ H ₉ NO ₂	2.986	151.0623	151.0633	-7.06	-1.07
AM1	C ₈ H ₈ ClNO ₂	3.713	185.0244	185.0246	1.27	0.23
AM2	C ₁₆ H ₁₆ N ₂ O ₄	3.436	300.1110	300.1115	1.59	0.48
AM3	C ₁₆ H ₁₅ ClN ₂ O ₄	4.157	334.0720	334.0724	1.12	0.38
AM4	C ₈ H ₇ Cl ₂ NO ₂	4.822	218.9854	218.9847	-3.23	-0.71
AM5	C ₁₆ H ₁₄ Cl ₂ N ₂ O ₄	4.673	368.0331	368.0328	-0.82	-0.30
AM6	C ₂₄ H ₂₃ N ₃ O ₆	4.051	449.1578	449.1587	-1.94	-0.87
AM7	C ₂₄ H ₂₂ ClN ₃ O ₆	4.567	483.1200	483.1197	0.59	0.29

The mass spectrum of each individual metabolite found (7 in total) are included in Appendix I. The mass accuracy of the standard drug (APAP) was calculated and the values ranged between 0.37 ppm and 9.75 ppm. The relative mass differences of metabolites were between 0.59 ppm and 3.23ppm. The mass differences of all compounds were less than 1.1 mDa. This method was proved to be efficient for determination of the metabolites of APAP.

Dimer (AM2) and Trimer (AM6) were formed, their chlorinated products were observed as AM3, AM7 respectively. For chlorinated metabolites, the isotope peaks were detected as the conformation of addition of chlorine atom. For AM1, AM3 and AM7, the two major peaks of each spectra separated by 2 m/z units and peak heights are in the ratio of 3:1, proved these molecules contain one chlorine atom. For AM4 and AM5, there were 3 lines in the molecular ion region

(M+, M+2 and M+4) with gaps of 2 m/z units between them, and with peak heights in the ratio of 9:6:1, it was confirmed that both compounds contain 2 chlorines.

The structures of each metabolite were confirmed in targeted MS/MS by retention time and fragment ions (Fig. 2.2). The concentration of AM7 was low, the majority form of AM7 was [M+Na]⁺ (472.1453 m/z).

2.3.3 Triple-quadruple LC/MS/MS

Agilent Technologies 6460 Triple-quadrupole LC/MS/MS in multiply reaction monitoring (MRM) mode was applied in investigation of metabolites of APAP. Data were analyzed with Agilent MassHunter Qualitative Analysis software. After the formula of metabolites was confirmed by LC-Q-TOF-MS, Individual metabolites were assessed with a more sensitive analytical technique (LCQQQ-MS). For example, AM1 showed one solid peak with a mass corresponding to m/z 186.03 in Q-TOF both in full scan mode. The use of an MRM method in Triple-quadrupole LC/MS/MS, two peaks were clearly eluted at different retention times. For detection of isomers in complex biological matrix, Triple-quadrupole shows excellent sensitivity and selectivity for target compounds by filtering out the purities with the same molecular weight as targeted products.

The specific parameters, including optimized fragmentor voltage and collision energy (CE) for different MRM transition has been determined by flow injection analysis without column (FIA) with MassHunter Optimizer software (Appendix II). Routine MRM mode, more than one MRM transition per compound is used to

avoid false-positive results, two transitions are monitored for one compound in most cases.

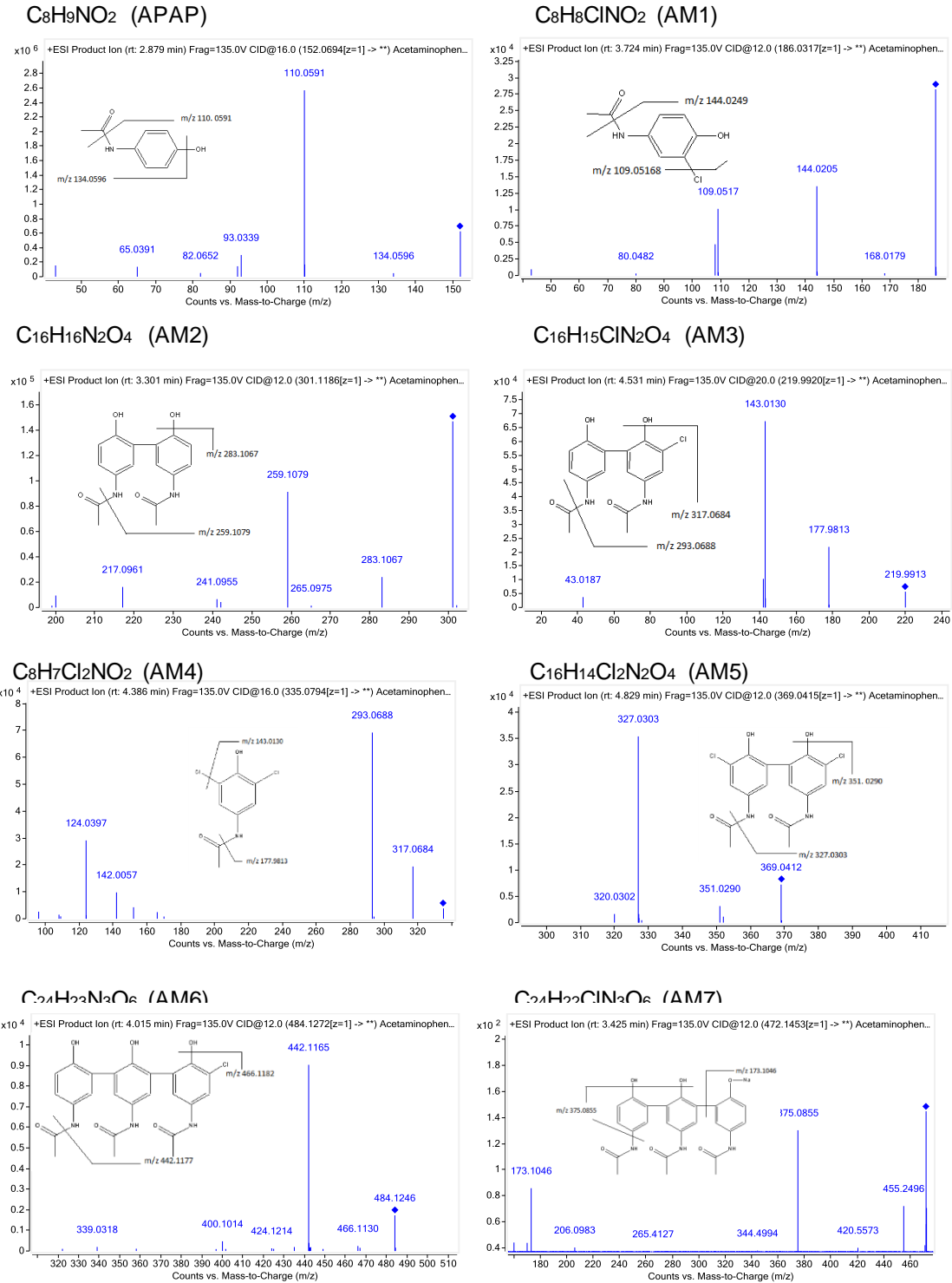


Figure 2.2 The targeted MS/MS spectra of APAP and its metabolites.

The relative area in chromatogram was used to measure the abundance of each metabolite (Fig. 2.3a). AM1 and AM2 were the major product. To investigate the mechanism of the degradation, limited concentration of H₂O₂ was added to the reaction, the ratio of APAP and H₂O₂ was 10:1. At first 3 minutes, the formation of AM2 was predominant within 5 minutes. The proportional area was consistent with the degradation by higher concentration H₂O₂. (Fig. 2.3b). There were no other metabolites observed at the first reaction stage, suggesting the mechanism that AM3, AM4, AM5, AM6 and AM7 were formed from AM1 and AM2 (Fig 2.4).

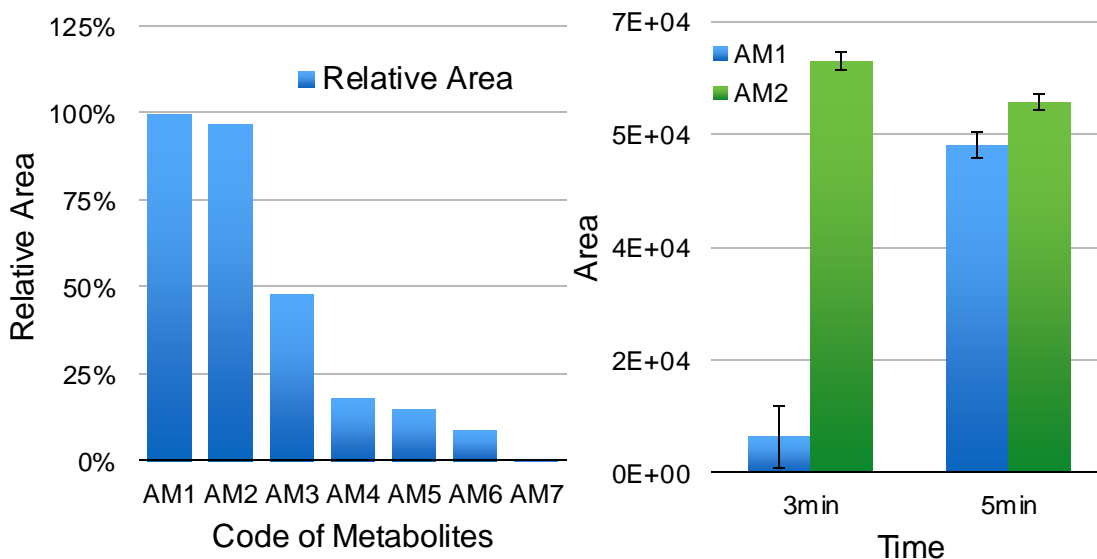


Figure 2.3 The relative area of each metabolite. (a) In high concentrated sample, the area of AM1 was set as 100%, compared with AM1, AM2 -AM6 is 96.94%, 48.08%, 18.12%, 8.93%, respectively. The area of AM7 was only 0.06%. (b) The area of AM1 at 3min was 5602 with error is 4879, at 5min increases dramatically to 50800 with error 2103; AM2 is 63866 at 3min with error 1452, and 57423 at 5min with error 1201. Each experiment was run in triplicate.

The different elution times of the same formula was considered as isomers. In addition, the exist of isomers could also be suggested with distinctive product

ions by the same fragmentor voltage at different retention time (Table 2.2). The concentration of AM7 is too low to detect the different elution time of isomers. The other 6 metabolites showed a good resolution.

To consider the relatively low concentration isomers, all optimized MRM transitions were loaded into the MassHunter Acquisition software for performing data analysis. The chromatograph of each formula was extracted by Agilent MassHunter Qualitative Analysis software with the proposed structures, the first structure shown on the chromatogram is the proposed primary structure with highest concentration (Fig 2.5.)

Table 2.2 Information of the proposed isomers (RT presents retention time).

Code	RT (min)	Area	Share transitions	Specific transitions
AM1-1	4.220	517761	43,54, 73,81, 82, 109, 168	53, 80, 144
AM1-2	3.923	34544		
AM2-1	3.664	812260	108, 259, 283	43, 127, 154 , 172, 182, 200, 217
AM2-2	4.292	64986		
AM3-1	4.405	223747	43	142, 170, 198, 199,215, 257, 293,317
AM3-2	4.890	66386		124, 142, 199, 293, 317
AM3-3	9.397	111378		
AM4-1	5.090	77208	43, 52, 79, 143, 178	
AM4-2	4.776	4866		
AM5-1	5.423	375540		218, 326
AM5-2	5.704	104506		218,326
AM5-3	4.943	71328		326
AM5-4	5.551	54057		326
AM6-1	9.714	36531	57	191, 253, 433
AM6-2	9.046	5142		71
AM6-3	8.480	5122		71
AM6-4	8.838	2809		71

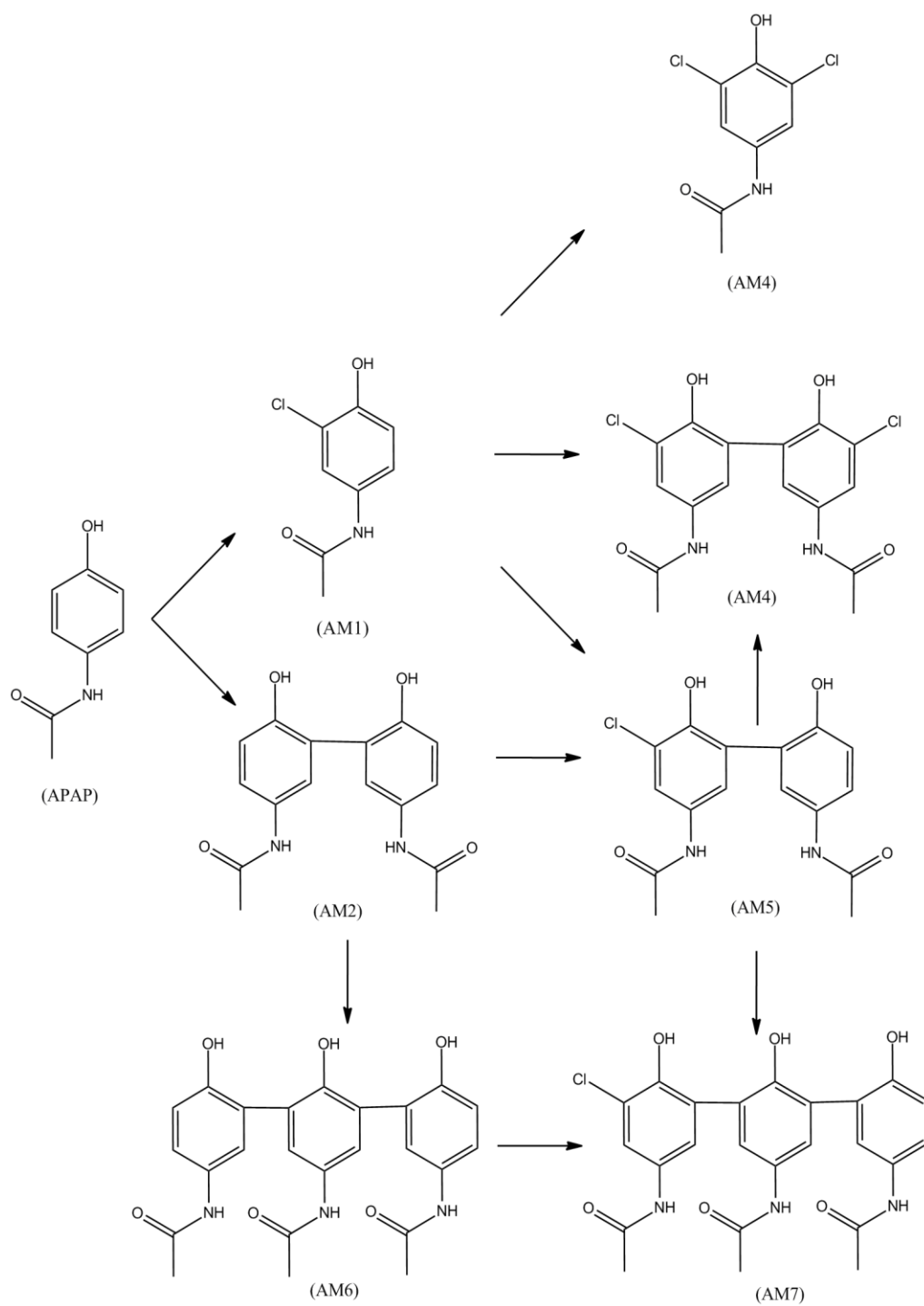


Figure 2.4 The proposed mechanism of the degradation of APAP catalyzed by CPO present by primary structure of each metabolites.

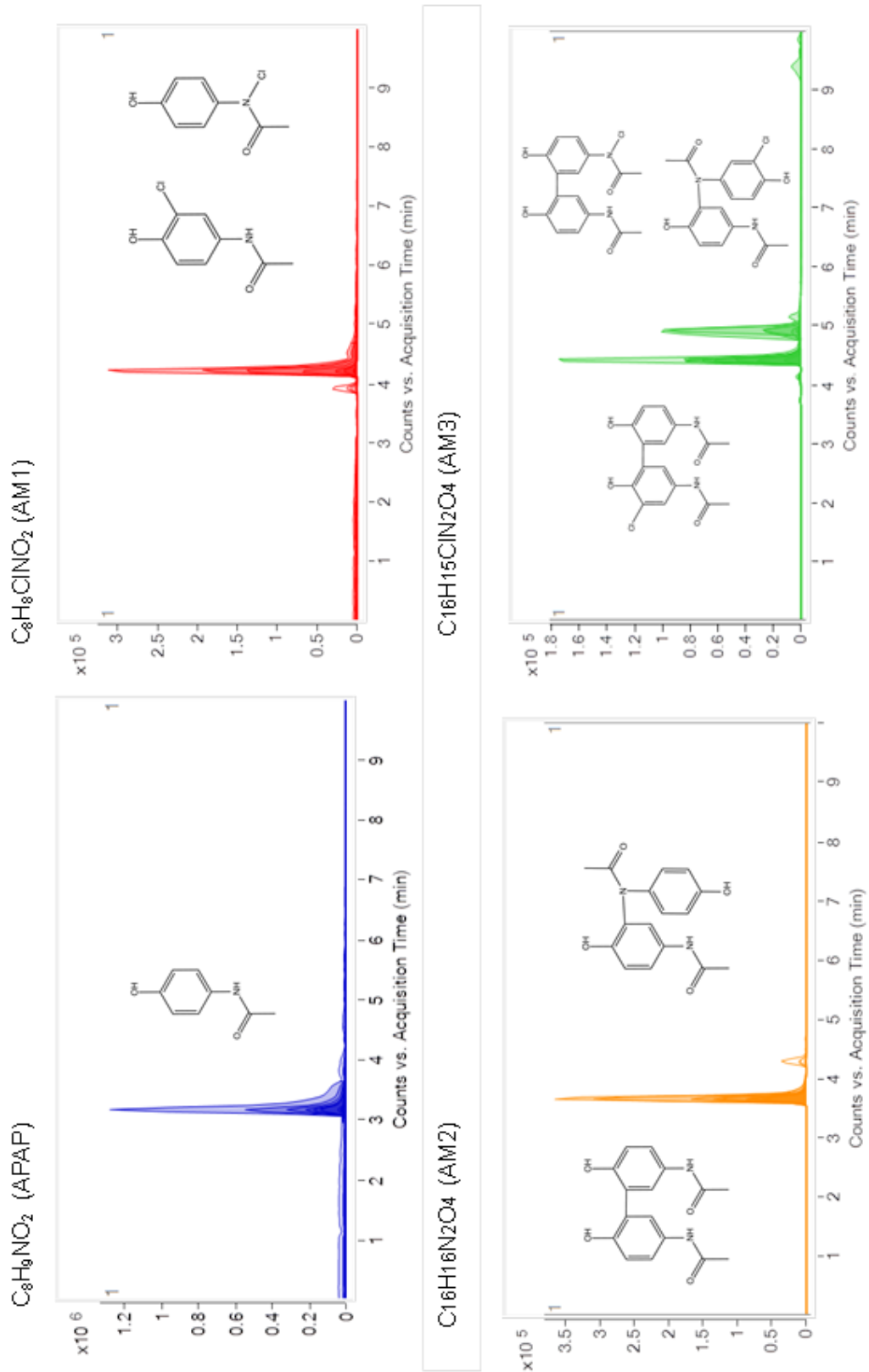
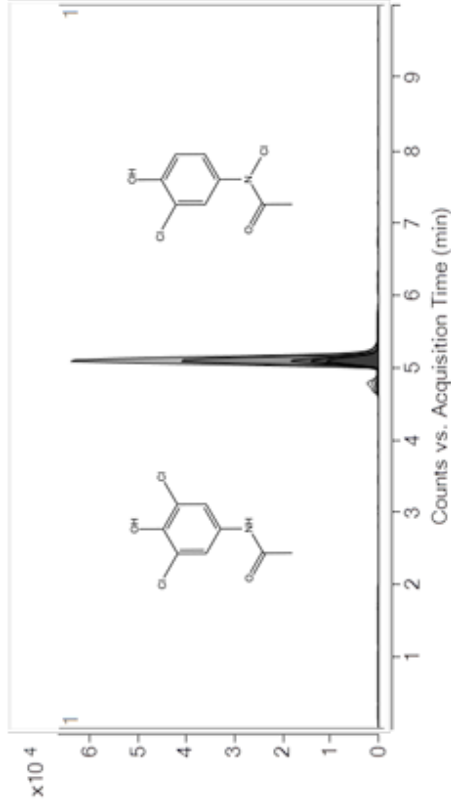
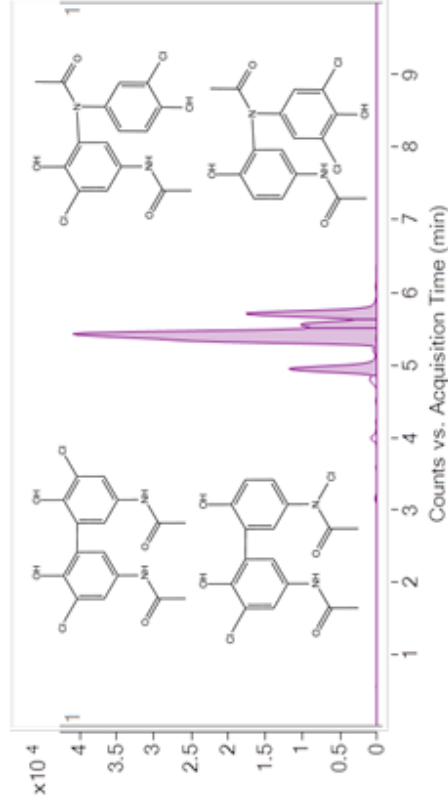


Figure 2.5 Extracted chromatogram of APAP and its metabolites detected by Triple-Quadrupole LC/MS/MS.

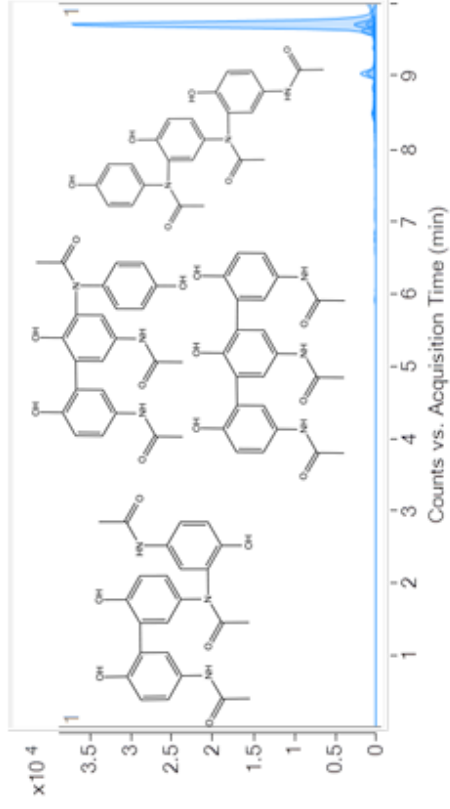
C₈H₇Cl₂NO₂ (AM4)



C₁₆H₁₄Cl₂N₂O₄ (AM5)



C₂₄H₂₃N₃O₆ (AM6)



C₂₄H₂₂ClN₃O₆ (AM7)

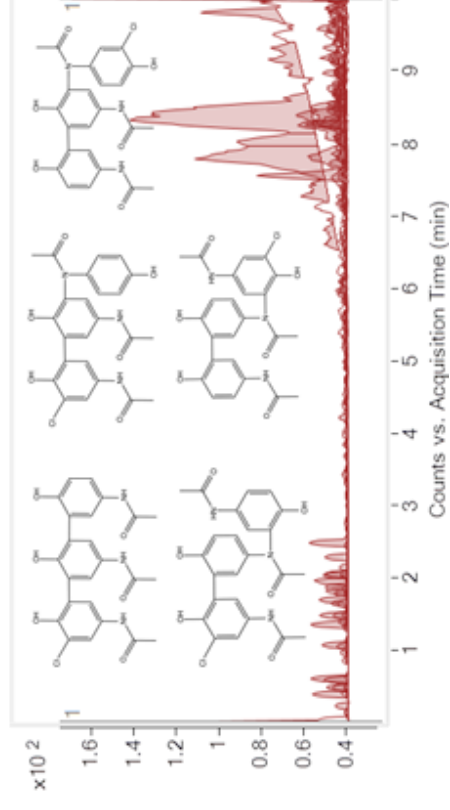


Figure 2.5 (Cont.) Extracted chromatogram of APAP and its metabolites detected by Triple-Quadrupole LC/MS/MS.

2.4 Discussion

NAPQI is the significant hepatotoxicity intermediate product of APAP catalyzed by the cytochrome P450 enzyme.[49] CPO shares the similar structure of P450 in proximal heme iron thiolate ligand,[50] but obviously, for catalyzing the degradation of APAP, the function of chlorination and dimerization is preferred instead of oxidation. For degradation of APAP, CPO-H₂O₂-Cl⁻ system works differently from hypochlorite and P450, suggesting the specific ability of detoxification of APAP. AM1 is a chlorinated APAP product, previously AM1-1 was reported in nitration processes of acetaminophen in nitrifying activated sludge as a low concentration transformation product. [51]

AM1-1 and AM4-1 are two ring chlorination metabolites of APAP. They were detected after APAP (10 µmol/L) reacted with hypochlorite (57 µmol/L) for 1 hour, 88% APAP was transformed. The approximate concentration of two chlorinated metabolites was 7% of the initial APAP. The concentration was relatively low when compared with the experiment catalyzed by CPO. When APAP mixed with hypochlorite, two toxic quinoidal oxidation products were produced, 1,4-benzoquinone and *N*-acetyl-*p*-benzoquinone imine (NAPQI) accounted for 25% and 1.5% of the initial acetaminophen concentration, respectively, which were not detected in CPO-H₂O₂-Cl⁻ system. Evaluation on the toxicity of the final products indicated that, CPO has the potential application in the purification of waste water when compared with regular chlorine disinfection systems.

AM4 was two electron-withdrawing chlorine substituent, compared the LDH leakage in hepatocytes with APAP, the LDH leakage was 36%, and APAP was

about 51%. Other analogues at the 3,5 positions were tested (R=-F, -Br, and -I), the value were from 42% to 15%. Besides, these halogenated products decreased the inhibitory potency towards cyclooxygenase, showed the decreased function of drug, both evidences implied that the halogenation of APAP in waste water by CPO-H₂O₂-Cl⁻ system could decrease the cytotoxicity and drug effect in human body.[49]

Dimer (AM2), trimer (AM6) and their chlorinated products (AM3, AM5, and AM7) were identified in CPO catalyzed reaction. Both dimer and trimer were detected in the horseradish peroxidase catalyzed polymerization of APAP, there were two dimers and three trimers detected by 500-MHz proton magnetic resonance spectroscopy.[35] The number of polymerized isomers generated by CPO catalyzed reaction were consistent with horseradish peroxidase catalyzed polymerization, and we proposed the same structure of each isomers. In the polymerization by horseradish peroxidase, the polymers formed primarily through a covalent bond between carbons *ortho* to the hydroxyl group due to the high unpaired electron density, and to a lesser extent, between the carbon *ortho* to the hydroxyl group and the amino group of another APAP molecule, as the isomer ratios observed from chromatograms of CPO catalyzed reaction.

CHAPTER III.

CPO-CATALYZED DEGRADATION OF CARBAMAZEPINE

3.1 Background

Carbamazepine (CBZ) is widely used in the treatment of epilepsy, trigeminal neuralgia and bipolar disorder. [52] CBZ has been studied as persistent anthropogenic pollutant which is detectable in surface water, ground water, and even in drinking water. In Germany, the annual consumption of CBZ was over 80 tons, and the concentrations detected were 6.3 µg/L in STP effluent, 26 ng/L in urban groundwater, 762 ng/L in surface water, 1640 ng/L in raw sewage, and 65-86 ng/L in tap water.[4, 7, 53] In other European surface water, the highest concentration was reported from 110-800 ng/L. [1] In addition, 420 ng/L CBZ was detected in the ground water used for public drinking water supply in USA. [46]

10 µg/L CBZ showed obviously cytotoxic to gill cell of fish.[54] It was reported that CBZ administration caused tumors in rats for 2 years drug treatment, and reduced the humoral and cellular immune responses, and induced spleen cellularity.[55, 56] Therefore, Long time exposure to CBZ in drinking water is a potential risk to human health.

The common water treatment is effective to degrade CBZ, even with some new biodegradation method was investigated such as biodegradation by algae, fungus, photocatalysis, etc. [4, 57-59] CPO has the potential to apply in degradation of CBZ due to its high efficiency (catalyzed within minutes), less expensive (work with nanomolar level enzyme) and its stability in acidic wastewater (pH 2.0-5.0). The CBZ degradation efficiency in water, the kinetic

parameters and the products of CBZ catalyzed by CPO was investigated in this experiment.

The aim of this experiment was to investigate the potential application of CPO in the degradation of CBZ. The efficiency of CPO in the degradation of CBZ was measured. The operating conditions including the concentration of Cl^- , reaction buffer pH, and the concentration of H_2O_2 was optimized, and under the optimized conditions, the enzyme kinetic and degradation pathway was studied.

3.2 Experimental Procedure

3.2.1 Material

All material and chemicals used were the same as described in section 2.2.1.

3.2.2 UV-Visible spectrophotometry

3.2.2.1 UV-Vis spectrum of degradation

A VARIAN UV-Vis spectrophotometer (Cary 200 Bio) was used to collect the UV spectra of the degradation products. The drug solution was scanned by dissolving 0.07 mM CBZ in 100 mM KH_2PO_4 buffer with 20 mM KCl at pH 2.75. The same solution was monitored after mixed with 0.35mM H_2O_2 . UV spectra were recorded after the addition of 5 nM CPO for 1minute, 2.5 minutes and 4 minutes. The degradation efficiency was calculated according to Equation (1)

$$\text{Efficiency (\%)} = \frac{A_0 - A_t}{A_0} \times 100 \quad (1)$$

3.2.2.2 Effect of diverse parameters on CPO degradation

The effect of the concentration of chloride was investigated. Degradation was carried out in 100 mM phosphate buffer at pH 3.0 with 0.07 mM CBZ and 0.07

mM H₂O₂, concentration of chloride was increased from 0 to 20 mM, 285 nm wavelength was monitored immediately after 2.5 nM CPO was added.

The degradation rate at pH range of 2.0 to 5.0 was investigated to probe the effect of pH on CPO catalyzed reaction. The reaction was carried out in 100 mM phosphate buffer with 20 mM KCl, 0.07 mM CBZ, and 0.07 mM H₂O₂. H₃PO₄ and KOH were used to adjust pH, 285 nm wavelength was monitored immediately after the addition of 2.5 nM CPO. The calculated time was from 0.2 to 0.4 minute.

The degradation rate of CBZ was determined by different concentration of hydrogen peroxide from 0.07-0.71 mM in 100 mM phosphate buffer with 20 mM KCl and 0.07 mM CBZ at pH 3.0. 285 nm wavelength was monitored immediately after the addition of 5 nM CPO. Rate from 0.1 minute to 03 minute was calculated as degradation rate.

It was assumed that the degradation would follow Michaelis-Menten kinetics, and the Lineweaver-Burk plot Equation was used to calculate Michaelis-Menten constant (K_m) and maximum reaction rate (V_{max}) (2), where the $[S]$ presents the concentration of substrate (CBZ), V presents the initial reaction rate, the rate was calculated by monitoring at 285 nm absorbance from 0.1-0.2 minute. The reaction was carried out in 100 mM concentration of KH₂PO₄ buffer with 20 mM KCl at pH 2.75, the concentration of CBZ was varying from 0.02 mM to 0.11 mM. UV was started to monitor immediately after adding 0.35 mM H₂O₂.

$$\frac{1}{V} = \frac{K_m}{V_{max}} \times \frac{1}{[S]} + \frac{1}{V_{max}} \quad (2)$$

The turnover number (k_{cat}) was obtained by the equation (3), calculated from the maximum reaction rate (V_{max}) and the concentration of CPO (E_0).

$$V_{max} = k_{cat} [E_0] \quad (3)$$

All experiments were triplicated and data reported were mean values of three independent measurements with standard deviation.

3.2.3 Liquid chromatography and mass spectroscopy

3.2.3.1 Sample preparation

To investigate the degradation efficiency, CBZ was dissolved in methanol to make stock solution (21.19 mM), 10.59 μ M (2.5 mg/L) CBZ was reacted with 107.19 μ M H₂O₂ and 2.9 nM CPO for 10 minutes at room temperature. Mixture was centrifuged at 3,000 g in Centriprep[®] centrifugal filter unit with 30,000 Dalton cut-off membrane (EMD Millipore, Billerica, MA, USA). The filtrate was collected after centrifuged for 1min. Ethyl acetate was used to extract the filtrate while shaking vigorously. To remove the organic solvent, nitrogen gas purge was applied to dry the sample. The dried residues were dissolved in H₂O /methanol (95:5 v/v) to make the final concentration approximate 1 mg/L (ppm). The sample was stored at -20 °C in a freezer, or immediately run in LC-Q-TOF-MS mass spectrometer system.

To detect all metabolites of CBZ, CBZ was dissolved in methanol to make stock solution (21.19 mM), a high concentration of CBZ sample was prepared by mixing 62.56 μ M (14.8 mg/L) CBZ with 0.4 nM CPO, H₂O₂ stock solution (41.16 mM) was added to reaction system at 56.5 μ L/minute to make the final

concentration of H₂O₂ up to 316.56 μM. The total reaction time was 55 minutes. The solution was extracted by ethyl acetate, and the supernatant was evaporated by using nitrogen gas. Metabolites were dissolved in 2.0 mL H₂O/methanol (95:5 v/v) to make the final concentration approximately 5 mg/mL (ppm). The sample was centrifuge at 1200 g for 10 minutes, 1.5 mL supernatant was removed by syringe. Filtration was applied by using 0.22 μM polyethersulfone syringe filter. The sample was stored at -20 °C in freezer, detected both in LC-Q-TOF/MS system and Triple-Quadrupole LC/MS/MS system.

To investigate the mechanism of degradation, samples were prepared with low concentration of H₂O₂. 6.86 μM H₂O₂ was added directly to Centriprep[®] centrifugal filter unit (30,000 Dalton) with 42.28 μM CBZ, catalyzed by 1.3 nM CPO in the 100 mM phosphate buffer with 20 mM KCl for 1 minute, 3 minutes and 5 minutes, filter units were centrifuged at 3000g for 1min at room temperature, and extracted the filtrate by ethyl acetate, purged the organic phase with nitrogen gas to dryness. The dried metabolites were dissolved in H₂O/methanol (95:5 v/v) to make the final concentration approximate 1 mg/L (ppm), and detected by LC-Q-TOF-MS system immediately. Experiments were run in duplicate.

3.2.3.2 Instrumentation and chromatographic separation

The instrumentation and chromatographic separation were the same as in section 2.2.3.2.

3.2.3.3. Data Mining and Database development

The data Mining and Database development were the same as in section

2.2.3.3.

3.3 Result and discussion

3.3.1 UV-Vis study of CPO-catalyzed degradation of carbamazepine

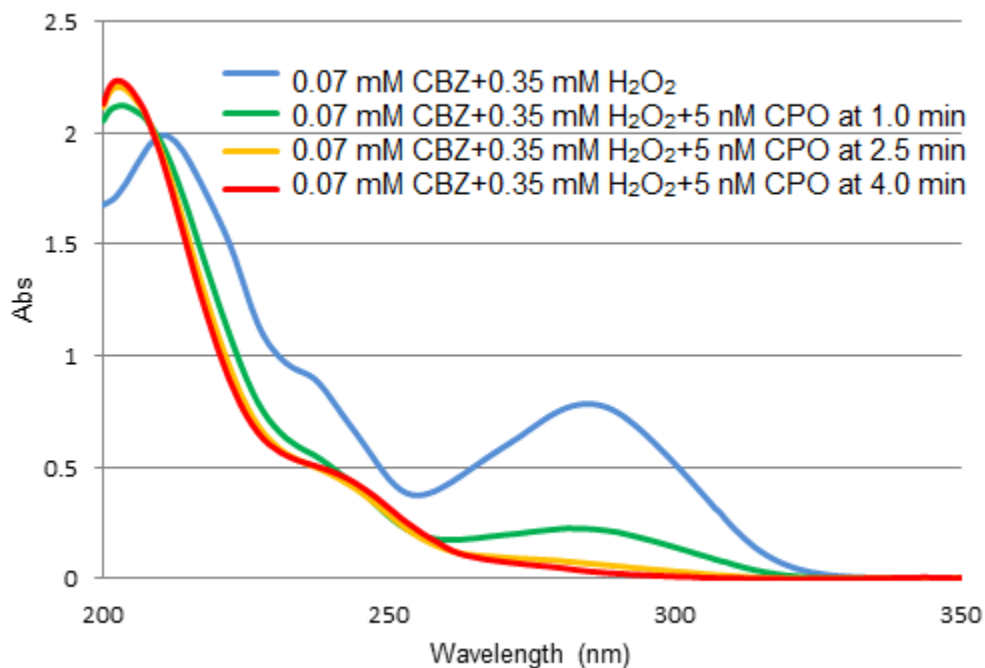


Figure 3.1 UV-Vis Spectra of CBZ with H₂O₂ and its metabolites at 1min, 2.5min and 4min.

UV-Vis Spectra of CBZ (0.07 mM / 16.53 mg/L) and H₂O₂ (0.75 mM) were scanned in 100 mM KH₂PO₄ buffer, 20 mM KCl at pH 2.75 (Fig.3.1). The Spectrum of CBZ showed a strong absorption at 285 nm. 1 minute after addition of 5 nM CPO, the 285 nm absorption decreased, and stopped increasing at 4 minutes (Fig. 3.1). Wavelength at 285 nm was used to measure kinetic parameter of CBZ degradation catalyzed by CPO.

The same reaction was carried out under the same condition except for the chlorine ion (KCl) in phosphate buffer. Without KCl, the absorbance did not

change after the addition of CPO. Chlorine ion is necessary in the degradation of CBZ in CPO-H₂O₂-Cl⁻ system.

According to Equation (1), The efficiency of degradation catalyze by 5 nM CPO was 96% within 4 minutes, the efficiency might be more than 96% since the the tail of the UV peak of product seemed cover the original drug (285 nm).

3.3.2 The effect of chloride on the degradation of CBZ

Degradation rate was calculated from 0.2-0.6 minute. The degradation rate increased from 0 to 18.89 $\mu\text{M}/\text{min}$. The obsevation was consistent as described in section 3.2.1, suggested that chloride participates in the degradation of CBZ. (Fig. 3.2).

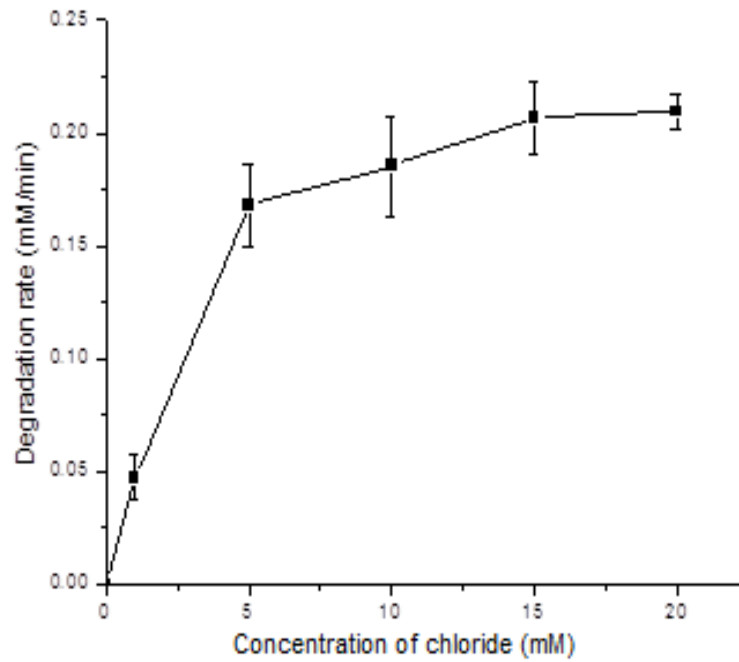


Figure 3.2. The effect of chloride on the degradation of CBZ. Data were collected from triplicate experiment in 100 mM phosphate buffer at pH 3.0, with 0.07 mM CBZ, 0.07 mM H₂O₂, and 2.5 nM CPO.

3.3.3 The effect of pH on the degradation of CBZ

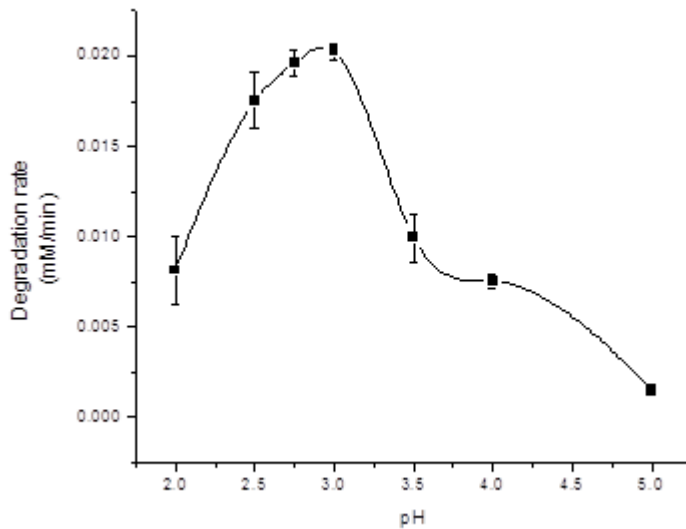


Figure 3.3 The effect of pH on CBZ degradation. Data were collected from triplicate experiment in 100 mM phosphate buffer (20 mM KCl) with 0.07 mM CBZ, 0.07 mM H_2O_2 , and 2.5 nM CPO at pH 3.0.

The optimum pH for the degradation of CBZ is 3.0 in the presence of 20 mM Cl^- , the degradation efficiency decreased from pH 3.5 to 5. This curve was close to the expected chlorination reaction and oxidation reaction, [60] suggested CPO could be applied in the acid wastewater treatment. (Fig. 3.3).

3.3.4 The effect of H_2O_2 concentration

The degradation rate was increased as the concentration of H_2O_2 increased to 0.53 mM. From 0.53 to 0.71 mM, the rate was still stable, only decreased slightly. This could be due to the degradation of CPO by the high concentration of H_2O_2 . [61] The stability of CPO in the presence of H_2O_2 compared with other peroxidase is suggested that CPO has a better prospect of application than the same class enzyme. (Fig. 3.4).

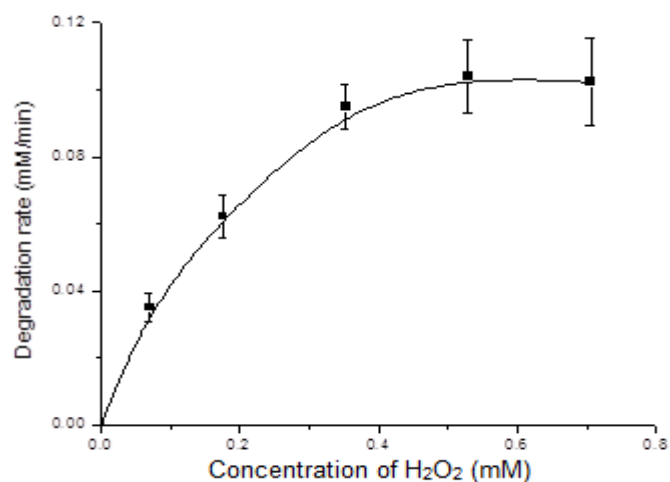


Figure 3.4 The effect of H₂O₂ concentration, Data were collected from triplicate experiment in 100 mM phosphate buffer (20 mM KCl) with 0.07 mM CBZ and 5 nM CPO at pH 3.0.

3.3.5 The kinetic parameters of CBZ degradation catalyzed by CPO

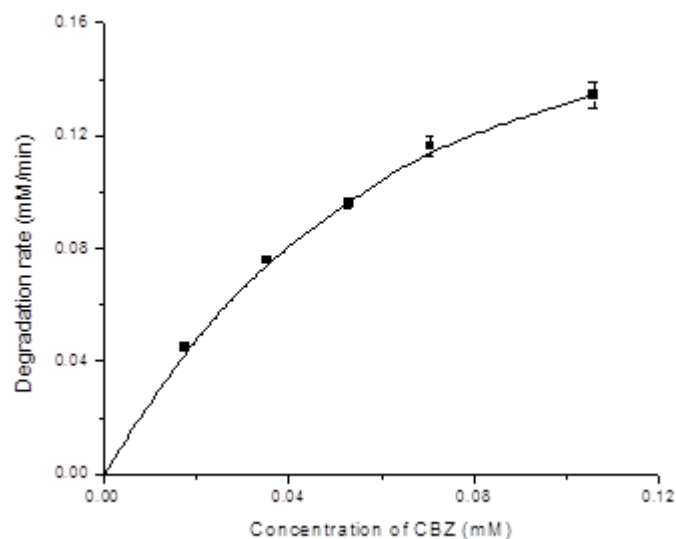


Figure 3.5 The effect of CBZ concentration. Data were collected from triplicate experiment in 100 mM phosphate buffer (20 mM KCl) with 0.07 mM H₂O₂, and 5 nM CPO at pH 3.0, concentration of CBZ was varied from 0.02 mM to 0.11 mM.

Different concentrations of CBZ were reacted with 0.07 mM H₂O₂ with 5 nM

CPO (Fig. 3.5). According to Equation 2, the kinetic parameters of CBZ degradation catalyzed by CPO was calculated (Table 3.1)

Table 3.1 The kinetic parameters of CBZ degradation catalyzed CPO.

K_m (μM)	V_{max} ($\mu\text{M s}^{-1}$)	k_{cat} (s^{-1})	k_{cat}/K_m ($\mu\text{M}^{-1}\text{s}^{-1}$)	R^2
73.35	3.87	733	10.54	0.9995

3.3.6 LC-Q-TOF- MS

To investigate the degradation efficiency of CBZ in CPO-H₂O₂-Cl⁻ system, 10.59 μM CBZ was reacted with 107.19 μM of H₂O₂ and CPO (2.9 nM) for 10 minutes, the sample was analyzed by LC-Q-TOF-MS, CBZ was not observed, the degradation efficiency by low concentration of CPO could achieved 100%, suggesting the potential of the application of CPO in large-scale waste water treatment.

Samples were detected in Agilent Technologies 6530 Accurate-Mass LC-Q-TOF-MS in full scan MS mode, the accurate mass data of the molecular ions were processed through the Agilent MassHunter Qualitative Analysis software. There were 15 CBZ metabolites (coded from CM1 to CM15) confirmed by different retention times and accurate mass-to-charge ratios (m/z). The elemental formula, retention time, the relative mass difference between the observed mass and the mass of the target compound (in parts per million), and the difference between the observed mass and the mass of target compound (in milliDaltons)

were collected (Table 3.2).

Table 3.2 Accurate-Mass LC-Q-TOF-MS data for the identification of CBZ and its metabolites.

Code	Formula	Retention time (min)	Experimental mass (m/z)	Theoretical mass (m/z)	Diff (ppm)	Diff (mDa)
CMZ	C ₁₅ H ₁₂ N ₂ O	5.901	236.0943	236.0950	-2.73	-0.64
CM1	C ₁₅ H ₁₂ N ₂ O ₂	4.314	252.0914	252.0899	6.21	1.56
CM2	C ₁₅ H ₁₄ N ₂ O ₃	3.366	270.1004	270.1004	-0.08	-0.02
CM3	C ₁₄ H ₁₁ NO ₂	2.839	225.0790	225.0790	-0.06	-0.01
CM4	C ₁₄ H ₉ NO	6.776	207.0680	207.0684	-1.84	-0.38
CM5	C ₁₃ H ₉ N	3.970	179.0728	179.0735	-4.12	-0.74
CM6	C ₁₃ H ₉ NO	5.185	195.0678	195.0684	-3.23	-0.63
CM7	C ₁₅ H ₁₃ NO ₂	3.793	239.0938	239.0946	-3.64	-0.87
CM8	C ₁₄ H ₉ NO ₂	2.379	223.0630	223.0633	-1.64	-0.37
CM9	C ₁₅ H ₁₁ NO ₃	3.959	253.0748	253.0739	3.53	0.89
CM10	C ₁₆ H ₁₄ N ₂ O ₂	4.863	266.1058	266.1055	0.88	0.23
CM11	C ₁₅ H ₁₂ ClNO ₂	6.061	273.0559	273.0557	0.90	0.25
CM12	C ₁₄ H ₈ ClNO	7.985	241.0298	241.0294	1.36	0.33
CM13	C ₁₃ H ₈ ClN	7.442	213.0356	213.0345	5.14	1.10
CM14	C ₁₃ H ₈ ClNO	6.222	229.0291	229.0294	-1.48	-0.34
CM15	C ₁₄ H ₈ ClNO ₂	3.111	257.0240	257.0244	-1.46	-0.38

All the relative mass difference of the standard drug (CBZ) and metabolites were less than 5.0 ppm except for CM1 (6.21 ppm) and CM13 (5.14 ppm). The relative mass difference of metabolite CM1 and CM13 in all experiments were between 0.19 ppm and 9.54 ppm, 0.74 ppm and 5.14 ppm, respectively. The mass differences of all compounds were less than 2.0 mDa. This method was proved to be efficient for determination of the metabolites of CBZ.

The mass spectra of each individual metabolite were collected in positive mode by MassHunter Workstation software (Appendix I). Since it was in positive

mode, all the compounds were detected as molecular ion $[M + H]^+$ except for CM9, the detected molecular ion was $[M + NH_4]^+$ adduct (271.1085 m/z), the ammonium adduct formation was favored in the ion source probable due to the ion pairing effect on the functional group responsible of ionization.

For chlorinated metabolites, the isotope peaks were detected as the conformation of addition of chlorine atom, the two major peaks of each spectra separated by 2 m/z units and peak heights are in the ratio of 3:1, proved these molecules contain one chlorine atom.

The structures of each metabolite were confirmed in targeted MS/MS by retention time and fragment ions (Fig. 3.6). There were 2 types of metabolites based on their structure. The first type contained CM1, CM2, CM9, CM10 were suggestive of oxygen insertion into the CBZ-based structure. The other structures were the second type, structures were based on acridine (CM5), the decarbonylation product of parent compound. All chlorinated metabolites were from acridine-based structures. CM11, CM12, CM13, CM14, CM15 was the chlorinated product of CM7, CM4, CM5, CM6, CM8, respectively. CM7 was generated from CM3 by methylation of hydroxyl group. CM8 was the hydroxylated product of CM4.

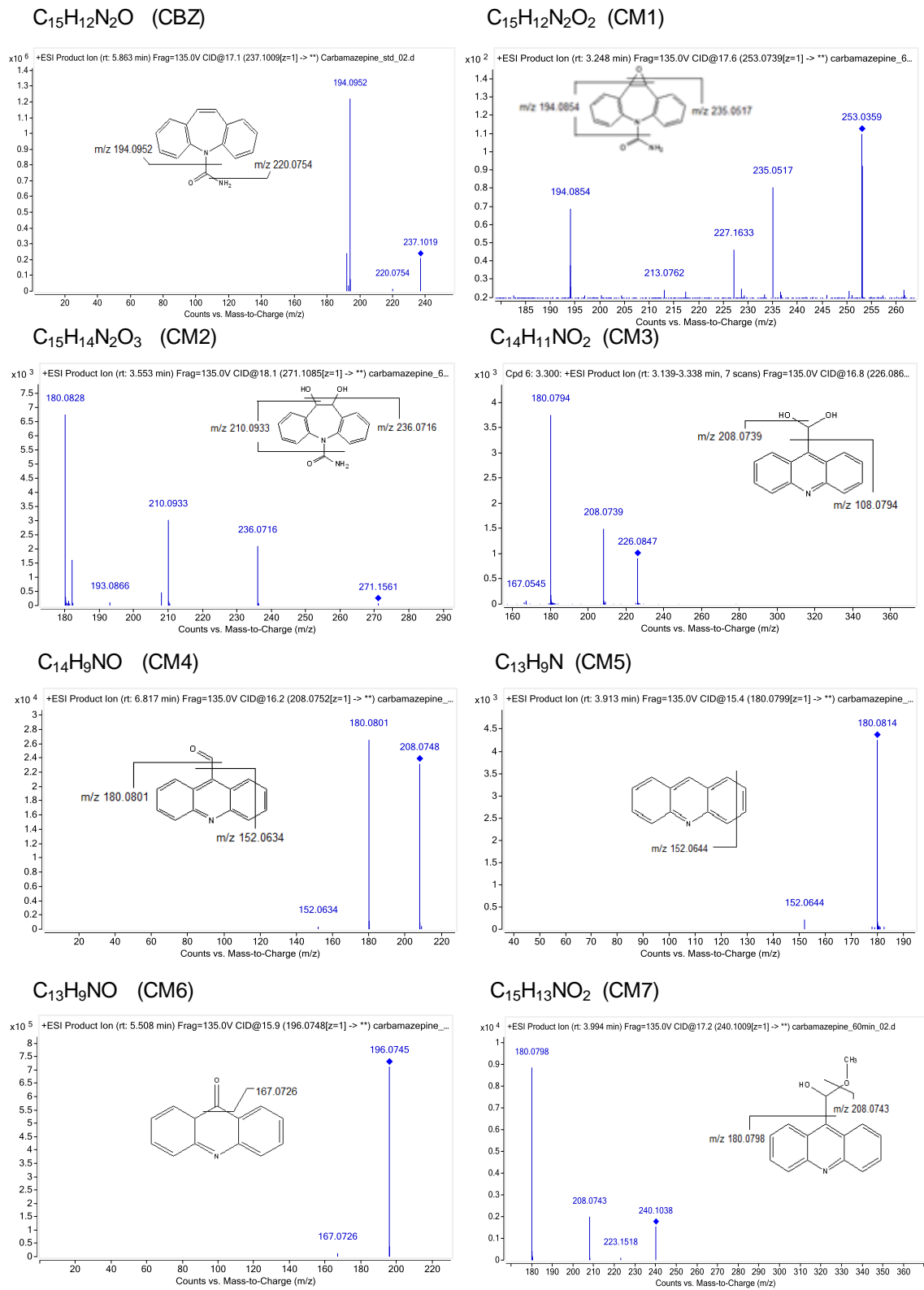


Figure 3.6 The targeted MS/MS spectra of CBZ and its metabolites.

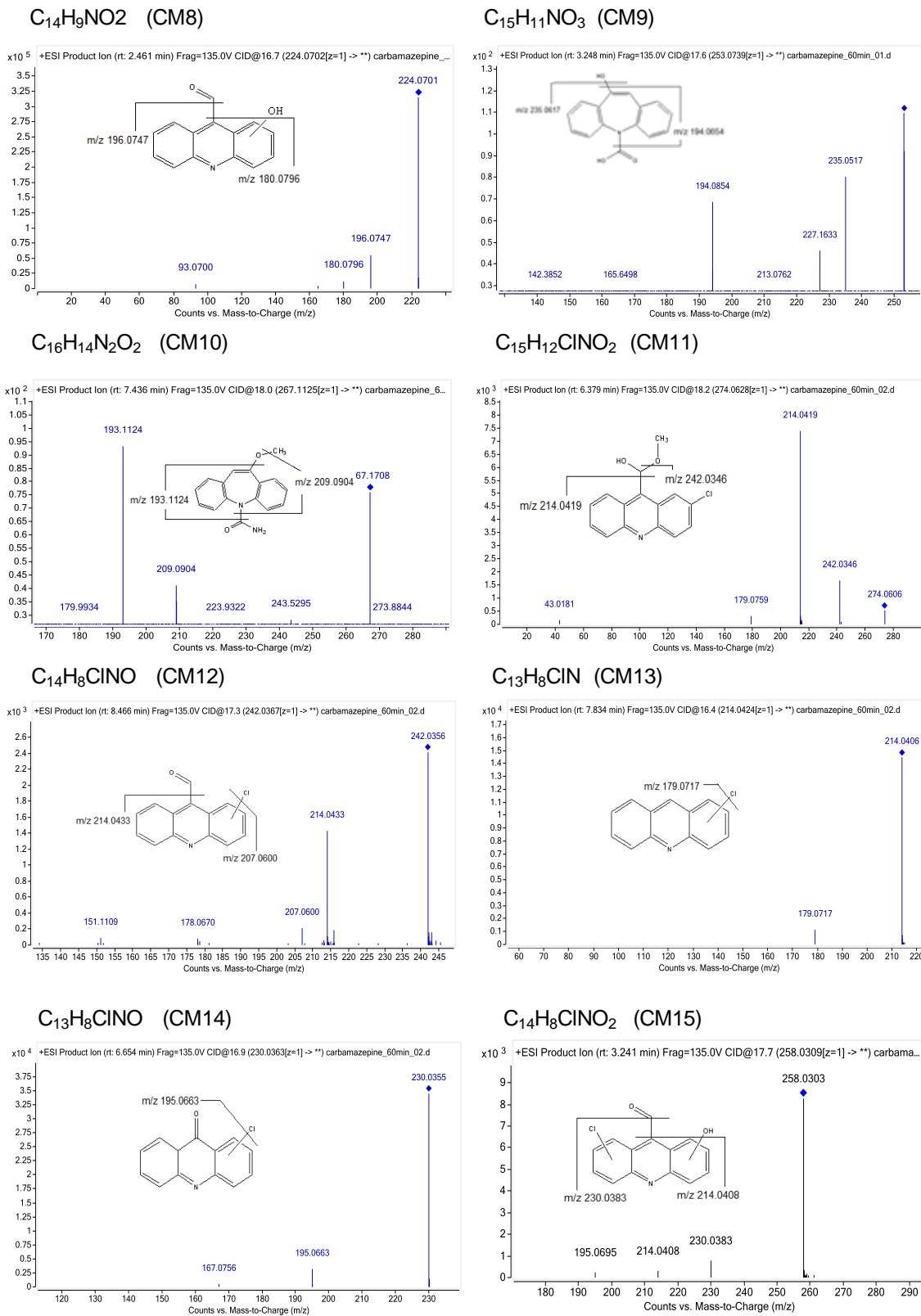


Figure 3.6 (Cont.). The targeted MS/MS spectra of CBZ and its metabolites.

The concentrations of all metabolites were measured as compound area by MassHunter Workstation software, and presented by percentage of all compounds as pie chart, all chlorinated compounds were showed in the second pie chart at right side (Fig. 3.7)

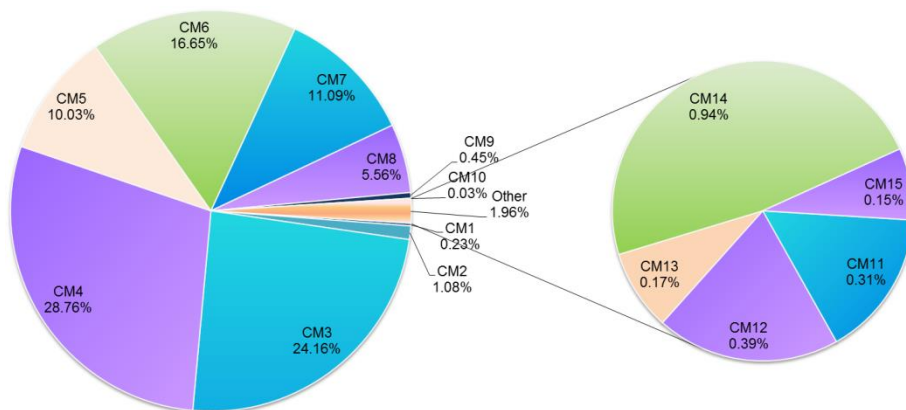


Figure 3.7. The percentage of each metabolites measured by compound area. Metabolites shared the same structure presented by the same color.

To investigate the mechanism of degradation process, the experiment was carried out for limited reaction time (1,3 and 5 minutes) with low concentration of H_2O_2 ($6.86 \mu M$), the ratio of the concentration of CBZ and H_2O_2 was about 7:1. Only part of CBZ was degraded, and only several metabolites were detected which could be suggested as the first formed metabolites (Fig 3.8). At the first minute, only CM1, CM2, CM9, CM10 were formed, the four proposed structures were suggestive of oxygen insertion into the CBZ-based structure, produced directly from CBZ without decarbonylation, CM1 was the most abundant metabolite, suggested the first step of degradation was the epoxidation of CBZ. The percentage of these four compounds decreased significantly after reacted with higher concentration of H_2O_2 for longer time (Fig. 3.7). From 3 minutes,

acridine (CM5) was formed, CM7 and CM8, two acridine-based metabolites were detected at 5 minutes. The final concentrations of them were the relatively high. Compared with the CBZ-based structure compounds, acridine-based structure were suggested as the major products, acridine (CM5), the decarbonylation product of parent compound, with CM6, CM7 and CM8 were the major metabolites of the degradation catalyzed by CPO, CBZ-based structures existed as intermediates of the degradation. CM5, CM6, CM7 and CM8 were the most abundant metabolites, suggested they were the major metabolites of the degradation catalyzed by CPO.

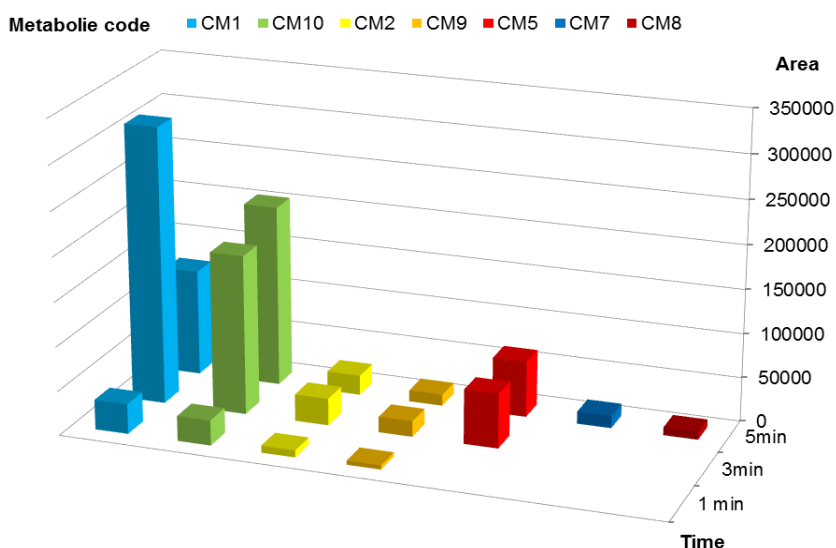


Figure 3.8 The area of metabolites with limited H_2O_2 at 1 min, 3 min and 5 min detected by Accurate-Mass LC-Q-TOF-MS. All experiments were duplicates and data reported were mean values of two independent measurements.

The chlorinated products were observed as CM11-CM15, the concentration of them were relatively low (Fig. 3.7) and they were not observed at the first stage of reaction (Fig. 3.8), these metabolites were not the major product of the

degradation catalyzed by CPO.

The chromatograms of CBZ and its metabolites were collected with their proposed structures (Fig. 3.9). In the chromatograms of CM1, CM2, CM9, CM11, CM12, CM13, CM14 and CM15, there were isomers identified by different retention time. For CM1, CM9, CM11 and CM12, metabolites had problem of signal to noise ratio might due to the low concentration, chromatograms of the four compounds were collected by Agilent Technologies 6460 Triple-quadrupole LC/MS/MS in multiply reaction monitoring (MRM) mode.

3.3.7 Triple-Quadruple LC/MS/MS

Agilent Technologies 6460 Triple-Quadrupole LC/MS/MS in multiply reaction monitoring (MRM) mode was applied in the investigation of metabolites of CBZ, especially for the 3 compounds (CM1, CM9, CM11 and CM12) which the resolution were low in Q-TOF. Data was analyzed in Agilent MassHunter Qualitative Analysis software. After the formula of metabolites was confirmed by LC-Q-TOF-MS, different retention times of individual metabolites could be recognized by Triple quad with less noise than in Q-TOF. (Fig. 3.9)

The specific parameters, including optimized fragmentor voltage and collision energy (CE) for different MRM transition has been determined by flow injection analysis without column (FIA) with MassHunter Optimizer software (Appendix II).

Four transitions were selected to monitor for one compound.

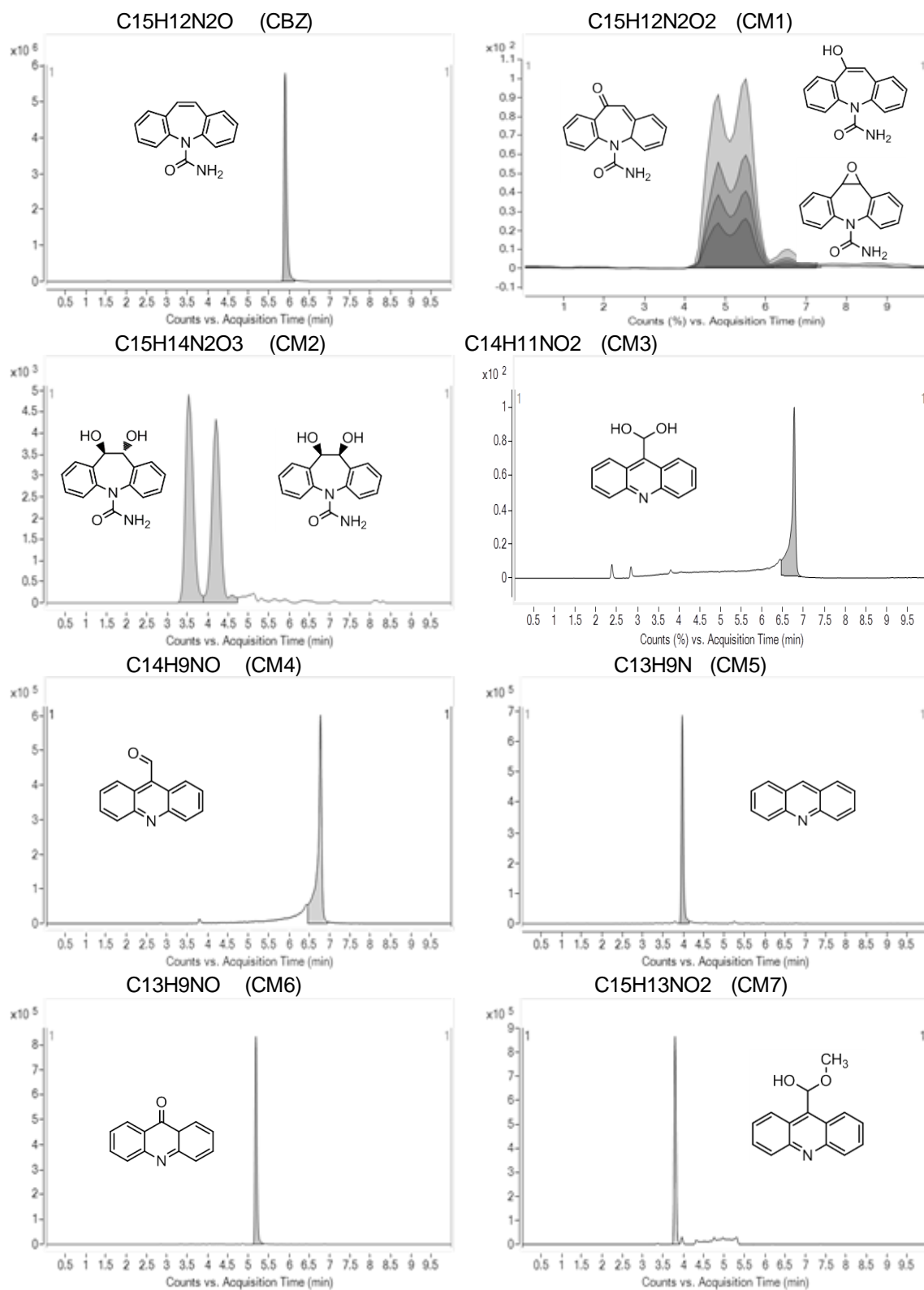


Figure 3.9 The chromatograms of CBZ and its metabolites.

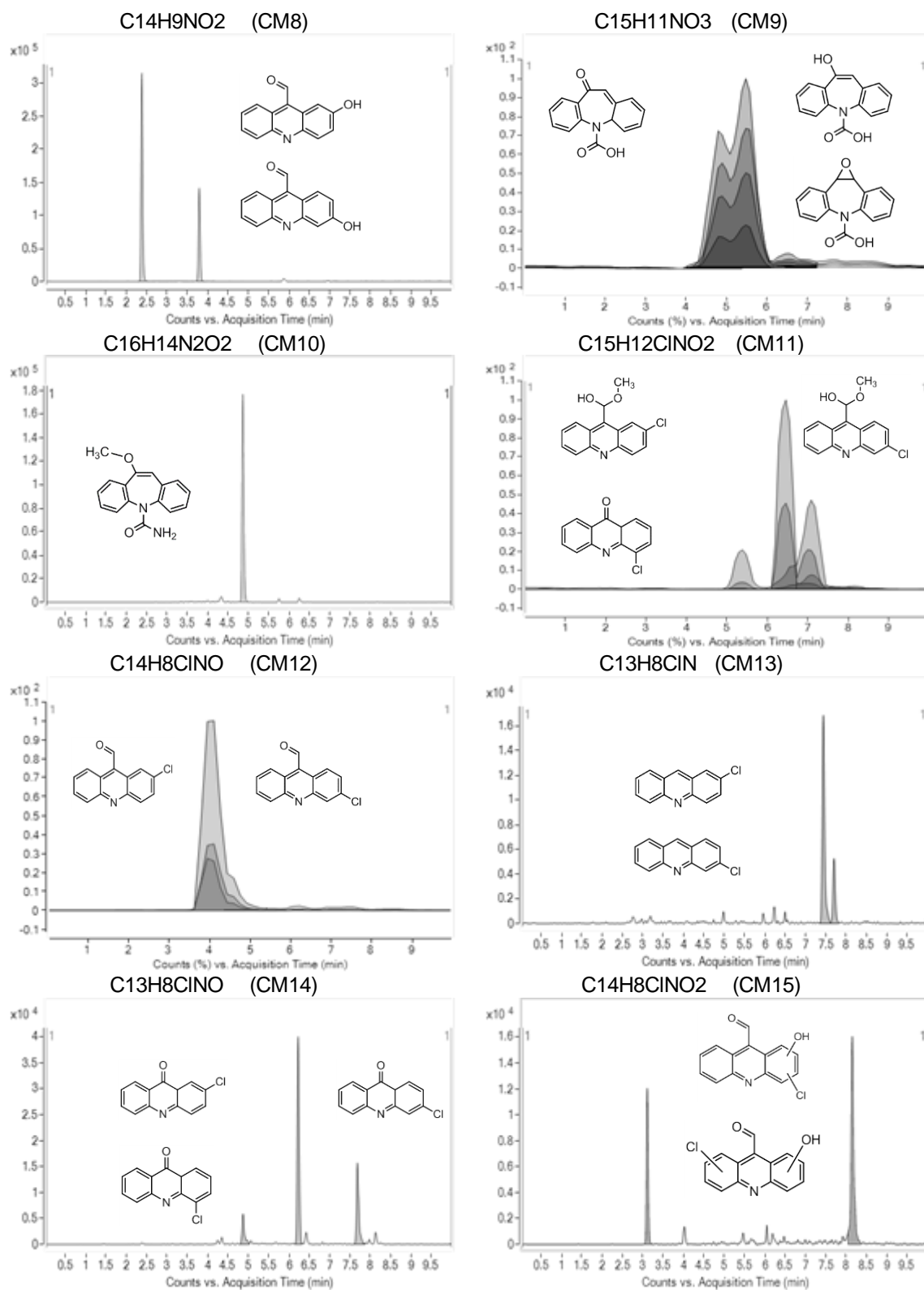


Figure 3.9 (Cont.) The chromatograms of CBZ and its metabolites.

The information of produced ions gave a better understanding of the structure of metabolites than the targeted MS/MS, it provided all the fragment information of parent compound to help to analyze, several same transitions could suggest the structural similarity. For example, CM4, CM5, and CM7 shared most of their product ions (Table 3.3).

Table 3.3 The optimizer data of CM4, CM5 and CM7.

Precursor ion	Precursor ion (m/z)	Shared product ions (m/z)	Independent product ions (m/z)
C ₁₄ H ₉ NO (CM4)	208	<i>180, 152, 128, 127, 77, 101, 51</i>	75, 102, 154,
C ₁₃ H ₉ N (CM5)	180		75, 102, 153, 140
C ₁₅ H ₁₃ NO ₂ (CM7)	240		208, 153, 154

The bold values were the mass of precursor ions. The italic values were estimated as the same fragments adducted with vary hydrogens.

The different elution times of the same formula was considered as isomers. In addition, the existence of isomers could also be suggested with distinctive product ions by the same fragmentor voltage at different retention time.

3.3.8 The proposed mechanism of degradation catalyzed by CPO

With all information above, the pathway for CBZ metabolism catalyzed by CPO was proposed (Fig 3.10.) The main pathway of degradation was to form the 10,11-epoxy carbamazepine (CM1), the C₁₀-C₁₁ bond was likely the most reactive site. The 10,11-dihydroxy carbamazepine (CM2) produced by addition of H₂O, with both trans and cis isomers. They were major transient intermediates further underwent cleavage of the carbamoyl moiety and rearrangement of heterocycles, from azepine ring to a pyridine structure, to form 9-acridine-

caboxaldehyde hydrate form (CM3). Hydroxyl group of CM3 was exchanged with methanol in phosphate buffer (pH 3.0), to generate methylated product CM7. Dehydration was the reaction happened at the same time, 9-acridine-caboxaldehyde (CM4) was generated. CM8 was hydroxylated from CM4. Both CM3 and CM4 were not observed on mass spectra, because they transferred to their product quickly at the beginning of reaction (Fig. 3.8). Acridine (CM5) was formed from CM4 by cleaving aldehyde group of CM4. Further, the derivatives of CM5 was generated as CM6' and CM6. CM6' was the hydroxylated product of CM5, hydroxylation was at 9 position due to its low electron density. The oxidized metabolite, acridone (CM6) was from CM6' by kept oxidizing at hydroxyl group and considered as more abundant than CM6' according to its stable structure.

The minor path way was from CM1'a, hydrolysis of the carbamoyl moiety, to form a carboxylic acid group CM9a, and further CM9a' underwent the oxidation to form CM9b. CM1'a was transformed from CM2 by losing water molecule, by exchanged the carbamoyl moiety, CM9a was also formed. Oxcarbazepine (CM1'b) was oxidation of CM1'a on the hydroxyl group, and CM1'b produced CM9b by the same way as CM1'a to CM9a. The methylation of hydroxyl group of CM1a generated CM10. CM11, CM12, CM13, CM14 and CM15 were the chlorinated metabolites from CM7, CM4, CM5, CM6, respectively.

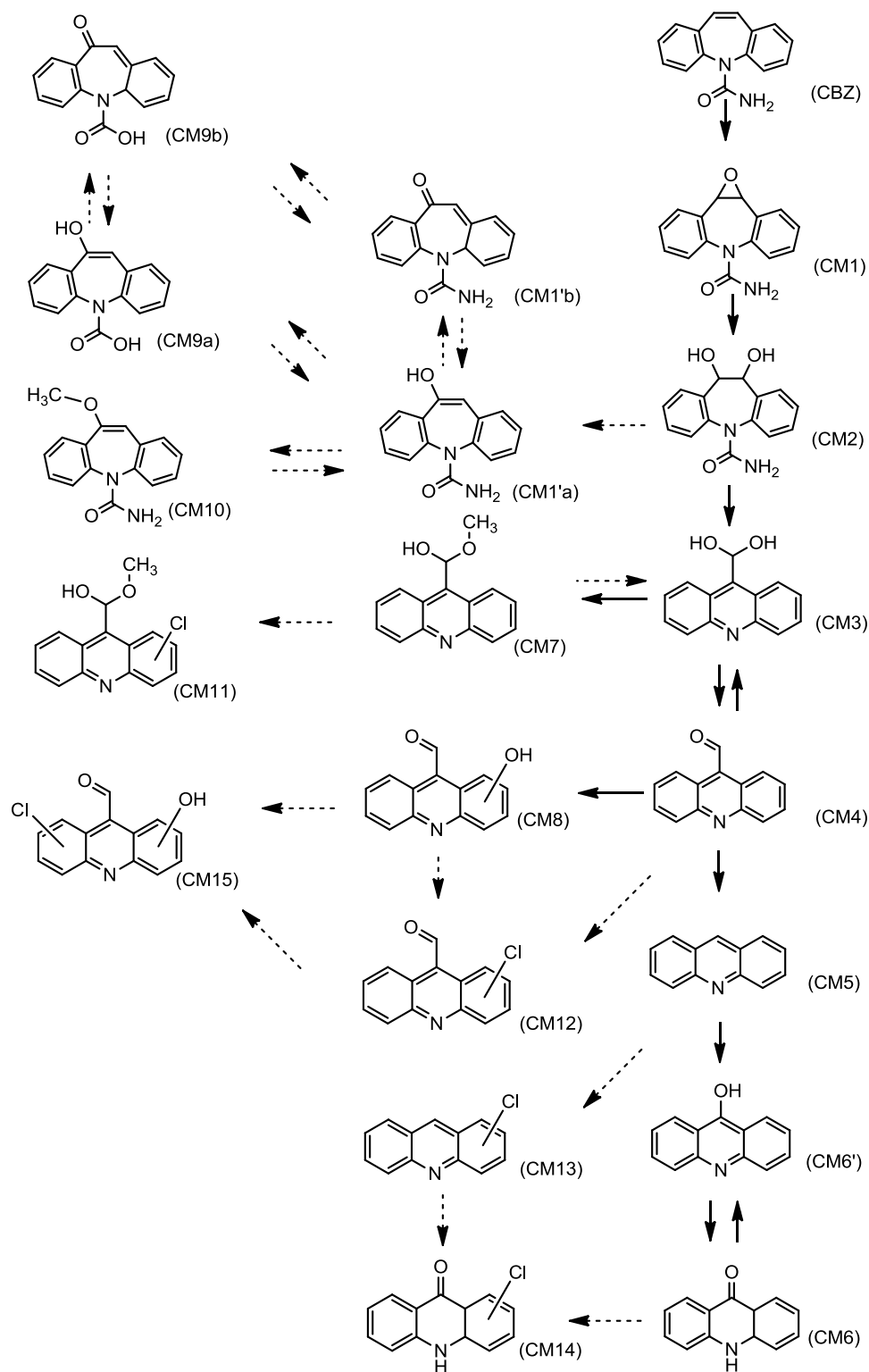


Figure 3.10 The proposed mechanism of the degradation of CBZ catalyzed by CPO.

3.4 Discussion

The process of CBZ degradation catalyzed by CPO was efficient, 100 % CBZ was depleted at the concentration from 2.5 mg to 14.8 mg/L for minutes, or $\geq 96\%$ with 16.5 mg/L for 4 minutes, all in nanomolar level CPO. The degradation rate and concentrations were conservative, removal ability are mostly likely more than parameters used in the experiment due to the LC samples were not monitored by shorter time period.

Compared with some biological treatment in water, such as white rot fungus, the efficiency of CPO-catalyzed reaction was dramatically improved. For example, it was reported that 57% to about 70% of CBZ was removed by *Trametes versicolor*, and 46% was degraded by *Ganoderma. Lucidum* for 7 days, at the original concentration of 10 mg/L (ppm). [58]

The UV treatment, the most efficient common water treatment in degrading CBZ, compared with ClO_2 oxidation and active sludge treatment. The UV radiation with 0.1 mg/L CBZ, could remove 93% of parent compound after 10 minutes. The concentration of CBZ was 0.1 mg/L in ClO_2 to remove 54% CBZ; in active sludge treatment with 0.2 mg/L CBZ, 16% of drug was removed. [62] For the other active sludge degradation experiment with 30 $\mu\text{g/L}$ CBZ, the removal of CBZ was not observed.[63] TiO_2/UV method could reach 74% CBZ conversion for 2 hours with TiO_2 at 100 mg/L.[59] The complete CBZ degradation (10mg/L) by Fenton-like oxidation was achieved at 2 mg/L iron for 1 hour, at 50 °C.[64] The new CBZ biodegradation was investigated by using freshwater microalgae for 10 days the percentage of degradation was 30%-37%, with initial CBZ

concentration at 1 mg/L (ppm). With the increased of CBZ concentration, the degradation rate was decreased.[57] Ozonation of CBZ was likely the rapidest degradation treatment to CBZ in drinking water treatment system by ppm level ozone.[65] However, to consider about the application in large scale environment, CPO showed the stronger degradation ability to high concentration of CBZ at simple conditions (low concentration of catalyst, easy operation and proper reaction time), which was a potential choice industrial wastewater treatment.

Most of CBZ metabolites generated by CPO-H₂O₂-Cl⁻ system were the same as products in the common water treatment and in environment.[58, 59, 62, 63, 66] The CPO-H₂O₂-Cl⁻ system could be used as the environmental model to learn the chlorinated and oxidized reaction of specific pollutants.

To consider the toxicity and the persistence of CBZ products, the possible environmental impact of metabolites should be emphasized. Although simple acridines were not carcinogens, acridine and its derivatives were suggestive of mutagenic activities.[67] Acridine and acridone showed more toxic than CBZ itself in different ecotoxicity assays.[53]

There are still abundant acridine, acridone, and their derivatives after degradation catalyzed by CPO. The acridine and acridone are more susceptible to biological treatments. CPO might be applied in active sludge or with other microorganism to digest the major metabolites. The UV treatment showed a outstanding removal of acridine and acridone. CPO catalyzed degradation could be coupled with UV-treatment to increase the degradation efficiency. The

investigation of improving the depletion of toxicologically relevant metabolites of CBZ, such as by coupling CPO catalyzed degradation with other treatment should be considered in the future experiments

CHAPTER IV.

CPO-CATALYZED DEGRADATION OF SULFAMETHAZINE

4.1 Background

Over 10,000 tons level of antibiotics are estimated to be used in the U.S.A per year. [68] Sulfonamide pharmaceutical substances are widely used in human and veterinary antibacterial treatments and they are frequently detected in wastewater and surface water with the active sulfonamide concentration detected as 20 mg/L.[69] Sulfamethazine or sulfadimidine (SMZ) belongs to heterocyclic sulfonamides, and the concentration of SMZ has been detected to 8.7 mg/kg in manure.[70] Nine sulfonamide antibiotics were detected in surface water with SMZ as the highest one with concentration of 78.3 ng/L, SMZ resistant bacteria was found in the sample.[8] The detection of SMZ resistant bacteria implied the extensive use of SMZ increased the risk of antibacterial resistance..

CPO showed its ability to degrade/ detoxicate drugs in our previous study, and the aim of this experiment was to investigate the potential application of CPO in degradation of antibiotics. To evaluate CPO-H₂O₂-Cl⁻ system, the reaction efficiency of CPO in the degradation of SMZ would be investigated and the structures of metabolites and degradation pathway would be proposed.

4.2 Experimental Procedure

4.2.1 Material

All material and chemicals used were the same as described in section 2.2.1.

4.2.2 UV-Visible spectrophotometry

A VARIAN UV-Vis spectrophotometer (Cary 200 Bio) was used to collect the

UV spectra of the degradation products. SMZ was dissolved in methanol to make 3.59 mM stock solution. The drug solution was scanned by dissolving 0.06 mM SMZ in 100 mM KH_2PO_4 buffer with 20 mM KCl at pH 2.75, mixed with 0.06 mM H_2O_2 . UV spectra were recorded after the addition of 5 nM CPO for 1 minute, 2.5 minutes and 4 minutes.

4.2.3 Liquid chromatography and mass spectrometry

4.2.3.1 Sample preparation

To investigate the degradation efficiency, SMZ was dissolved in methanol to make a stock solution (3.59 mM), 62.45 μM (17.38 mg) of SMZ was mixed with 1.3 nM CPO for 30 minutes at room temperature. H_2O_2 stock solution (41.16 mM) was added to reaction system at 56.5 $\mu\text{L}/\text{minute}$ to make the final concentration of H_2O_2 achieved 314 μM . Mixture was centrifuged at 3,000 g in Centriprep[®] centrifugal filter unit with a 30,000 Dalton cut-off membrane (EMD Millipore, Billerica, MA, USA). The filtrate was collect after centrifuged for 1 min. Ethyl acetate was used to extract the filtrate while shaking vigorously. The get rid of the organic solvent, The supernatant was evaporated to dryness. The dried residues were dissolved in H_2O /methanol (95:5 v/v) to make the final concentration approximate 1 mg/L (ppm). Sample was stored at -20 °C in a freezer or immediately detected by LC-Q-TOF-MS mass spectrometer system.

To detect all metabolites of SMZ, the same experiment above was carried out (3.59 mM SMZ, 314 μM H_2O_2 and 1.3 nM) for 1.5 hour, extracted directly by ethyl acetate. And nitrogen gas purge was used to get sample dried. The dried metabolites were dissolved in 2.0 mL H_2O /methanol (95:5 v/v) to make the final

concentration approximate 5 mg/L (ppm). Centrifuge the sample with 1200g for 10 minutes, 1.5 mL supernatant was removed by syringe. Filtration was applied by using 0.22 μ M polyethersulfone syringe filter. The sample was stored at -20 °C in a freezer and detected both in LC-Q-TOF-MS.

To investigate the mechanism of degradation in CPO-H₂O₂-Cl⁻ system, the sample reacted with low concentration of H₂O₂ was prepared. 6.86 μ M H₂O₂ was added directly to Centriprep[®] centrifugal filter unit (30,000 Dalton cut-off) with 35.90 μ M SMZ, catalyzed by 1.3 nM CPO in the 100 mM phosphate buffer with 20 mM KCl for 1 minute, 3 minutes and 5 minutes, filter units were centrifuged at 3000g for 1min at room temperature, and extracted the filtrate by ethyl acetate, purged the organic phase with nitrogen gas to dryness. The dried metabolites were dissolved in H₂O/methanol (95:5 v/v) to make the final concentration approximate 1 mg/L (ppm), and detected by LC-Q-TOF-MS system immediately. Experiments ran in triplicate.

To investigate the brominated products, the reaction was also carried out in the buffer contained KBr instead of KCl, 62.45 μ M SMZ, 2 mM H₂O₂, catalyzed by 2 nM CPO for 30 minutes. After extraction and purge procedure, the final concentration dissolved in the H₂O/methanol (95:5 v/v) was approximate 1 mg/L (ppm).

4.2.3.2 Instrumentation and chromatographic separation

Instrumentation and chromatographic separation were the same as in section 2.2.3.2. without the application of Triple-Quadrupole LC/MS/MS mass spectrometry.

4.2.3.3. Data Mining and Database development

The data Mining and Database development were the same as in section 2.2.3.3 without the application of FIA.

4.3 Result and discussion

4.3.1 UV-Vis study of CPO-catalyzed degradation of carbamazepine

UV-Vis Spectra of SMZ (0.06 mM) and H₂O₂ (0.06 mM) were scanned in 100 mM KH₂PO₄ buffer with 20 mM KCl at pH 2.75 (Fig.4.1). The Spectrum of SMZ showed the absorption at 241 nm, 263 nm and 306 nm. 1 minute after addition of 5 nM CPO, the 241 nm absorption increased, and stopped increasing at 2.5 minutes, the 263 nm peak kept decreasing. And the wavelength at 306 nm increased from 1minute to 2.5 minutes. The UV spectrum at 4 minutes was monitored, the line was the same as the wavelength at 2.5 minutes. H₂O₂ was added to the mixture solution, to make the total concentration of H₂O₂ increase to 0.30 mM, after 1 minute, the 241 nm peak decreased and a strong absorption was observed at 273 nm (Fig. 4.1). There was no wavelength could be used to measure kinetic parameter of SMZ degradation catalyzed by CPO.

The same reaction was carried out under the same condition except for the chlorine ion (KCl) in phosphate buffer. Without KCl, the absorbance did not change after the addition of CPO. Chlorine ion is imperative in the degradation of SMZ in CPO-H₂O₂-Cl⁻ system.

4.3.2.1 CPO-H₂O₂-Cl⁻ system

To investigate the degradation efficiency of SMZ in CPO-H₂O₂-Cl⁻ system, 62.45 μM SMZ was reacted with 314 μM of H₂O₂ and CPO (1.3 nM) for 30

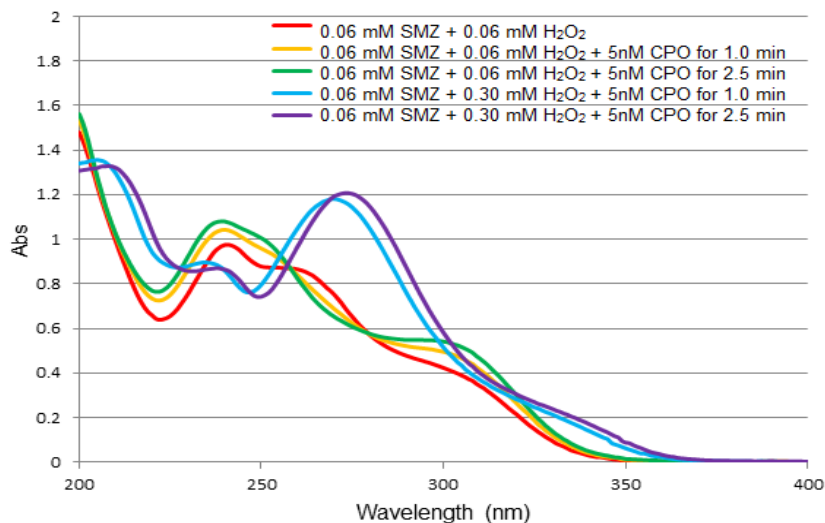


Figure 4.1 UV spectrum of SMZ degradation catalyzed by CPO

minutes, the sample was detected by LC-Q-TOF-MS, SMZ was not observed, the

4.3.2 LC-Q-TOF- MS

Degradation efficiency by nanomolar level of CPO could achieved 100%, suggesting the potential of the application of CPO in large-scale waste water treatment.

Samples were detected in Agilent Technologies 6530 Accurate-Mass LC-Q-TOF-MS in full scan MS mode, the accurate mass data of the molecular ions were processed through the Agilent MassHunter Qualitative Analysis software. To detected all metabolites, samples were concentrated 5 folds, there were 8 SMZ metabolites (coded from SM1 to SM8) confirmed by different retention times and accurate mass-to-charge ratios (m/z). SM9 was detected only in the reaction with limited H_2O_2 within 5 minutes as an intermediate product. The elemental formula, retention time, the relative mass difference between the observed mass and the mass of the target compound (in parts per million), and the difference

between the observed mass and the mass of target compound (in milliDaltons) were collected (Table 4.1).

Table 4.1 Accurate-Mass QTOF-LC/MS data for the identification of SMZ and its metabolites catalyzed in CPO-H₂O₂-Cl⁻ system.

Code	Formula	Retention time (min)	Experimental mass (m/z)	Theoretical mass (m/z)	Diff (ppm)	Diff (mDa)
SMZ	C ₁₂ H ₁₄ N ₄ O ₂ S	4.245	278.0832	278.0837	-1.93	-0.54
SM1	C ₁₂ H ₁₄ N ₄	3.219	214.1211	214.1218	-3.27	-0.70
SM2	C ₁₂ H ₁₃ ClN ₄	4.106	248.0829	248.0829	0.00	0.00
SM3	C ₁₂ H ₁₂ Cl ₂ N ₄	7.295	282.0440	282.0439	0.23	0.07
SM4	C ₁₂ H ₁₁ Cl ₃ N ₄	7.400	316.0044	316.0049	-1.71	-0.54
SM5	C ₁₂ H ₁₃ ClN ₄ O ₂ S	4.894	312.0447	312.0448	-0.13	-0.04
SM6	C ₁₂ H ₁₂ Cl ₂ N ₄ O ₂ S	5.414	346.0054	346.0058	-1.04	-0.36
SM7	C ₁₂ H ₁₃ ClN ₄ O ₃ S	2.980	328.0398	328.0397	0.25	0.08
SM8	C ₁₂ H ₁₁ Cl ₃ N ₄ O ₂ S	7.267	379.9668	379.9668	-0.16	-0.06
SM9	C ₁₂ H ₁₄ N ₄ O ₃ S	1.020	294.0790	294.0787	1.17	0.34

All the relative mass difference of the standard drug (SMZ) and metabolites were less than 4.0 ppm. The mass differences of all compounds were less than 1.0 mDa. This method was proved to be efficient for determination of the metabolites of SMZ.

The mass spectra of each individual metabolite were collected in positive mode by MassHunter Workstation software (Appendix I). Since it was in positive mode, all the compounds were detected as molecular ion [M + H]⁺. SM7 and SM9 were detected as molecular ion [M + Na]⁺ adduct (351.0287 m/z and 317.0677 m/z, respectively), the sodium adduct formation was favored in the ion source probable due to the ion pairing effect on the functional group responsible of ionization.

For chlorinated metabolites with one chlorine atom in compound (SM2, SM5 and SM7), the isotope peaks were detected as the conformation of addition of

chlorine atom, the two major peaks of each spectrum separated by 2 m/z units and peak heights are in the ratio of 3:1, proved these molecules contain one chlorine atom. For SM3 and SM6, there were 3 lines in the molecular ion region (M^+ , $M+2$ and $M+4$) with gaps of 2 m/z units between them, and with peak heights in the ratio of 9:6:1, it was confirmed that both compounds contain 2 chlorines. For SM4 and SM8, compounds had the pattern 27:27:9:1.[71]

The structures of each metabolite were confirmed in targeted MS/MS by retention time and fragment ions (Fig. 4.2). There were 2 types of metabolites based on their structures. The first type products were SO_2 extrusion structures. (SM1, SM2, SM3 and SM4). SM1 was the product lost the sulfonyl group of SMZ, SM2, SM3 and SM4 were the chlorinated metabolites of SM1. The other structures were directly chlorination of SMZ (SM5, SM6 and SM8), and the hydroxylation product of SM5 was SM7. SM9 was the metabolic intermediate of SM7, the hydroxylated product of SMZ, it could only be detected at the beginning of the reaction.

The concentrations of all metabolites were measured as compound area by MassHunter Workstation software, and presented by percentage of all compounds as pie chart, percentage less than 1% were showed in the second pie chart at right side (Fig. 4.3)

To investigate the mechanism of degradation process, a experiment was carried out for limited reaction time (1,3 and 5 minutes) with low concentration of H_2O_2 (6.86 μM), the ratio of the concentration of drug and H_2O_2 was about 5:1. Only part of SMZ was degraded, and 3 metabolites were detected which could

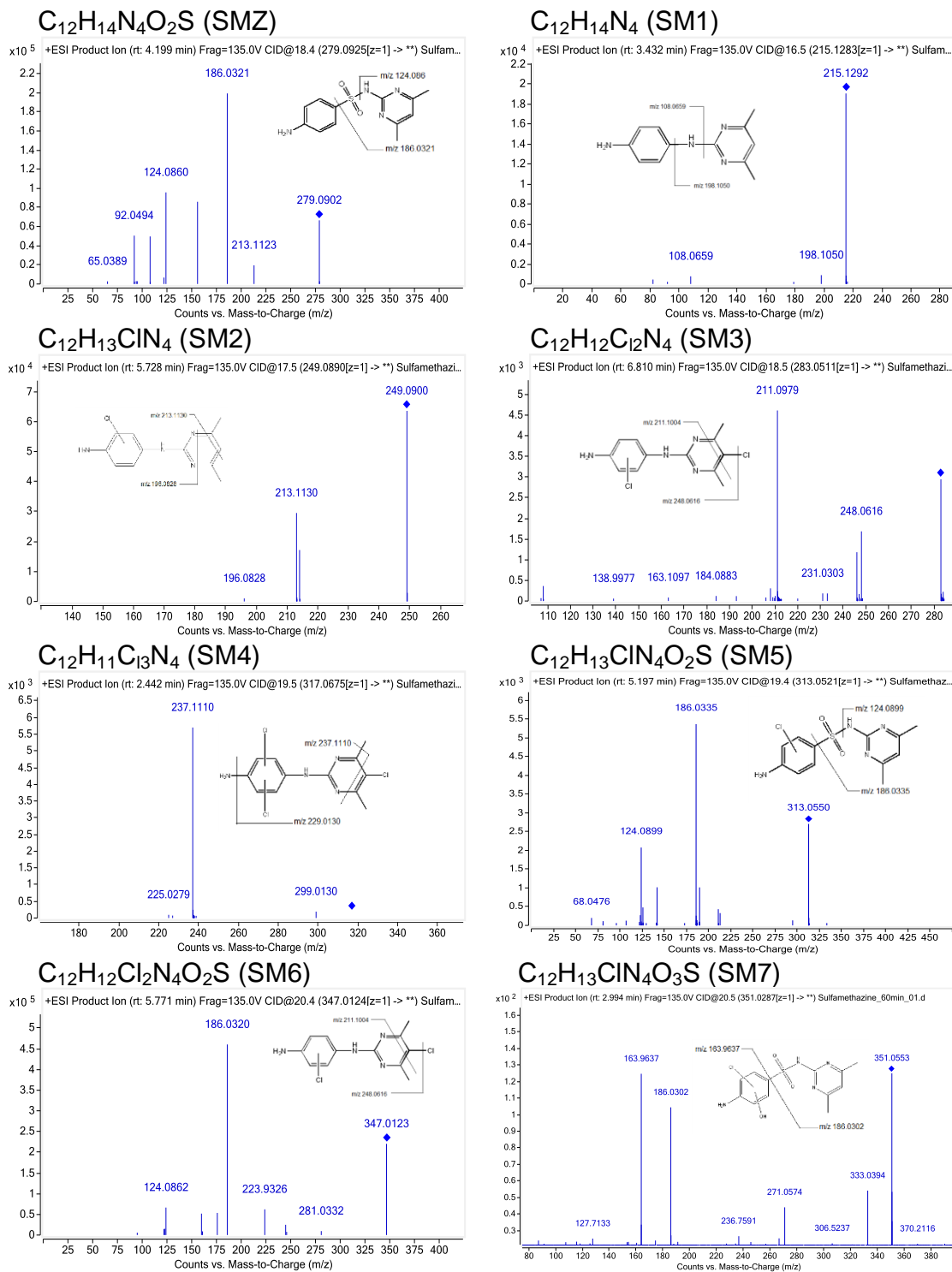


Figure 4.2 The targeted MS/MS spectra of APAP and its metabolites.

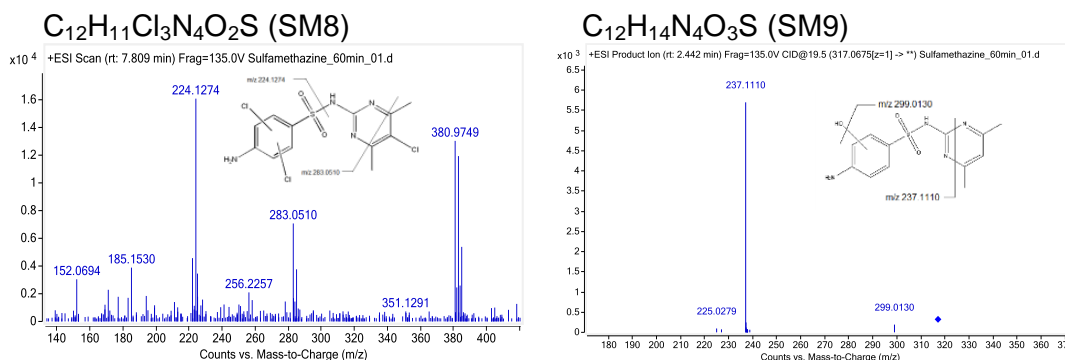


Figure 4.2 (cont.) The targeted MS/MS spectra of APAP and its metabolites.

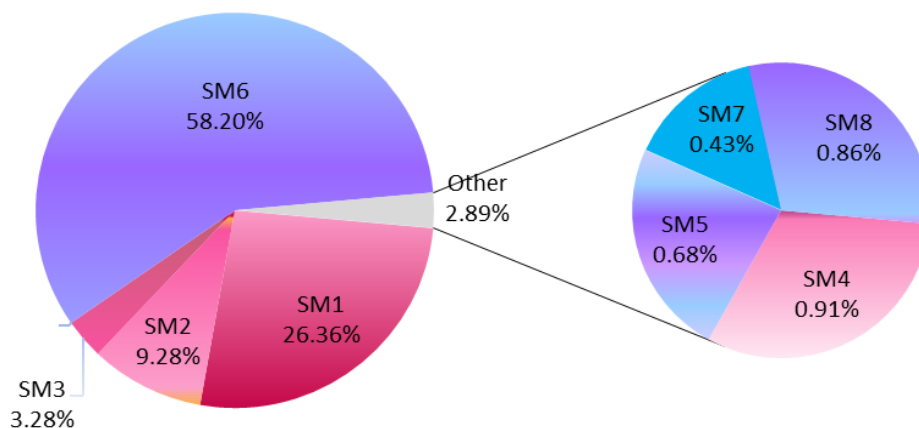


Figure 4.3 The percentage of each metabolites measured by compound area. Metabolites shared the same structure presented by the same color (pink color represent the desulfonated structure, purple represent the SMZ-based group and blue presents the hydroxylated group).

be

suggested as the first formed metabolites (Fig 4.4). SM1 was the most abundant metabolite within 5 minutes, and SM5, SM9 generated at the same time in lower amounts, suggested that the first step of degradation was the oxidation, chlorination and the loss of sulfonyl group, SM1 formed preferentially.

The area of SM1 kept stable at first 3 minutes and showed decreased tendency at 5 minutes, it might due to the transformation of SM1 to chlorinated metabolites which under the limit of detection. The percentage of SM1 was 26.35% in the reaction with higher concentration of H₂O₂ for longer reaction time,

whereas SM6 was the primary product finally, suggested that the desulfonylation reaction was predominant at the first reaction stage, and then the rate of chlorination significantly increased.

SM5 had the increased tendency from 1 minute to 5 minute, the finally concentration of SM5 was low but its chlorinated product SM6 was the major metabolites, SM5 was suggested as the major intermediate metabolite. SM9 was not observed after reaction with high concentration H_2O_2 for 30 minutes, but its chlorinated product was detected as 0.43% of all metabolites, it was suggested that hydroxylated metabolites were the byproducts in the reaction. Chlorination and desulfonylation were the major reactions, hydroxylation was the minor reaction. (Fig.4.3).

For desulfonylated metabolite SM1 and its chlorinated products SM2, SM3 and SM4, the total concentration of them was 39.83% and the 3 chlorine atom addition structure (SM4) was only 0.91%. Chlorination of the desulfonylated structure by 3 chlorine atoms was not favored in the reaction which may be due to the structure of CPO binding pocket and the polarity in the pocket. The same limitation of chlorine atoms addition also applied in SMZ based structure, the total concentration of them was 60.17%, SM8 (0.86%) were the minor product of the degradation catalyzed by CPO. Two chlorine atoms were preferentially inserted to SMZ molecule (SM6, 58.20%) in contrast to the three chlorine atoms addition. (Fig 4.4)

The chromatograms of SMZ and its metabolites were collected with their proposed structures (Fig. 4.5). In the chromatograms of SM2, SM3, SM4, SM5,

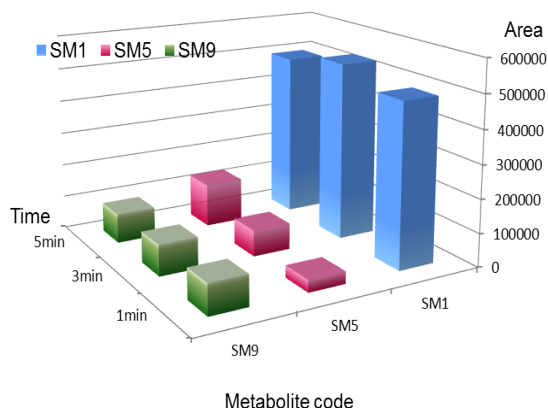


Figure 4.4 The area of metabolites with limited H₂O₂ at 1 minute, 3 minutes and 5 minutes detected by Accurate-Mass LC-Q-TOF-MS. All experiments were duplicates and data reported were mean values of two independent measurements.

SM7, SM8 and SM9, there were isomers identified by different retention times.

The extrusion of SO₂ structure (SM1) was reported previously with structural rearrangement. There were two structures proposed for SM1 (Table 4.2). One is N1-(4,6-dimethylpyrimidin-2-yl)benzene-1 (a), 4-diamine, another is 4-(2-imino-4,6-dimethylpyrimidin-1(2H)-yl)aniline (b). Proposed structures were presented by form (a) in all the spectra and chromatograms, form (a) was probably the actual structure of metabolite in the reaction catalyzed by CPO because of its less rearrangement than form

(b). SM2-SM4 were the chlorinated products of SM1. In SM2, there were 5 isomers according to the 5 different retention times. The two major isomers were chlorinated on

Table 4.2 Possible identities of C₁₂H₁₄N₄ (SM1).

Structure	Reference
<p>(a)</p>	[72-75]
<p>(b)</p>	[75-80]

position 1 and 2 because of the high electron density of aniline group and the metabolite chlorinated at position 1 (Fig. 4.5) was assumed as the most abundant product because of its electron density, $-NH_2$ group on benzene ring was an electron donating group (EDG), whereas sulfonyl group was electron withdrawing group. Other isomers were also suggested first be chlorinated or hydroxylated on the aniline group at the carbon atoms which located close to amine.

SM5 had 5 different chlorinated sites which corresponded to 5 different retention time, major metabolites were chlorinated at position 1,2 and 3, the 3rd position was on the dimethylpyrimidine group (Fig 4.5). The other two were proposed to assign to the two amine groups. SM6 only showed one retention time, there was one structure was stable, other structures may exist but with the amount under the limit of detection. The chlorine atoms probably added to the aniline group near primary amine due to the high electron density and it was a typical chlorination catalyzed by CPO.[39] SM8 was the byproduct with one more chlorine atom addition based on SM7, the two retention times suggested 2 isomer structures, one additional chloride sites were on the aniline group near $-NH_2$ or on the dimethylpyrimidine.

SM7 and SM9 were the hydroxylated products of SMZ, although in TiO_2/UV method, the pyrimidinyl moiety of SMZ was suggested to be hydroxylated, in CPO reaction, phenyl portion were proposed to be hydroxylated according to the MSMS spectrum. [81] The hydroxylation of aromatic amine in SMZ was also reported in the biodegradation catalyzed by white rot fungus.[72] However,

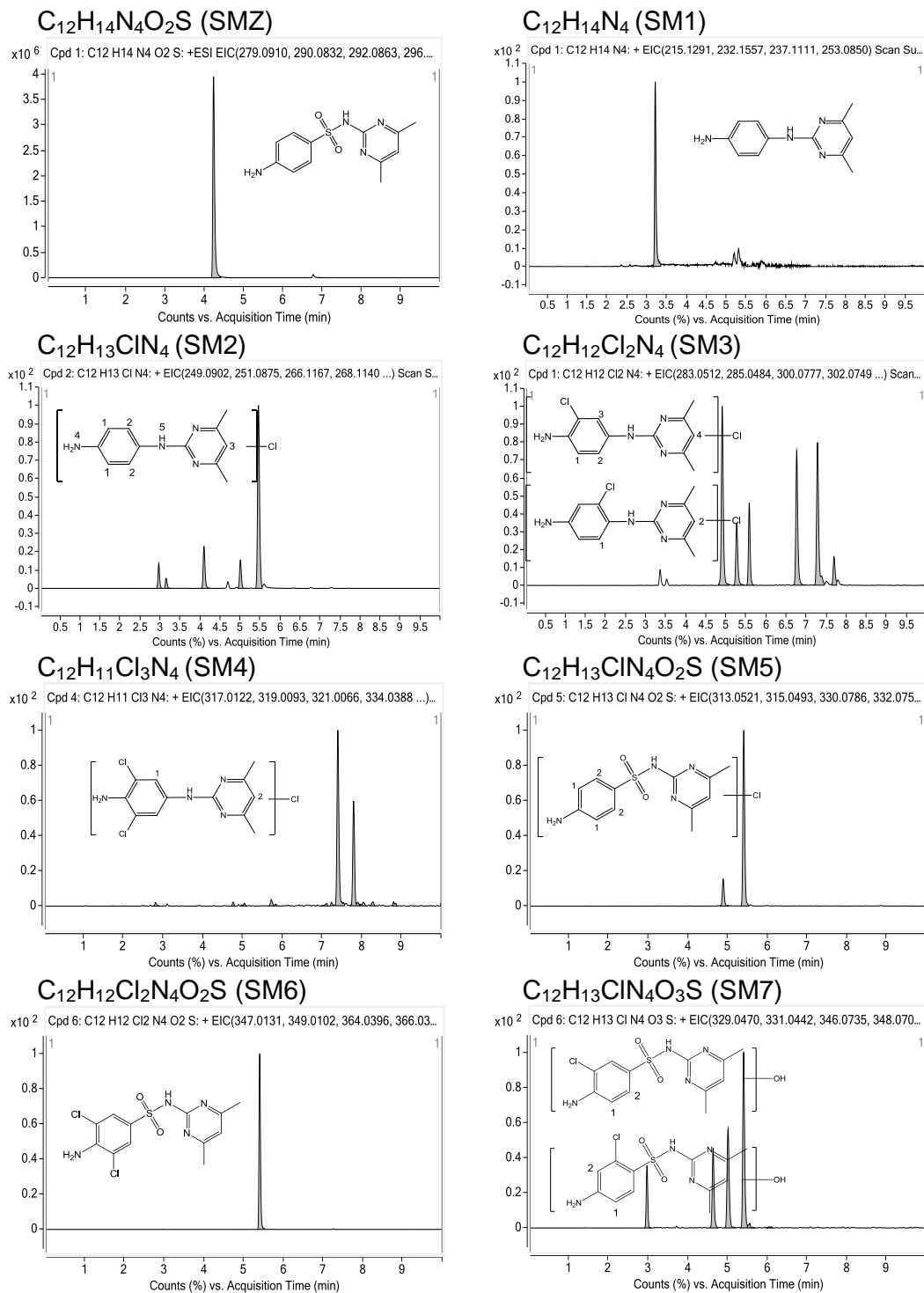


Figure 4.5. The chromatograms of CBZ and its metabolites.

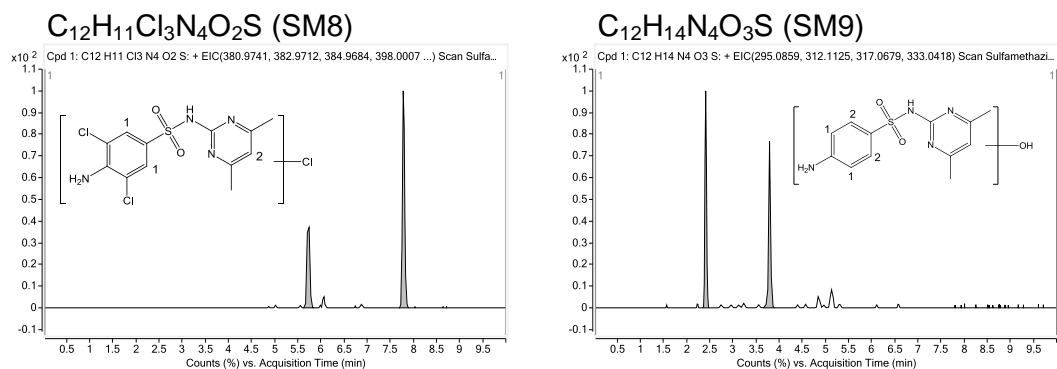


Figure 4.5. (cont.) The chromatograms of CBZ and its metabolites.

according to CPO chlorination preference, the hydroxylation was recommended mainly at phenyl portion.

The mechanism of degradation catalyzed by CPO was proposed considering all information above, the pathway for SMZ metabolism catalyzed by CPO was proposed, each metabolite showed by one of its proposed chemical structures instead of all isomers. For CPO-H₂O₂-Cl⁻ system (Fig 4.6), the chlorinated steps with one and two chlorine atoms addition and desulfonylation of SMZ were the major pathways. The minor path way was hydroxylation and chlorination with three chlorine atoms.

4.3.2.2 CPO-H₂O₂-Br⁻ system

To investigate the halogenation of SMZ catalyzed by CPO, 20 mM KBr was applied in the buffer instead of KCl, the CPO-H₂O₂-Br⁻ system reaction was carried out at the room temperature, and the product spectrum was obtained (Appendix I) There were only 3 metabolites detected. All of them were brominated products. (Table 4.3) [71] There were two peaks (357.0027 m/z and

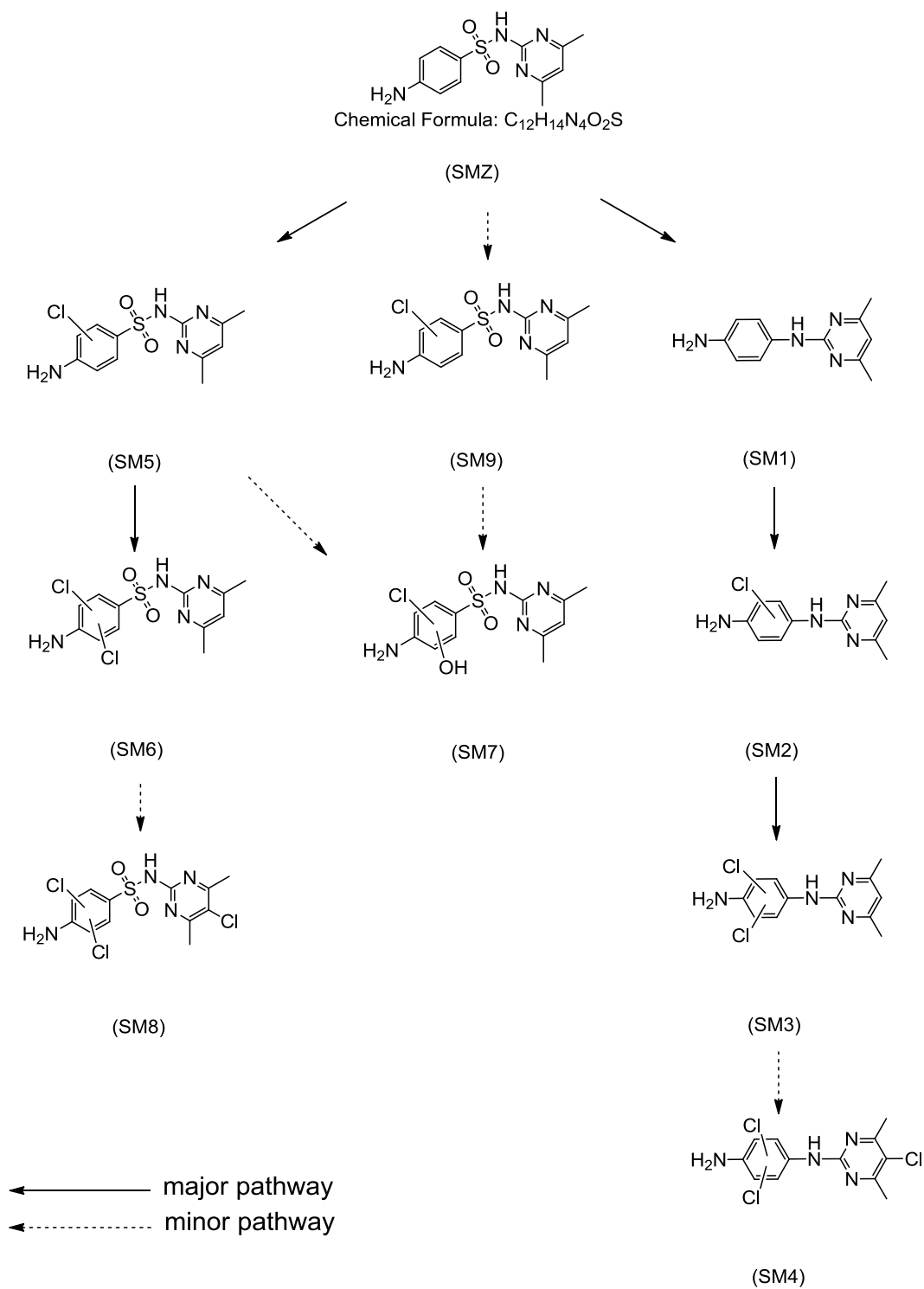


Figure 4.6. The proposed mechanism of the degradation of SMZ catalyzed by CPO-H₂O₂-Cl-system presented by primary structure of each metabolite.

Table 4.3 Accurate-Mass LC-Q-TOF-MS data for the identification of SMZ and its metabolites catalyzed in CPO-H₂O₂-Br⁻ system.

Code	Formula	Retention time (min)	Experimental mass (m/z)	Theoretical mass (m/z)	Diff (ppm)	Diff (mDa)
SM5-Br	C ₁₂ H ₁₃ BrN ₄ O ₂ S	5.390	355.9948	355.9943	1.65	0.59
SM6-Br	C ₁₂ H ₁₂ Br ₂ N ₄ O ₂ S	6.095	433.9042	433.9048	-1.28	-0.55
SM8-Br	C ₁₂ H ₁₁ Br ₃ N ₄ O ₂ S	8.258	511.8144	511.8153	-1.66	-0.85

368.9995 m/z) in approximately 1:1 ratio in the mass spectrum of SM5-Br, confirming compound contained 1 bromine atom. For SM6-Br, there were three peaks (434.9117 m/z, 436.9090 m/z and 438.9074) in 1:2:1 ratio, suggested 2 bromines addition to the parent compound. The ratios of 3 bromine atoms contained molecule are 1:3:3:1, which was observed in the mass spectrum of SM8-Br, suggested the number of bromine in this metabolite.

In the CPO-H₂O₂-Br⁻ system, neither the loss of sulfonyl group, nor the

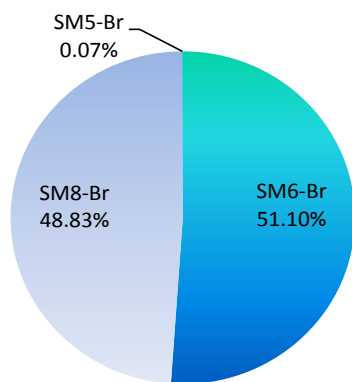


Figure 4.7 The percentage of the three metabolites measured by compound area (catalyzed by CPO-H₂O₂-Br⁻ system).

hydroxylation was observed (Fig 4.7). Compared with the chlorination of SMZ, bromination was favorable to form the product with 3 halogen atoms addition (48.83%).

Halogenation, hydroxylation and desulfonylation were suggested as competitive reactions in the SMZ degradation catalyzed by CPO. When buffer contained bromide, with competitive pathway was predominantly changed to halogenation. This

result was consistent with our previous result that the rate of halogenation in the presence of bromide was higher than chloride.[28]

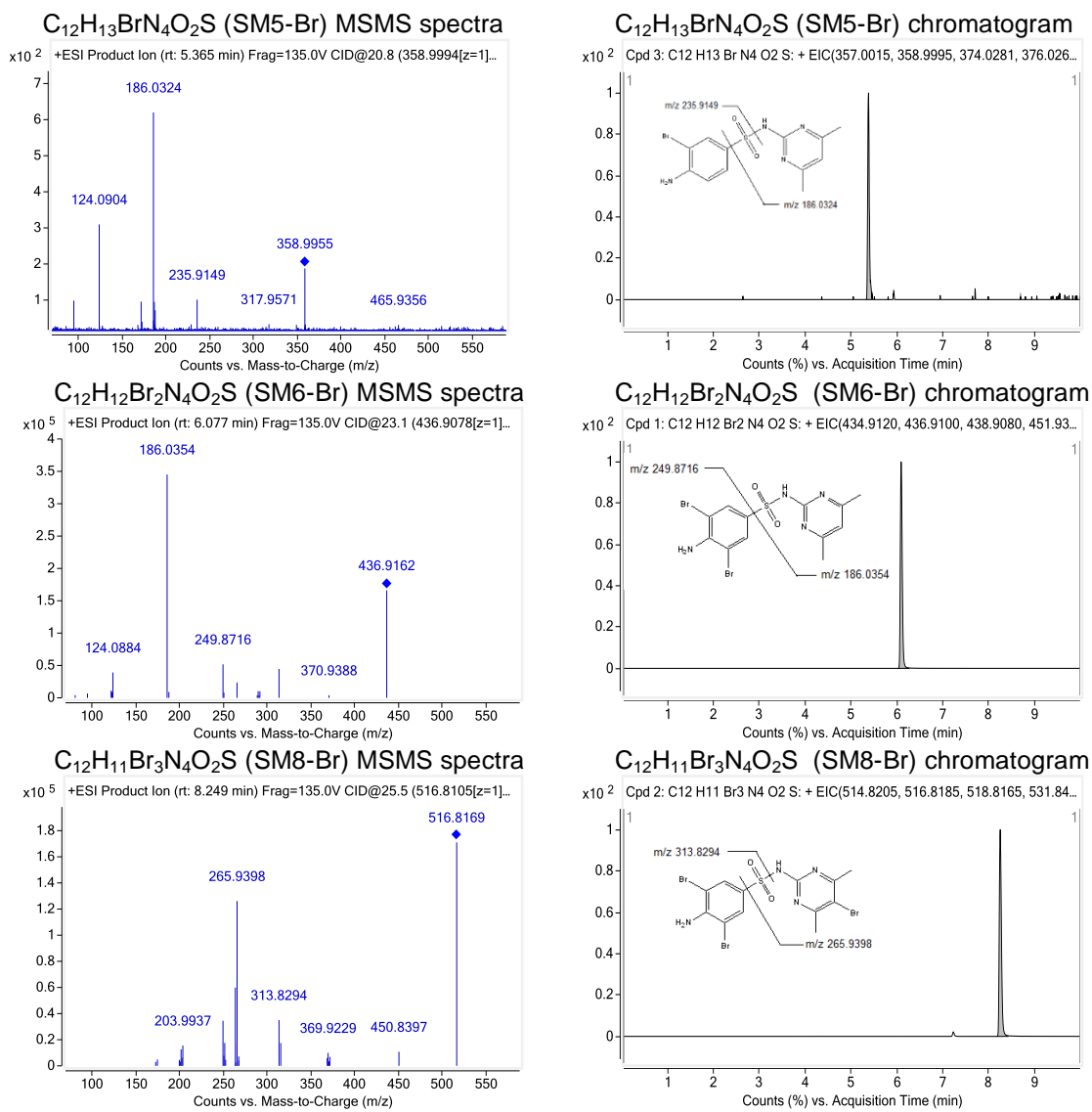


Figure 4.8 The mass spectra and chromatograms of SMZ brominated metabolites.

The structures were confirmed by targeted MSMS, and the chromatograms of each metabolite were collected. (Fig 4.8).

There was only one peak in each chromatogram, demonstrated that there was no isomer of brominated product. Bromination showed higher halogenated selectivity in the SMZ, it was presumably due to the formation of Br_2 during the CPO catalyzaion. The halogenation might occur in the solution or the wide

channel of CPO, reacted with the free bromine. This assumption also consistent with the only one retention time of SM6, Cl_2 might release and reacted with SMZ directly by two chlorinated sites. It was suggested that HClO formed in the catalyzation to chlorinate substrate, however in chlorination of SMZ by hypochlorite, the product was only reported as SM5, HClO would not be the only crucial intermediate involved in the chlorination.[82]

For $\text{CPO-H}_2\text{O}_2\text{-Br}^-$ system, there was only one pathway to elucidate the mechanism of SMZ halogenation. (Figure 4.9)

4.4 Discussion

The process of SMZ degradation catalyzed by CPO was efficient, 100 % SMZ was depleted at the concentration from 17.38 mg/L for minutes by the

nanomolar level CPO. The degradation rate and substrate concentrations were conservative, removal ability are mostly likely more than parameters used in the experiment due to the LC samples were not monitored by shorter time period.

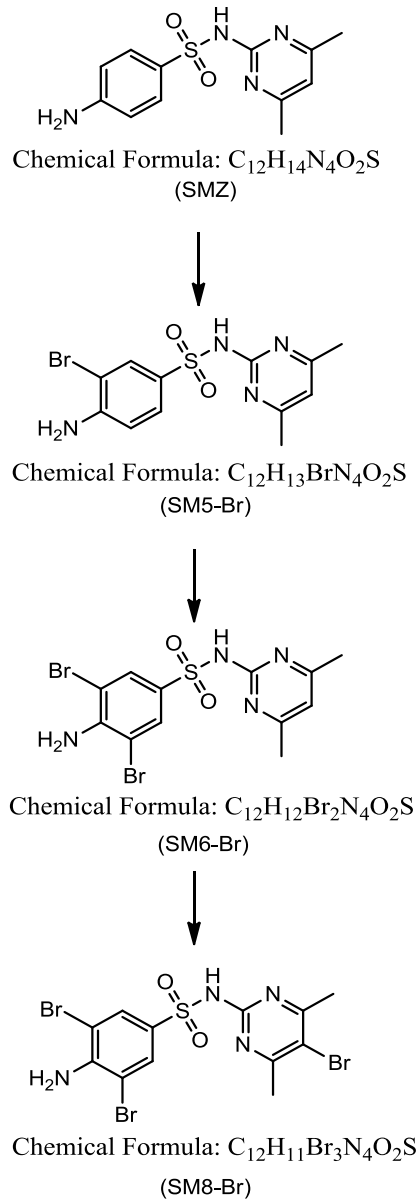


Figure 4.9. The mechanism of SMZ bromination catalyzed by CPO

The major metabolite in environment was N⁴-acetyl-sulfamethazine. The desulfonylated products generated by CPO-H₂O₂-Cl⁻ system are more susceptible to future biological degradation.[70]

Compared with some biodegradation treatment in water, such as white rot fungus, the efficiency of CPO-catalyzed reaction was dramatically improved. For example, it was reported 9 mg/L SMZ was removed by *Trametes versicolor* for 20 hours.[72] The 62%±4% SMZ was removed within 8 minutes when 36 μM SMZ reacted with 360 μM MnO₂. [8]

It was reported that in different types of treatments (photolysis, UV/H₂O₂, UV/persulfate and persulfate oxidation) with 20 μM SMZ for 45 minutes, the removal rate of SMZ achieved 15.1% to 96.5%. The UV/H₂O₂ achieved 87.5%, the most effective method was UV/persulfate, however this reaction required 200 μM sulfate to accomplish 96.5% degradation, 500 μM sulfate to accomplish 100% degradation. As it stated by the author, the persulfate addition may cause environmental problem.[79]

The degradation of SMZ was not significantly observed after 8 hours when treated by sodium hypochlorite, and used more than one month to degrade substrate.[83]

CPO catalyzed degradation has the potential to apply in large scale wastewater treatment considering about the nanomolar level enzyme and the rapid sample preparation.

The oxidation and chlorination products of SMZ generated in CPO-H₂O₂-Cl⁻ system could be found in most of the water chlorination treatment and

biodegradation process.[72, 75, 83] CPO-H₂O₂-Cl⁻ system might be used as the environmental model to learn the chlorinated and oxidized reaction of specific pollutants.

CHAPTER V.

ENGINEERING THE HYDROGEN BOND OF CPO BY MUTANT H105R

5.1 Introduction

Glutamic acid 183 (Glu 183) of CPO located closely to the heme iron in the distal pocket, suggested its function to in the cleavage of the peroxide O-O bond. [20] It is an important acid-base catalyst in the formation of compound I. In a mutagenesis study, Glu 183 was replaced by histidine residue, the mutant's chlorination and dismutation activity were decreased to 15% and 50%, respectively.[23] The result implied that the Glu 183 affects predominately

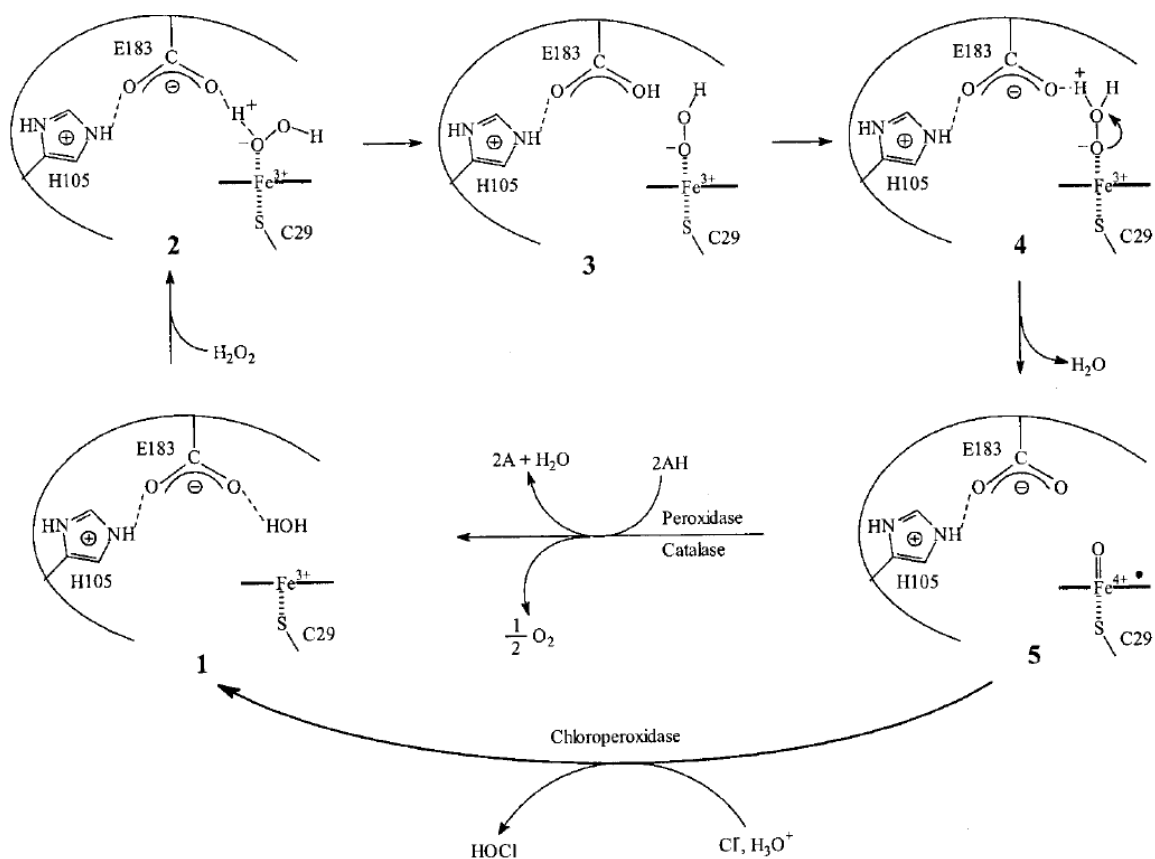


Figure 5.1 The Proposed mechanism of His 105 in the cleavage of the peroxide O-O bond.

chlorination activity, but not essential for it. The hydrogen bond linked to 183 and the distal pocket structure might affect the enzyme activity, mutant E183H could still form hydrogen bond with histidine 105(His 105) to facilitate the cleavage of peroxide O-O bond.

His 105 was located in the heme distal pocket, formed hydrogen bond with glutamic acid 183. His 105 is 3.5 Å from the propionate carboxyl group, it might be critical in peroxide O-O cleavage by forming a hydrogen bond with Glu183 which position the carboxyl group toward the heme iron. The hydrogen bond between H105 and E183 was suggested to play an essential role in modulating the chlorination activity. (Fig. 5.1) [1, 21] When H105 was replaced by a small and nonpolar amino acid alanine (H105A) to decrease the polarity and destroyed chlorination decreased. [85]

To investigate the function of the hydrogen bond between histidine and glutamic acid, mutant H105R was created by changing histidine 105 to arginine to increase the hydrogen bonding strength.

5.2 Experimental Procedure

5.2.1 Materials

A filamentous fungus *Aspergillus niger* (A. niger, MGG029) were purchased from American Type Culture Collection (Manassas, VA). Gene expression vector pCPO3.I-Amds which is coding for WT CPO and co-transformation plasmid pAB4.1 with *PyrG* selection marker (GenBank accession no. AJ300448) were obtained TNO Microbiology and Systems Biology, Netherlands. Ultra-Pfu DNA

polymerase and The QuikChange II XL sitedirected mutagenesis kit were purchased from Stratagene (La Jolla, CA). Lysing enzyme (L1412) was from Sigma- Aldrich (St. Louis, MO) Purified oligonucleotide primers were obtained from Eurofins MWG Operon (Huntsville, AL). All other chemicals were purchased from Thermo Fisher scientific (Waltham, MA). De-ionized water was produced by using a Milli-Q® Biocel™ Ultra-Pure water purifier system equipped with 0.22 µM membrane filter cartridge (EMD Millipore, Billerica, MA, USA), purification cartridge and an organic removal cartridge (Evoqua Water Technologies, Lowell, MA, USA).

5.2.2 Construction of H105R mutant and plasmid propagation

To investigate the function of His 105 and the relation between His 105 and Glu183, the H105R mutation was created by site-directed mutagenesis. Vector pCPO3.I-*Amds*, a 14 kb plasmid was used as template. *A.nidulans* acetamidase gene (*AmdS*) was inserted into *NotI* restriction enzyme digestion site as a selection marker, to allow the mutant contains *Amds* to grow on acetamide plate, consuming acetamide as the sole source of nitrogen. The full encoded CPO gene, pCPO3.I is placed under control of the *A. niger* glucoamylase promoter

(*PglaA*) and *A. nidulans* anthranilate synthetase terminator (*TtrpC*). (Fig. 5.2)

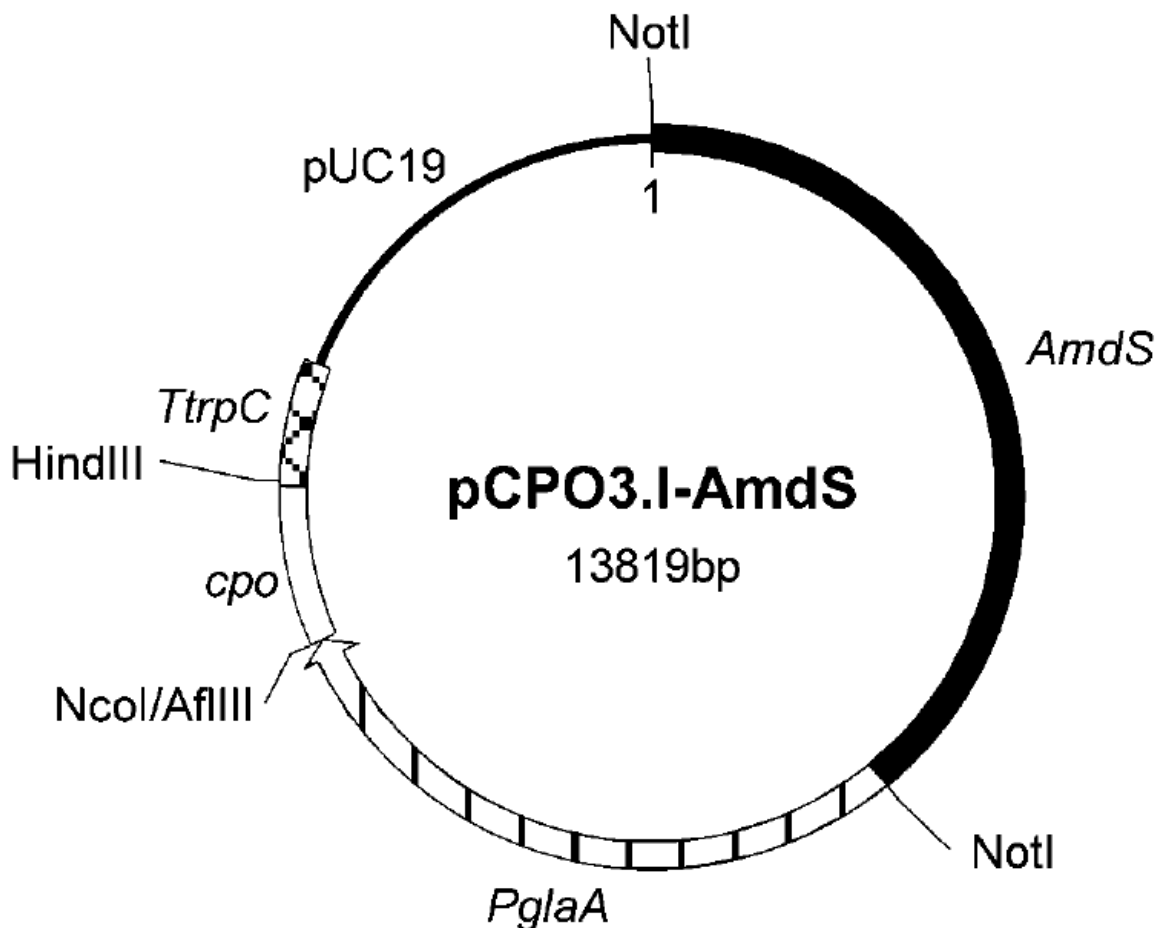


Figure 5.2 The CPO expression vector pCPO3.1-AmdS for transformation of *A.niger* strain.[2]

Encoded primers for H105R mutant was 5'-gag ccc cac gct ttc gag cgc gac c-3'(primer 1) and 5'-gcg gga gaa gga gtg gtc gcg ctc g-3'(primer 2), both with the melting temperature of 74.42°C. The PCR was carried out by QuikChange II XL sitedirected mutagenesis kit and Eppendorf thermal cycler (Mastercycler gradient) , PfuUltra HF DNA polymerase was added to reaction. The PCR reaction was set up at 98 °C for 50 seconds, followed by 18 cycles of 98°C for 30

seconds for denaturation, 63 °C for 30 seconds for annealing, 72 °C for 14 minutes for extension, the last cycle was hold at 72 °C for 10 minutes.

DPN I restriction endonuclease was applied to digest the templates. PCR product was propagated in *E. coli* strain (H105R). Plasmids from *E. coli* was extracted by QIAGEN DNA extraction mini kit (QIAGEN, CA). The extracted DNA was examined by DNA electrophoresis and confirmed by DNA sequencing (Fig. 5.3)

5.2.3 Transformation into *A. niger* and selection for expression

The *A. niger* MGG029 strain was inoculated in 50 mL minimal medium (MM) containing maltose (5%), glucose (1%), casamino acids (0.5%), yeast extract (0.5%), NaNO₃ (70mM), KCl (7 mM), K₂HPO₄ (6 mM), MgSO₄ (2 mM), uridine (10 mM), carbenicillin (50 mg/L), the Hutner trace elements solution (50 µL).[84] The culture was incubated for 37 °C at 250 rpm for 1 day and change to 30 °C for 2-5 days, homogenizer was used to disrupted mycelia for 20 seconds, repeated 3 times. Then the culture was transferred to 1 L media with the same compositions as in 50 mL MM, incubated at 30 °C for 20 hours at 250 rpm.

Mycelia was resuspended in 1.7 Osm solution (0.27 M CaCl₂ and 0.6 M NaCl) after filtered through sterile myra cloth. Protoplasts were incubated with lysing enzyme (L1412) at 37 °C for 4 hours at 150 rpm, resuspended protoplasts and incubated on ice for 20 minutes, then centrifuged at 3500 rpm for 15-30 minutes at 0 °C to get precipitate. The supernatant was decanted, precipitate was

washed twice by STC 1700 buffer (1.2 M sorbitol, 10 mM Tris-HCl, 50 mM CaCl₂ and 35 mM NaCl at pH 7.5), resuspended by STC 1700 and incubated with 10 µg mutant plasmid and 1 µg pAB4.1 co-transformation plasmid at 25 °C for 25 minutes. The incubated protoplast was mixed with 60% PEG 4000 in 10 mM Tris-HCl buffer at pH 7.5 and 50 mM CaCl₂ carefully in three steps. The PEG-treated protoplast was diluted to 10 mL with STC 1700 and collected through centrifugation. The protoplast was resuspended in the leftover of STC1700 and spread onto 1.2 M sorbitol selective agar medium plate, incubate for 3-5 days at 22 °C.

5.2.4 Expression of the H105R mutant protein

Mutant colonies on the selective plates were inoculated in MM (without uridine and yeast extract, addition of 0.1 mM 5-Aminolevulinic acid hydrochloride (heme precursor) for 22 °C at 250 rpm for 7 days.

MCD assay and ABTS assay of the culturing medium were used to determine the protein yield by its chlorination and peroxidation activity, respectively.

MCD assay was measured at 278 nm by UV-Vis spectroscopy. 0.17 mM monochlorodimedone (MCD) was mixed with 50-500 µL culture medium in 100 mM KH₂PO₄ buffer with 20 mM KCl at pH 2.75, after addition of 2 mM H₂O₂, absorbance at 278 nm was monitored for 1 minute.

1.7 mM 2, 2'-azino-bis-3-ethy-benzthiazoline-6-sulfonic acid (ABTS) was mixed with 50 µL clear culture medium in 100 mM KH₂PO₄ buffer with 25 mM

citric acid at pH 3.0, after addition of 2 mM H₂O₂, the UV started to collect the absorbance at 405 nm for 1 minutes.

Due to decreased tendency of ABTS activity after 2-3 days since inoculation, and totally destroyed activity after Amicon stirring pressure cell, 0.05 mM ferriprotoporphyrin IX chloride (hemin) was added to culture to stabilized the mutant.

5.2.5 Purification of the mutant protein

After 7 days, the 12 Liter medium was filtered through myracloth and glass fiber filter circles G6 to remove fungus, concentrated to 50 mL in the Amicon ultrafiltration cell. 50 mL crude sample was dialyzed in 4 liters 25 mM phosphate buffer at pH 5.9 for 12 hours, and repeat dialysis again with fresh buffer. The sample was filtered by 0.45 µM membrane.

Ion exchange chromatography was applied by diethylaminoethyl (DEAE) sepharose fast flow column with 50 mL DEAE resin. 25 mM phosphate buffer at pH 5.9 with ionic strength gradient was used to wash the column, gradually increase the concentration of NaCl from 0.0 to 0.5 M. Different eluted portions were collected and concentrated by Centriprep[®] centrifugal filter unit (30,000 Dalton). Absorption spectrum was scanned and SDS-PAGE was used to check the existence of mutant.

All buffers used in column were filtered through 0.45 µM membrane and degassed for 15 minutes to remove solid and gas particles. Purification by columns was carried out in 4 °C to keep protein stable.

Sodium dodecyl sulfate polyacrylamide gel electrophoresis (SDS-PAGE) was used to check the molecular size of eluted products.

5.3 Result and discussion

5.3.1 Mutant DNA sequencing

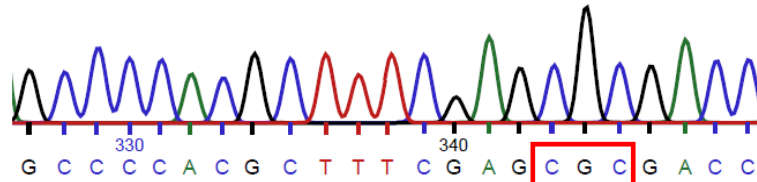


Figure 5.3 DNA sequence of H105R mutant.

In the sequencing result, the Histidine codon CAC was replaced by Arginine codon CGC successfully. The GC content was as high as 72%, but PCR protocol still work effectively.

5.3.2 Transformaiton and expression result

H105R mutant grown on 1.2 M sorbitol selective agar plate after transformation suggested the transformation was successful. The colonies were inoculated to 12 L medium and monitored the expression of protein by MCD and ABTS assays. There was no MCD activity showed in mutant medium, only ABTS assay could be used to evaluate the expression. The ABTS activity was high at the second day of inoculation, and

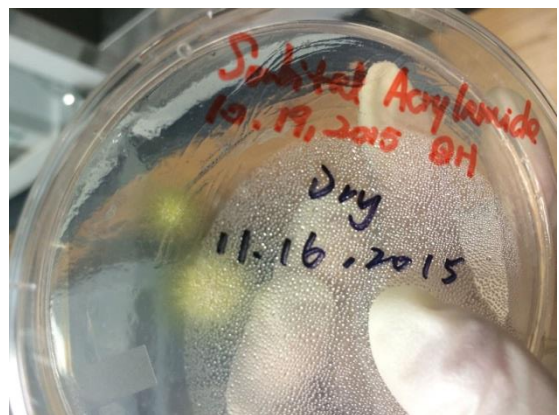


Figure 5.4 H105R mutant grown on 1.2 sorbitol selective agar plate after 24 hours.

quickly decreased. (Fig. 5.5).

50 μM hemin was added to culture to stabilize the protein, repeated the same protocol to 12 liters culture.

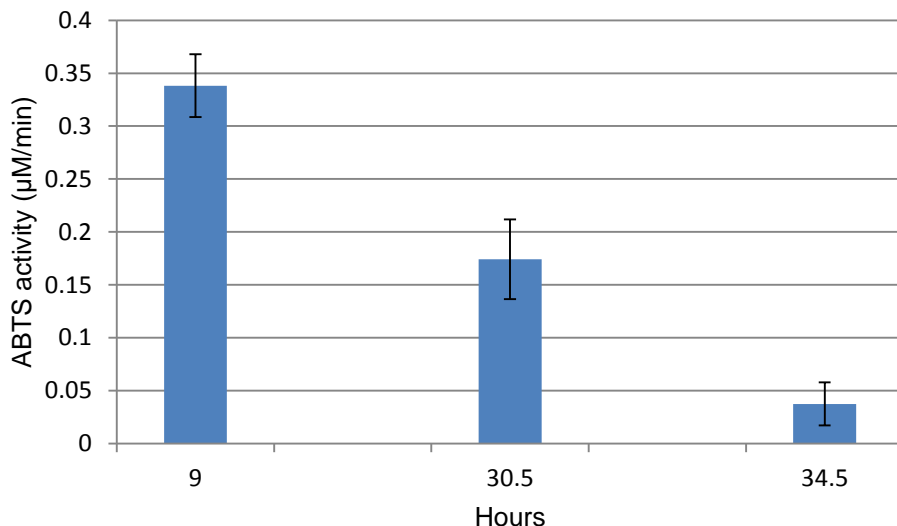


Figure 5.5 The ABTS activity of H105R cultures since the second day of inoculation. Samples were run in triplicate.

5.3.3 Purification

The purification of concentrated sample was collected to run SDS-PAGE with samples from the crude medium and other portion of elution product. (Fig. 5.6) The band of mutant was presented in SDS-PAGE, the concentrated sample (lane 2) was of transparent color, implying the heme was not incorporated into protein.

In UV-Vis spectrum of concentrated sample (lane 2), the low-spin ferric heme protein typically with a Soret band around 420 nm was not observed (Fig. 5.7), indicating the heme incorporation was not efficient in H105R mutant, the recombinant H105R mutant was apoprotein.

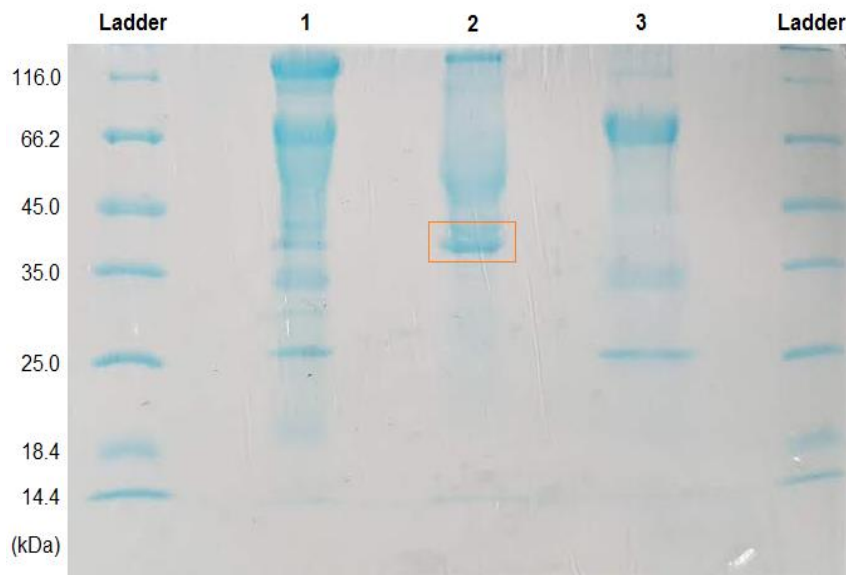


Figure 5.6 SDS-PAGE of mutated protein. Lane 1-the crude sample before ion exchange; lane 2-ion exchange eluted products (band of H105R in red rectangle); lane 3-products eluted by buffer with 1M NaCl.

5.4 Discussion

The apoprotein H105R was suggested that arginine might change the distal pocket due to its charge or structure, and even result in the instability of heme

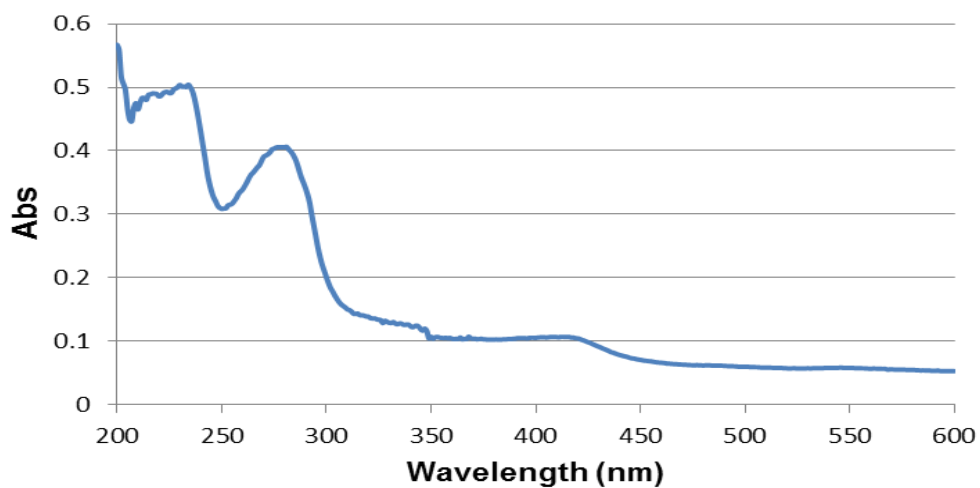


Figure 5.7 UV-Vis spectra of H105R mutant.

porphyrin. Although H105 could be changed to alanine (A), the structure of CPO would not change much due to the smaller size of alanine.

The chlorination activity was not found during all the process, suggested that the chlorination active site in CPO was not formed. The change of distal pocket affected the chlorination dramatically and the role of H105 site was crucial in supporting the CPO construction near the heme center.

The peroxidation decreased during culturing and amicon concentration, implied that mutated protein was easy to be denatured. The H105 has the ability to stabilize E183 by hydrogen bond, changing it to a larger and more polar amino acid might destroy the structure and function of CPO by affected E183.

There is also possibility that the change from histidine to arginine might directly change the tertiary structure of mutant protein. In conclusion, the amino acid at 105 site could be changed to arginine but could not express active protein due to heme incorporation failure.

CHAPTER VI

DEGRADATION OF NON-STEROIDAL ANTI-INFLAMMATORY DRUGS DICLOFENAC AND NAPROXEN BY CHLOROPEROXIDASE

THIS PAPER IS SUBMITTED AND ITS FORMAT IS KEPT

**Degradation of Non-steroidal Anti-inflammatory Drugs Diclofenac and
Naproxen by Chloroperoxidase**

Xiaohong Li^{a,†}, Qinghao He^{b,†}, Haiyun Li^a, Mancheng Hu^{a,c}, Shuni Li^{a,c}, Quanguo
Zhai^{a,c}, Yucheng Jiang^{a,c*}, Xiaotang Wang^{b*}

*a School of Chemistry & Chemical Engineering, Shaanxi Normal University, Xi'an,
710062, P.R. China*

*b Department of Chemistry and Biochemistry, Florida International University,
Miami, Florida 33199, USA*

*c Key Laboratory of Macromolecular Science of Shaanxi Province, Shaanxi
Normal University, Xi'an, 710062,
P.R. China*

†These authors contributed equally to this work

*Corresponding authors

Dr. Yucheng Jiang

Mailing Address: School of Chemistry & Chemical Engineering
Xi'an, No. 620 West Chang'an Road, Chang'an District
710119, P.R. China

E-mail: jyc@snnu.edu.cn

Phone: +86 29 81530763

Dr. Xiaotang Wang

Mailing Address: Department of Chemistry and Biochemistry
Florida International University
11200 S.W. 8th Street,
Miami, Florida 33199. USA

E-mail: wangx@fiu.edu

Phone: (305) 348-7544

Abstract

Non-steroidal anti-inflammatory drugs (NSAIDs), such as diclofenac and naproxen, are widely used for the treatment of arthritis, ankylosing spondylitis, and acute muscle pain. However, most NSAIDs are usually not metabolized and simply pass through human body. These drugs are difficult to be decomposed by general waste treatment strategies and have caused serious environmental concerns. Here we report a rapid and efficient enzymatic degradation of diclofenac and naproxen by chloroperoxidase (CPO), a heme protein isolated from *Caldariumyces fumago* (*C. fumago*). Complete degradation of diclofenac and naproxen was achieved in only 9 and 7 min for diclofenac and naproxen, respectively, under mild conditions with nanomolar enzyme concentration. The degraded products were identified by both HPLC-MS and NMR, suggesting the involvement of multiple steps in CPO catalyzed degradation of the two drug molecules. Moreover, our work demonstrated that CPO treatment followed by existing bioremediation technologies (activated sludge) greatly improved the efficiency and completeness of decontaminating these two drugs from waste water. Most significantly, our eco-toxicity test using green algae, *Chlorella Pyrenoidos*, showed that the products had noticeably lower toxicity than the parent drugs, demonstrating the potential of CPO in large-scale treatment of sewage contaminated with diclofenac and naproxen.

Keywords: enzymatic degradation; diclofenac; naproxen; chloroperoxidase; eco-toxicity

1. Introduction

Both diclofenac (2-[(2,6-dichlorophenyl)amino]benzeneacetic acid; sodium salt) and naproxen (2-(6-methoxynaphthalen-2-yl)propionic acid) (Fig. 1) are non-steroidal anti-inflammatory drugs (NSAIDs). They are widely used in the treatment of arthritis, ankylosing spondylitis, acute muscle pain, and other symptoms associated with inflammation ([Grenni et al., 2013](#); [Sathishkumar et al., 2012](#)). The widespread

application of these drugs coupled with their resistance toward metabolic breakdown in human body inevitably resulted in the release of large amount of these drugs into the aquatic environment. In recent years, diclofenac and naproxen has been detected in surface water, groundwater, wastewater, and even in drinking water at concentrations ranging from $\text{ng}\cdot\text{L}^{-1}$ to $\mu\text{g}\cdot\text{L}^{-1}$ (Zhang et al., 2008; Zhao et al., 2009). It has been reported that naproxen has adverse effects on biota, such as impairing the lipid peroxidation system of bivalves and altering microbial community structure to yield antibiotic resistance in environmental microbial communities (Gagné et al., 2006). Diclofenac was recently designated as a devastating environmental pollutant because of its bioaccumulation in the food chain (Ilic et al., 2011). Therefore, effective degradation of these drugs is of paramount significance for reducing their accumulation in the environment.

Unfortunately, conventional sewage treatment is inefficient in removing or degrading diclofenac and naproxen (Hartmann et al., 2008; Nakada et al., 2006). For example, no noticeable breakdown of diclofenac was observed over a period of 28 days either when it was the sole source of carbon or when an external carbon source was added for co-metabolic degradation (Quintana et al., 2005). Batch tests using an activated sludge system and membrane bioreactors also revealed very poor degradability of diclofenac in comparison with other pharmaceuticals (Samaras et al., 2013). Other conventional water treatment processes such as coagulation, sedimentation and filtration have all been proven to be ineffective to remove these two drugs (Brillas et al., 2010; Westerhoff et al., 2005). Consequently, physicochemical approaches including ultrasonic (Naddeo et al., 2010), electrochemical oxidation (Faber et al., 2012), photocatalytic (Arriaga et al., 2008), potassium permanganate oxidation (Álvarez et al., 2013) and ozone oxidation (Naddeo et al., 2009) have been adopted to improve the removal of these drugs from

drinking water or wastewater. However, limitations of these methods, such as cost, efficiency, and secondary pollution from use of chemicals, warrant further investigations on the removal/breakdown of these widely used drugs from environment.

Little evidence of diclofenac transformation by microbial communities is documented in the literature. White-rot fungi (WRF) were found to be efficient in degrading both diclofenac (Urrea et al., 2010) and naproxen (Urrea et al., 2010), but long treatment time (1 h and 5 h, respectively) was needed. Enzymatic degradation is an ideal approach because of the mild and environmentally friendly conditions employed. Thus, crude lignin peroxidase (LiP, a heme-imidazole peroxidase) from *Phanerochaete chrysosporium* (*P. chrysosporium*) has been used to convert diclofenac in various conditions and was found to be highly effective (Zhang et al., 2010). In addition, fungal unspecific peroxygenases (UPOs) have been shown to be able to hydroxylate/O-demethylate a diverse array of pharmaceuticals (including diclofenac and naproxen)(Hofrichter et al., 2014; Kinne et al., 2009; Piontek et al., 2013; Poraj-Kobielska et al., 2011; Wang et al., 2013). Inspired by the results of LiP and UPOs, we studied the degradation of diclofenac and naproxen by chloroperoxidase (CPO), a heme containing glycoprotein that is phylogenetically (heme-thiolate proteins) and functionally (haloperoxidases) related to UPOs with higher oxidation potential and thermal/chemical stability than LiP (Makino et al., 1976; Millis et al., 1989). High performance liquid chromatography-mass spectrometry (HPLC-MS) and nuclear magnetic resonance (NMR) spectroscopy were employed to identify the major degradation products. Based on the products identified, reaction pathways are postulated. Our results demonstrated that CPO can effectively convert both diclofenac and naproxen into compounds that are significantly less toxic based on their inhibitory effects and EC_{50} value on the growth of a freshwater green alga, *Chlorella pyrenoidos*.

2. Experimental

2.1 Enzyme preparation

Chloroperoxidase was isolated from the growth medium of *C. fumago* according to the method of Morris and Hager (Morris et al., 1966) with minor modifications, using acetone rather than ethanol in the solvent fractionation step. CPO with $R_z = 1.03$ (A_{398}/A_{280} , 1.44 for pure enzyme) was prepared and stored in 100 mM phosphate buffer (pH 5.0) at 4 °C. The halogenation activity of CPO used in this study was $4232 \text{ U}\cdot\text{mL}^{-1}$ based on the standard monochlorodimedon (MCD) assay (Hager et al., 1966). The aromatic hydroxylation activity ($3563 \text{ U}\cdot\text{mL}^{-1}$) of the enzyme was determined by monitoring the hydroxylation of naphthalene into 1-naphthol (Kluge et al., 2007). The classic peroxidase activity of the enzyme determined using ABTS (2,2'-azino-bis(3-ethylbenzothiazoline-6-sulphonic acid)) as substrate was $3071 \text{ U}\cdot\text{mL}^{-1}$ (Manoj et al., 2008).

2.2 Reagents and buffers

All reagents used in this study, including diclofenac, naproxen, dipotassium hydrogen phosphate, potassium dihydrogen phosphate, hydrogen peroxide (30 % in aqueous solution), ethyl acetate, and inorganic reagents for cultivating the green alga were obtained from Xi'an Chemical Co. Ltd (Xi'an, China) with highest purity ($\geq 98\%$). Other chemicals such as methanol and acetonitrile (chromatography grade) as well as standard degradation product of the two drugs, o-desmethylnaproxen and 4'-hydroxydiclofenac (chromatography grade) were purchased from Sigma Aldrich (St. Louis, MO USA).

Phosphate buffer ($0.1 \text{ mol}\cdot\text{L}^{-1}$) was prepared by mixing appropriate volumes of $1 \text{ mol}\cdot\text{L}^{-1} \text{KH}_2\text{PO}_4$ and K_2HPO_4 stock solutions and diluting the combined solutions to 1 L. Then the solution was adjusted to various pH with $1 \text{ mol}\cdot\text{L}^{-1} \text{H}_3\text{PO}_4$. All solutions were prepared using deionized water with a conductivity of $5.6 \times 10^{-8} \text{ s}\cdot\text{cm}^{-1}$.

2.3 Degradation of diclofenac and naproxen

Enzymatic degradation of both drugs was carried out in 0.1 mol·L⁻¹ phosphate buffer in a centrifugal tube with a total volume of 3.0 mL containing CPO (0.25-23 nmol·L⁻¹), 20 mmol·L⁻¹ KCl, and drugs (15 μmol·L⁻¹) at pH 2~6 at 298K. The reaction was started by adding H₂O₂ (0.015-0.3 mmol·L⁻¹) in the absence of light under magnetic stirring and was continued for 20 min. The supernatant of the reaction mixture was extracted 3 times using ethyl acetate. The combined organic extract was concentrated by rotary evaporation (0.09 MPa, 308K) to remove the solvent. The extracts were then dissolved in acetonitrile and methanol, respectively, for HPLC (LC-20AT, Shimadzu) analysis. The mobile phase consisted of 80:20 (v/v) acetonitrile and water for diclofenac and 90:10 (v/v) methanol and water for naproxen, and the flow rate was 0.5 ml·min⁻¹. The detector was set at 274 nm and 235 nm for diclofenac and naproxen, respectively. The quantitative analysis of the target compounds was based on the standard curve (correlation coefficients were > 0.999).

$$\text{Degradation efficiency } \eta = \left(\frac{C_0 - C_t}{C_0} \right) \times 100\% \quad (1)$$

The effect of reaction parameters (pH, concentration of enzyme/H₂O₂, and reaction time) on degradation efficiency was investigated and optimized.

All experiments were triplicated and data reported were mean values of three independent measurements.

2.4 Determination of products

Samples were treated as above for HPLC-MS analysis. An Esquire LC-ion trap mass spectrometer (Bruker Daltonics, Germany) equipped with an orthogonal geometry Electrospray Ionization (ESI) source was employed to determine the formulae of the products. Nitrogen was used as the drying (8 L·min⁻¹) and nebulizing (0.8 bar) gas at 180 °C. Scanning was performed from m/z 100 to 1000 in the standard resolution mode.

To establish the structure of the degradation products, the reaction was carried out using the same condition as stated above except a larger volume (300 mL) was used. Upon completion of the reaction, the reaction mixture was extracted with either ethyl acetate or chloroform. After removal of the solvent by rotary evaporation (0.09 MPa, 308K) the extracts were dissolved in either deuterated chloroform or methanol and transferred to 5 mm NMR tubes. NMR experiments were carried out on a Bruker 600 MHz NMR spectrometer operating at a proton frequency of 599.73 MHz. All spectra were recorded at 298 K using standard pulse programs from the manufacturer.

2.5 Elimination of COD and TOC

Total organic carbon (TOC) measurement was conducted on a TOC-VCPA analyzer (Shimadzu Corp.). The feed speed was 150 ml·min⁻¹. Chemical oxygen demand (COD) was measured by a quick method on a Rapid Autoanalyzer (5B-1(F), Lian-hua Tech.Co., Ltd). A solution containing 2.5 ml sample, 0.7 ml reagent D (potassium dichromate) and 4.8 ml reagent E (catalysts) in a 20.0 ml glass tube was heated to 438K and kept for 10 min together with a blank sample and a standard sample. After 2 min of air cooling, the heated solution was cooled by water for another 2 min. Then the absorbency of the samples was measured at 610 nm.

2.6 Treatment of drug effluent by activated sludge

A mixed population of activated sludge microorganisms was collected from Xi'an second sewage treatment plant (Xi'an, China). The sample of activated sludge was filtered on a Spectra Mesh polypropylene 149- μ m filter (Spectrum Laboratories Inc., Rancho Dominguez, CA, USA) to remove aggregates. The sample was then washed three times by centrifugation and suspended in the same volume of culture medium. To remove any excessive amounts of dissolved organic carbon, the suspension was stirred and maintained under oxygen at 298K for at least 24 h without exposure to the test materials.

The volatile ratio f of activated sludge was 0.74.

90 mL of $15 \mu\text{mol}\cdot\text{L}^{-1}$ drug effluent was put into the activated sludge suspension before /after enzymatic treatment (to ensure a final drug concentration of $7.5\mu\text{mol}\cdot\text{L}^{-1}$). The samples were stirred for the duration of the study with a magnetically coupled stirrer when air was used as the aerated gas. The sample was then left to stand for 1-2 h. The supernatant was taken for determination of COD.

2.7 Toxicity Tests

Freshwater unicellular green alga, *C. pyrenoidosa* (provided by the Institute of Wuhan Hydrobiology, Chinese Academic of Science), was cultivated in nutrient media of blue green medium (BG11) at 298K and illuminated with cool-white fluorescent lights at a continuous light intensity of 2000 Lx. For cell experiments, *C. Pyrenoidosa* was exposed, during its log growth phase, to the toxicant at five different concentrations (maintain final concentration ranging from 0.01 to 0.36 mg/L) for 3-4 days at 298K. The concentration of the alga was determined by monitoring the change of absorption at 680 nm (Ma et al., 2006). The toxicity tests for each drug concentration were conducted in triplicate.

The growth inhibition rate i for each sample was calculated from Equation (2) and (3) (Lange et al., 2006),

$$\mu = (\ln OD_t - \ln OD_{t_0}) / (t - t_0) \quad (2)$$

$$i = (\mu_c - \mu_t) / \mu_c \times 100\% \quad (3)$$

where $t-t_0$ is incubation time (min); OD_{t_0} is absorbance at t_0 ; OD_t is absorbance at t ; μ is growth rate of all life (min^{-1}); μ_c is growth rates of control culture without toxin addition (min^{-1}); and μ_t is growth rates of cultures in the presence of drugs (min^{-1}). EC_{50} (drug concentration required to cause 50% reduction in growth) values were calculated using linear regression analysis of drug concentration as natural logarithm versus percentage

inhibition. All correlation coefficients were > 0.99 .

3. Results and discussion

3.1 Effect of reaction parameters on drug Degradation

Since various physicochemical parameters influence the degradation efficiency, it is essential to optimize these factors in order to make the process more efficient and practically applicable.

The pH range investigated was 2-6 due to poor stability and activity of CPO at higher pH. Fig. S1 (A) showed that the degradation efficiency of naproxen and diclofenac increased rapidly with increasing pH, and reached maximum around pH 3.2. The degradation efficiency decreased sharply when pH was increased above 3.2. The preference for such a low reaction pH has been observed for most CPO catalyzed reactions and has been attributed to the protein's unique active site structure and catalytic mechanism (Liu et al., 2014; Zhang et al., 2012). CPO uses a glutamic acid (Glu 183) as the acid-base catalyst to aid the formation of compound I (Sundaramoorthy et al., 1995; Wang et al., 2003). The protonation of Glu183 is necessary for both the formation of compound I and the binding of negatively charged substrates to avoid unfavorable electrostatic interactions. Acidic environment is also needed to protonate compound X involved in most CPO catalyzed halide dependent reactions (Chiang et al., 1976; Dawson et al., 1988).

It is well known that high concentration of H_2O_2 (oxidant) inactivates most heme containing enzymes due to internal oxidative destruction of the porphyrin prosthetic group (Grey et al., 2007). Thus low concentrations of H_2O_2 are employed for reactions catalyzed by most heme peroxidases. This strategy cannot be simply applied to CPO because of its ability to disproportionate hydrogen peroxide. Therefore, the optimum concentration of hydrogen peroxide needs to be determined based on the actual

substrate. The effect of H_2O_2 concentration on CPO catalyzed degradation of diclofenac and naproxen is shown in Fig. S1B. As expected for all peroxidases, no degradation of either drug was observed before the addition of H_2O_2 . The degradation efficiency of both drugs increased as H_2O_2 concentration is increased. Maximum rate is achieved when total H_2O_2 concentration reached $0.1 \text{ mmol}\cdot\text{L}^{-1}$. Further addition of H_2O_2 , however, repressed the degradation of both drugs possibly due to formation of compound III caused by high concentrations of H_2O_2 (Ayala et al., 2011). Therefore, $0.1 \text{ mmol}\cdot\text{L}^{-1}$ of H_2O_2 was chosen in the degradation of both diclofenac and naproxen in all subsequent experiments.

Optimizing CPO concentration not only improves degradation efficiency but also saves cost of operation. The range of CPO concentration tested was $0.25\text{-}6.0 \text{ nmol}\cdot\text{L}^{-1}$ for diclofenac and $1\text{-}23.0 \text{ nmol}\cdot\text{L}^{-1}$ for naproxen. Fig. S1 (C) showed that degradation efficiency of both drugs increased rapidly as CPO concentration was increased. Complete degradation of the drugs was achieved when CPO concentration was above $5.0 \text{ nmol}\cdot\text{L}^{-1}$ for diclofenac, and $20.0 \text{ nmol}\cdot\text{L}^{-1}$ for naproxen, indicating that CPO is extremely efficient in the degradation of the subject drugs.

It is remarkable to note that CPO degrades both diclofenac and naproxen with a remarkable rate. As shown in Fig. S1 (D), about 70% of diclofenac and 75% of naproxen is degraded within 1 min. The complete degradation was achieved in only 9 and 7 min for diclofenac and naproxen, respectively, at optimum reaction condition.

3.2 Determination of products by HPLC-MS and NMR

Tremendous efforts have been made to characterize the intermediates and final products generated from diclofenac and naproxen degradation (Faber et al., 2012; Urrea et al., 2010). Plausible mechanisms have been proposed for both drugs based on the intermediates and final products identified from different processes. To understand the

mechanisms of CPO catalyzed degradation and to evaluate the potential of this enzymatic method in environmental and industrial applications, both HPLC-MS and NMR analyses are employed to establish the structures of the putative products from the two drugs.

The hydroxylation of aromatic rings and O-demethylation of esters have been reported for several unspecific peroxygenase (UPOs) (Hofrichter et al., 2014; Kinne et al., 2009; Piontek et al., 2013; Poraj-Kobielska et al., 2011; Wang et al., 2013), a class of heme-thiolate proteins related to CPO and cytochromes P450. However, these two activities have not been reported for CPO. In this work, CPO catalyzed hydroxylation of diclofenac and O-demethylation of naproxen were observed. The degradation of both diclofenac and naproxen was confirmed by HPLC analysis of the reaction product as shown in Fig. 2. The MS spectra of samples from diclofenac degradation (Fig.2) suggested the formation of six putative products. The peak that eluted at 2.6 min (Fig.2A) shows a molecular ion $[M-H]^-$ at m/z 311, indicating the addition of an oxygen atom to the parent compound. Multiple possibilities exist as oxygen can be added at all possible positions of the two benzene rings. However, NMR analysis (Fig.3) suggested compound [II] as the major product corresponding to this molecular ion. Since the coupling pattern of the chloride bearing ring remained in the product, the oxygen must have been added to the acetate bearing ring with oxygen added at the para-carbon of the imino group. The NOE between peak "a" at 3.77 ppm (singlet, 2H) and peak "b" at 7.25 ppm (Fig.S3), the COSY correlation and splitting pattern confirm the structure of compound [II] as reported previously (Blum et al., 1996; Calza et al., 2006; Coelho et al., 2009; Osorio et al., 2014; Sparidans et al., 2008). Product [I], 4'-hydroxydiclofenac, is commercially available and displays a quite different NMR spectral pattern as shown in Fig. S4 and Fig. S5). The peak eluted at 3.1 min (Fig.2B) displayed a molecular ion $[M-H]^-$ at m/z 328, indicating

the addition of two oxygen atoms to the parent compound or the addition of one oxygen atom to compound [II]. This product also showed a major fragmentation ion at m/z 284 (Fig.2B), assignable to the decarboxylation of the major product. Decarboxylation was also observed for diclofenac itself (Fig.S6). The NMR spectrum (Fig.S7) of this product showed the absence of a three proton coupling pattern in the aromatic region as displayed by both the parent compound and compound [II], suggesting the oxygen atom is added to the chloride bearing ring as shown in compound IV. This is in good agreement with observations made with other methods (Blum et al., 1996; Calza et al., 2006; Osorio et al., 2014). The peak eluted at 2.7 min showed a molecular ion $[M-H]^-$ at m/z 325 (Fig.2C), assignable to compound [V] or [VI] due to further oxidation of product [II] or [IV]. However, neither compound V nor VI was detected in NMR experiments, implicating that these products might form only in the ionization process within mass spectrometer.

Based on the products identified from our LC-MS and NMR analysis, the sequence of diclofenac degradation catalyzed by CPO is proposed (Fig.4). The diverse catalytic activity of CPO makes it possible to produce a broad array of products from diclofenac degradation, however, under the conditions employed in our study, only hydroxylation activity is observed. This can be appreciated by the similarity between CPO and cytochromes P450 that metabolize most xenobiotics via hydroxylation. Thus CPO converts diclofenac to either monohydroxylated or dihydroxylated products, the same as the major products observed in the metabolism of diclofenac (Blum et al., 1996; Osorio et al., 2014). The close similarity among possible hydroxylation products makes it difficult to isolate and purify individual product. This drawback does not comprise the aim of this study.

The identification of products from CPO catalyzed degradation of naproxen is

achieved by detailed NMR analysis of the products with the aid of MS. The most noticeable difference between proton NMR spectra of the products and the parent drug, naproxen, is the absence of the methoxy signal (peak "i" around 3.9 ppm, Fig.S8 and S9) in the products as shown in Fig.5. This suggests the demethylation of naproxen as reported previously (Sidelmann et al., 2001; Urrea et al., 2010). Although CPO catalyzed N-demethylation has been reported (Kedderis et al., 1980), the observed O-demethylation represents a novel activity of CPO. This is reminiscent of the activity displayed by P450 (Meunier et al., 2004) and UPOs (Hofrichter et al., 2014; Kinne et al., 2009) that are structurally related to CPO. The methyl (peak "a" at 1.53 ppm, doublet, $J=6.56$, 3H) and the methine (peak "b" at 4.99 ppm, quartets, $J=6.56$, 1H) signals from the product are indicative of the propionic acid part of naproxen. These signals are downfield shifted compared to the corresponding signals in the parent drug molecule, consistent with observations reported previously (Sidelmann et al., 2001; Urrea et al., 2010). Both the methyl and the methine signals displayed NOE to a peak at 7.42 ppm (peak "h", doublet, $J=1.18$, 1H) and a peak at 7.48 ppm (signal "c", doublet of doublet, $J=8.03$ and 1.18 , 1H) as shown in Fig.5 (A). The peak at 7.48 ppm is strongly coupled to a peak at 8.09 ppm (resonance "d", doublet, $J=8.03$, 1H) as shown in Fig.5 (B). The NOE and coupling pattern of this product suggests no modification occurred to the propionic group bearing ring of naproxen during degradation. The remaining aromatic signals, peak "g" at 7.44 ppm (doublet, $J=10.11$, 1H) and peak "f" at 6.44 ppm (doublet, $J=10.18$, 1H) are strongly coupled (Fig.5 (B)), demonstrating their vicinal relationship. Based on the above NMR spectral property, this product is proposed to be 2-(5,6-dihydroxynaphthalen-2-yl)propanoic acid due to modification at 5-C of naproxen. However, the NMR spectra of commercially available desmethylnaproxen (Fig. S10 and Fig. S11) do not support the proposed structure of this degradation product.

Furthermore, the MS of this product shows a molecular ion $[M-H]^-$ at m/z 311, also inconsistent with the structure proposed (expected m/z at 231). The difference of a mass of 80 between the expected and the observed mass, suggests the phosphorylation of one of the hydroxyl groups. Esterification of desmethylnaproxen has been reported previously (Sidelmann et al., 2001). The high phosphate concentration and the extremely low pH used in our degradation study make it feasible to phosphorylate 2-(5,6-dihydroxynaphthalen-2-yl)propanoic acid and give product (I) as shown in Figure 6. Product (I) can be further degraded to 2-(5,8-dihydroxy-6-(phosphonoxy)naphthalen-2-yl)propanoic acid via hydroxylation at the 8-C. However, this product is not observed in either NMR or MS experiments. The observation of a molecular ion $[M-H]^-$ at m/z 325 suggests the formation of product (II) as shown in Fig.6.

Based on the major products identified from our study, the reaction sequence of naproxen degradation catalyzed by CPO is proposed (Fig.7). Similar as the degradation of diclofenac, CPO catalyzed degradation of naproxen is achieved primarily via CPO's monooxygenase activity. Thus CPO degrades naproxen to either monohydroxylated or dihydroxylated products, similar as the major products observed in bacterial degradation of naproxen (Wojcieszńska et al., 2014). Initially, naproxen was degraded to desmethylnaproxen (Aresta et al., 2006; Urrea et al., 2010). The desmethylnaproxen is then phosphorylated to [(2-(6-(phosphonoxy)naphthalen-2-yl)acetic acid [a], not observed)] in the presence of high concentrations of phosphate and under low pH condition employed. Esterification of desmethylnaproxen has been reported in the literature (Sidelmann et al., 2001). Next, [a] was hydroxylated to 2-(5-hydroxy-6-(phosphonoxy)naphthalen-2-yl)propanoic acid [I] corresponding to m/z 311 observed in Figure 6. Product (I) was then degraded to 2-(5,8-dihydroxy-6-(phosphonoxy)naphthalen-2-yl)propanoic acid [b, expected $m/z=327$] which is instantly

oxidized to 2-(5,8-dioxo-6-(phosphonoxy)-5,8-dihydronaphthalen-2-yl)propanoic acid (II, $m/z=325$) as shown in Fig.6.

The products identified in our NMR and MS analysis are subjected to further oxidative transformation as supported by the results from activated sludge experiment as well as eco-toxicity test.

3.3 Reduction in chemical oxygen demand (COD) and total organic carbon (TOC)

Table 1 showed that only 4.9% , 9.1% of COD and 25%, 7.6% of TOC removal was achieved for diclofenac and naproxen, respectively. It is therefore proposed that CPO catalyzed degradation can serve as an efficient pre-treatment step in waste water treatment. This can be combined with subsequent bioremediation technologies (activated sludge) for complete decontamination of the two drugs in waste water.

3.4 Combined treatment of drug effluent by enzymatic oxidation and activated sludge

As indicated in Table 1, the COD value of drug effluent did not decrease noticeably after CPO-treatment. However, compared with the parent drugs, the products from CPO catalyzed degradation have improved solubility in aqueous media and are more vulnerable to further biodegradation. This conclusion was confirmed by the observation that treatment of CPO-catalyzed reaction mixture with activated sludge increased COD removal from 4.9% and 9.1% to 85% and 86% for diclofenac and naproxen, respectively. On the other hand, treatment by activated sludge alone only removes 49% and 54%, of the COD for diclofenac and naproxen, respectively, suggesting that more effective decontamination of the two drugs can be achieved through CPO pre-treatment followed by existing bioremediation technologies (activated sludge).

3.5 Evaluation of the eco-toxicity of the products

In some cases simple destruction of a drug is inadequate, since the resulting products may also be highly toxic, and special attention must therefore be paid to toxicity

assessment of products to ensure that the agent has been effectively detoxified. However, toxicity evaluation about the products from diclofenac and naproxen are not readily available. Biological assays offer a direct measure to evaluate the magnitude of the potential health risk of chemicals. Therefore, a growth-inhibitory test was carried out using *C. Pyrenoidosa*.

Fig.S10 showed that the 72-h EC_{50} increased with the increase in degradation efficiency. The value was $0.25 \text{ mg}\cdot\text{L}^{-1}$ for diclofenac and $0.33 \text{ mg}\cdot\text{L}^{-1}$ for naproxen at the end of degradation. These results demonstrated that the products had lower toxicity compared with the parent drugs, suggesting the great potential of using CPO as an efficient catalyst in the safe removal of these drugs from environmental.

4. Conclusion

In summary, our study demonstrated that CPO catalyzed oxidative degradation is a promising alternative for treatment of waste water containing non-steroidal anti-inflammatory drugs. Complete degradation of diclofenac and naproxen is reached in only 9 and 7 min, respectively, under mild conditions.

The products identified by HPLC-MS suggested the initial hydroxylation of the drug molecules followed by further oxidative transformation. The biodegradability of the decomposition products was significantly increased as confirmed by COD measurement after combining the enzymatic oxidation with activated sludge treatment. Most significantly, the products of both diclofenac and naproxen had dramatically lower toxicity than the original drugs as judged by the 72-h EC_{50} value of *C. Pyrenoidos*. Our results demonstrates that CPO can serve as an efficient, cost-effective, and

environmentally friendly catalyst for large-scale treatment of waste water contaminated with the two drugs studied in this work..

Acknowledgments

This work is supported by the National Natural Science Foundation of China (21176150) and the Fundamental Research Funds for the Central Universities (GK201505007) to YJ and the National Science Foundation via Grant CHE-0540763 to

X.W. (CAREER Award).

Nomenclature

NSAID, non-steroidal anti-inflammatory drugs; WRF, white-rot fungus; LiP, lignin peroxidase; CPO, chloroperoxidase; HPLC-MS, high performance liquid chromatography-mass spectrometry; NMR, nuclear magnetic resonance; NOE, nuclear overhauser effect; COSY, (homonuclear chemical shift) correlation spectroscopy; MCD, monochlorodimedon; ESI, electrospray ionization; TOC, total organic carbon; COD, chemical oxygen demand; BG, blue green medium; EC_{50} , median effective concentrations;

References

- Álvarez TR, Rodil R, Quintana JB, Triñanes S, Cela R. 2013. Oxidation of non-steroidal anti-inflammatory drugs with aqueous permanganate. *Water Res* 47: 3220-3230.
- Aresta A, Carbonara T, Palmisano F, Zambonin CG. 2006. Profiling urinary metabolites of naproxen by liquid chromatography-electrospray mass spectrometry. *J Pharmaceut Biomed* 41: 1312-1316.
- Arriaga FM, Esplugas S, Giménez J. 2008. Photocatalytic degradation of non-steroidal anti-inflammatory drugs with TiO₂ and simulated solar irradiation. *Water Res.* 42: 585-594.
- Ayala M, Batista CV, Vazquez-Duhalt R. 2011. Heme destruction, the main molecular event during the peroxide-mediated inactivation of chloroperoxidase from *Caldariomyces fumago*. *J Biol Inorg Chem* 16: 63-68.
- Blum W, Faigle JW, faar P U, Sallmann A. 1996. Characterization of a novel diclofenac metabolite in human urine by capillary gas chromatography-negative chemical ionization mass spectrometry. *J Chromatogr B* 685: 251-263.
- Brillas E, Segura SG, Skoumal M, Arias C. 2010. Electrochemical incineration of diclofenac in neutral aqueous medium by anodic oxidation using Pt and boron-doped diamond anodes. *Chemosphere* 79: 605-612.
- Calza P, Sakkas VA, Medana C, Baiocchi C, Dimou A, Pelizzetti E, Albanis T. 2006. Photocatalytic degradation study of diclofenac over aqueous TiO₂ suspensions. *Appl Catal B-Environ* 67: 197-205.
- Chiang R, Rand-Meir T, Makino R, Hager LP. 1976. Compound X an intermediate in enzymatic halogenations. *J Biol Chem* 251: 6340-6346.
- Coelho AD, Sans C, Agüera A, Gómez MJ, Esplugas S, Dezotti M. 2009. Effects of ozone pre-treatment on diclofenac: intermediates, biodegradability and toxicity assessment. *Sci Total Environ* 407: 3572-3578.
- Dawson JH. 1988 Probing structure-function relations in heme-containing oxygenases and peroxidases. *Science* 240: 433-439.

- Faber H, Melles D, Brauckmann C, Wehe CA, Wentker K, Karst U. 2012. Simulation of the oxidative metabolism of diclofenac by electrochemistry/(liquid chromatography) mass spectrometry. *Anal Bioanal Chem* 403: 345-354.
- Gagné F, Blaise C, Fournier M, Hansen PD. 2006. Effects of selected pharmaceutical products on phagocytic activity in *Elliptio complanata* mussels. *Comp Biochem Phys C* 143:179-186.
- Grenni P, Patrolecco L, Ademollo N, Tolomei A, Caracciolo AB. 2013. Degradation of Gemfibrozil and Naproxen in a river water ecosystem. *Microchem J* 107:158-164.
- Grey CE, Hedström M, Adlercreutz P. 2007. A mass spectrometric investigation of native and oxidatively inactivated chloroperoxidase. *Chembiochem* 8: 1055-1062.
- Hager LP, Morris DR, Brown FS, Eberwein H. 1966. Chloroperoxidase: II. Utilization of halogen anions. *J Biol Chem* 241: 1769-1777.
- Hartmann J, Bartels P, Mau U, Witter M, Tümping WV, Hofmann J, Nietschmann E. 2008. Degradation of the drug diclofenac in water by sonolysis in presence of catalysts. *Chemosphere* 70: 453-461.
- Hofrichter M, Ullrich R. 2014. Oxidations catalyzed by fungal peroxygenases. *Curr Opin Chem Biol* 19: 116-125.
- Ilic S, Drmic D, Franjic S, Kolenc D, Coric M, Brcic L, Klicek R, Radic B, Sever M, Djuzel V, Filipovic M, Djakovic Z, Stambolija V, Blagaic AB, Zoricic I, Gjurasin M, Stupnisek M, Romc Z, Zarkovic K, Dzidic S, Seiwert S, Sikiric P. 2011. Pentadecapeptide BPC 157 and its effects on a NSAID toxicity model: Diclofenac-induced gastrointestinal, liver, and encephalopathy lesions *Life Sci* 88: 535-542.
- Kedderis GL, Koop DR, Hollenberg PF. 1980. N-Demethylation reactions catalyzed by chloroperoxidase. *J Biol Chem* 255: 10174-10182.
- Kinne M, Poraj-Kobielska M, Aranda E, Ullrich R, Hammel KE, Scheibner K, Hofrichter M. 2009. Regioselective preparation of 5-hydroxypropranolol and 4'-hydroxydiclofenac with a fungal peroxygenase *Bioorg. Med Chem Lett* 19: 3085-3087.

- Kinne M, Poraj-Kobielska M, Ralph SA, Ullrich R, Hofrichter M, Hammel KE. 2009. Oxidative cleavage of diverse ethers by an extracellular fungal peroxygenase. *J Biol Chem* 284: 29343-29349.
- Kluge MG, Ullrich R, Scheibner K, Hofrichte M. 2007. Spectrophotometric assay for detection of aromatic hydroxylation catalyzed by fungal haloperoxidase–peroxygenase. *Appl Microbiol Biot* 75: 1473-1478.
- Lange F, Cornelissen S, Kubac D, Sein MM, Sonntag JV, Hannich CB, Golloch A, Heipieper HJ, Möder M, Sonntag CV. 2006. Degradation of macrolide antibiotics by ozone: A mechanistic case study with clarithromycin. *Chemosphere* 65: 17-23.
- Liu LX, Zhang J, Tan Y, Jiang YC, Hu MC, Li SN, Zhai QG. 2014. Rapid decolorization of anthraquinone and triphenylmethane dye using chloroperoxidase: Catalytic mechanism, analysis of products and degradation route. *Chem Eng J* 244: 9-18.
- Makino R, Chiang R, Hager LP. 1976. Oxidation-Reduction potential measurements on chloroperoxidase and its complexes. *Biochemistry* 15: 4748-4754.
- Manoj KM, Hager LP. 2008. Chloroperoxidase, a janus enzyme. *Biochem* 47: 2997-3003.
- Ma JY, Lu NH, Qin WD, Xu RF, Wang YB, Chen XN. 2006 Differential responses of eight cyanobacterial and green algal species, to carbamate insecticides. *Ecotox Environ Safe* 63: 268-274.
- Meunier B, de Visser SP, Shaik S. 2004. Mechanism of oxidation reactions catalyzed by cytochrome p450 enzymes. *Chem Rev* 104: 3947-3980.
- Millis CD, Cai D, Stankovich MT, Tien M. 1989. Oxidation-reduction potentials and ionization states of extracellular peroxidases from the lignin-degrading fungus *phanerochaete chrysosporium*. *Biochemistry* 28: 8484-8489.
- Morris DR, Hager LP. 1966. Chloroperoxidase: I. Isolation and properties of the crystalline glycoprotein. *J Biol Chem* 241: 1763-1768.
- Naddeo V, Belgiorno V, Ricco D, Kassinos D. 2009. Degradation of diclofenac during sonolysis, ozonation and their simultaneous application, *Ultrason. Sonochem* 16:

790-794.

- Naddeo V, Belgiorno V, Kassinos D, Mantzavinos D, Meric S. 2010. Ultrasonic degradation, mineralization and detoxification of diclofenac in water: optimization of operating parameters. *Ultrason Sonochem* 17: 179-185.
- Nakada N, Tanishima T, Shinohara H, Kiri K, Takada H. 2006. Pharmaceutical chemicals and endocrine disruptors in municipal wastewater in Tokyo and their removal during activated sludge treatment. *Water Res* 40: 3297-3303.
- Osorio V, Imbert-Bouchard M, Zonjia B, Aband JL, Pérez S, Varceló D. 2014. Simultaneous determination of diclofenac, its human metabolites and microbial nitration/nitrosation transformation products in wastewaters by liquid chromatography / quadrupole-linear ion trap mass spectrometry. *J Chromatogr A* 1347: 63-71.
- Piontek K, Strittmatter E, Ullrich R, Gröbe G, Pecyna MJ, Kluge M, Scheibner K, Hofrichter M, Plattner DA. 2013. Structural basis of substrate conversion in a new aromatic peroxygenase: cytochrome P450 functionality with benefits. *J Biol Chem* 288: 34767-34776.
- Poraj-Kobielska M, Kinne M, Ullrich R, Scheibner K, Kayser G, Hammel KE, Hofrichter M. 2011. Preparation of human drug metabolites using fungal peroxygenases. *Biochem Pharmacol* 82: 789-796.
- Quintana JB, Weiss S, Reemtsma T. 2005. Pathways and metabolites of microbial degradation of selected acidic pharmaceutical and their occurrence in municipal wastewater treated by a membrane bioreactor. *Water Res* 39: 2654-2664.
- Samaras VG, Stasinakis AS, Mamais D, Thomaidis NS, Lekkas TD. 2013. Fate of selected pharmaceuticals and synthetic endocrine disrupting compounds during wastewater treatment and sludge anaerobic digestion. *J Hazard Mater* 244-245: 259-267.
- Sathishkumar P, Chae JC, Unnithan AR, Palvannan T, Kim HY, Lee KJ, Cho M, Kannan S K, Oh BT. 2012. Laccase-poly(lactic-co-glycolic acid) (PLGA) nanofiber: highly

- stable, reusable, and efficacious for the transformation of diclofenac. *Enzyme Microb Tech* 51:113-118.
- Sidelmann UG, Bjørnsdottir I, Shockcor JP, Hansen SH, Lindon JC, Nicholson JK. 2001. Directly coupled HPLC-NMR and HPLC-MS approaches for the rapid characterisation of drug metabolites in urine: application to the human metabolism of naproxen. *J Pharmaceut Biomed Anal* 24: 569-579.
- Sparidans RW, Lagas JS, Schinkel AH, Schellens JHM, Beijnen JH. 2008. Liquid chromatography–tandem mass spectrometric assay for diclofenac and three primary metabolites in mouse plasma. *J Chromatogr B* 872: 77-82.
- Sundaramoorthy M, Turner J, Poulos TL. 1995. The crystal structure of chloroperoxidase: a heme peroxidase-cytochrome P450 functional hybrid. *Structure* 3: 1367-1377.
- Urrea EM, Trujillo MP, Blázquez P, Vicent T, Caminal G. 2010. Biodegradation of the analgesic naproxen by *Trametes versicolor* and identification of intermediates using HPLC-DAD-MS and NMR. *Bioresource Technol* 101: 2159-2166.
- Urrea EM, Trujillo MP, Morató CC, Caminal G, Vicent T. 2010. Degradation of the drug sodium diclofenac by *Trametes versicolor* pellets and identification of some intermediates by NMR. *J Hazard Mater* 176: 836-842.
- Wang XS, Peter S, Ullrich R, Hofrichter M, Groves JT. 2013. Driving force for oxygen-atom transfer by heme-thiolate enzymes. *Angew Chem Int Ed* 52: 9238-9241.
- Wang XT, Tachikawa H, Yi XW, Manoj KM, Hager LP. 2003. Two-dimensional NMR study of the heme active site structure of chloroperoxidase. *J Biol Chem* 278: 7765-7774.
- Westerhoff P, Yoon Y, Snyder S, Wert E. 2005. Fate of endocrine-disruptor, pharmaceutical, and personal care product chemicals during simulated drinking water treatment processes. *Environ Sci Technol* 39: 6649-6663.
- Wojcieszńska D, Domaradzka D, Hupert-Kocurek K, Guzik U. 2014. Bacterial degradation of naproxene-Undisclosed pollutant in the environment. *J Environ Manage* 145: 157-161.

- Zhang J, Feng MY, Jiang YC, Hu MC, Li SN, Zhai QG. 2012. Efficient decolorization / degradation of aqueous azo dyes using buffered H₂O₂ oxidation catalyzed by a dosage below ppm level of chloroperoxidase. *Chem Eng J* 191: 236-242.
- Zhang YJ, Geißen SU, Gal C. 2008. Carbamazepine and diclofenac: removal in wastewater treatment plants and occurrence in water bodies. *Chemosphere* 73:1151-1161.
- Zhang YJ, Geißen SU. 2010. *In vitro* degradation of carbamazepine and diclofenac by crude lignin peroxidase. *J Hazard Mater* 176: 1089-1092.
- Zhao JL, Ying GG, Wang L, Yang JF, Yang XB, Yang LH, Li X. 2009. Determination of phenolic endocrine disrupting chemicals and acidic pharmaceuticals in surface water of the Pearl Rivers in South China by gas chromatography-negative chemical ionization-mass spectrometry. *Sci Total Environ* 407: 962-974.

Figure captions:

Fig. 1 Chemical structures of diclofenac (a) and naproxen (b)

Fig. 2 ESI-ion trap mass spectra of the degradation products from CPO catalyzed oxidation of diclofenac recorded in negative mode.

Fig. 3 COSY of diclofenac product [II] in chloroform-d.

Fig. 4 Proposed degradation pathway of diclofenac during CPO-catalytic oxidative process.

Fig. 5 Proton NMR (A) NOESY and (B) COSY spectra of naproxen product [I]. The weak NOEs between peaks “a” and “c” and between peaks “b” and “c” can only be observed at lower contour levels. The NOE and coupling patterns unequivocally define the structure of this degradation product.

Fig. 6 ESI-ion trap mass spectra of the degradation products from CPO catalyzed oxidation of naproxen recorded in negative mode.

Fig. 7 Proposed degradation pathway of naproxen during CPO-catalytic oxidative process.

Table 1 Elimination of COD and TOC by CPO catalyzed oxidative degradation.

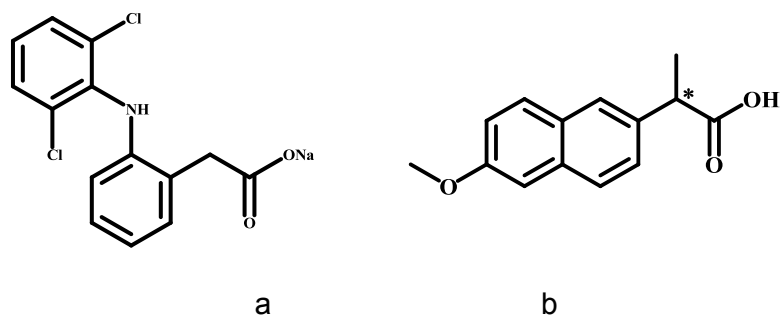


Fig. 1 Chemical structures of diclofenac (a) and naproxen (b)

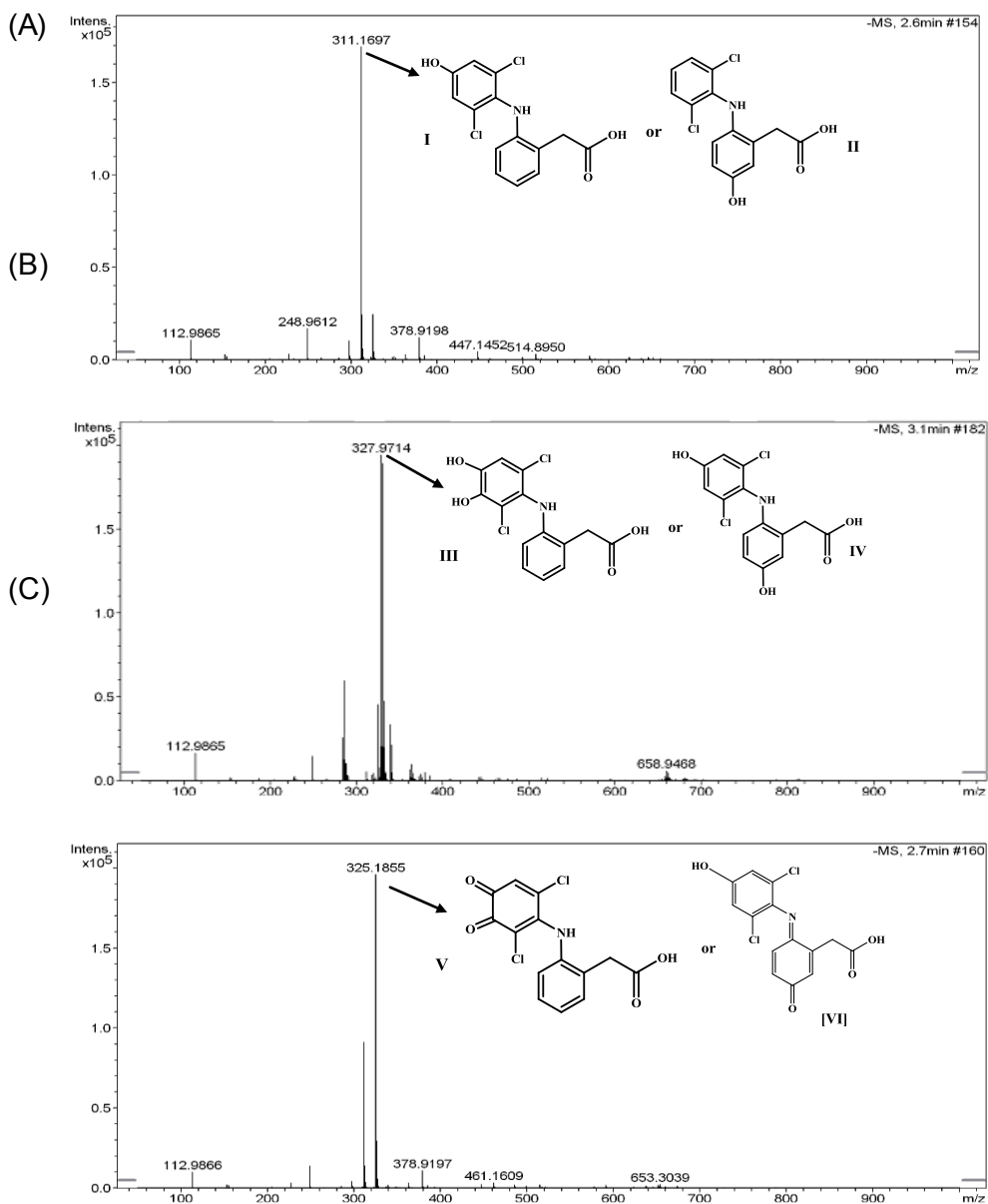


Fig. 2 ESI-ion trap mass spectra of the degradation products from CPO catalyzed oxidation of diclofenac recorded in negative mode.

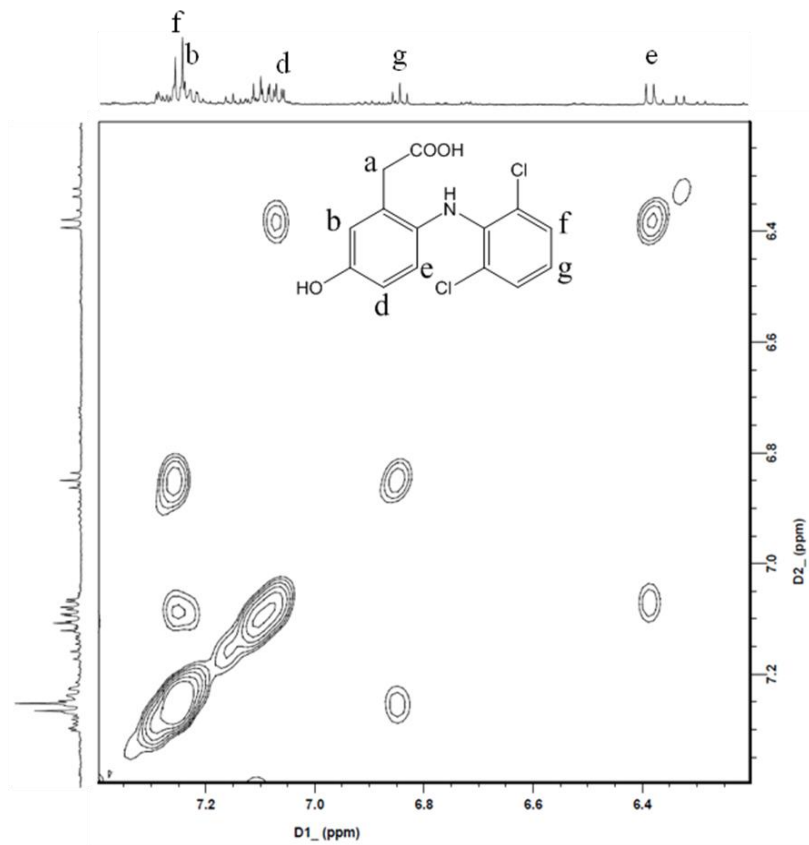


Fig. 3 COSY of diclofenac product [II] in chloroform-d.

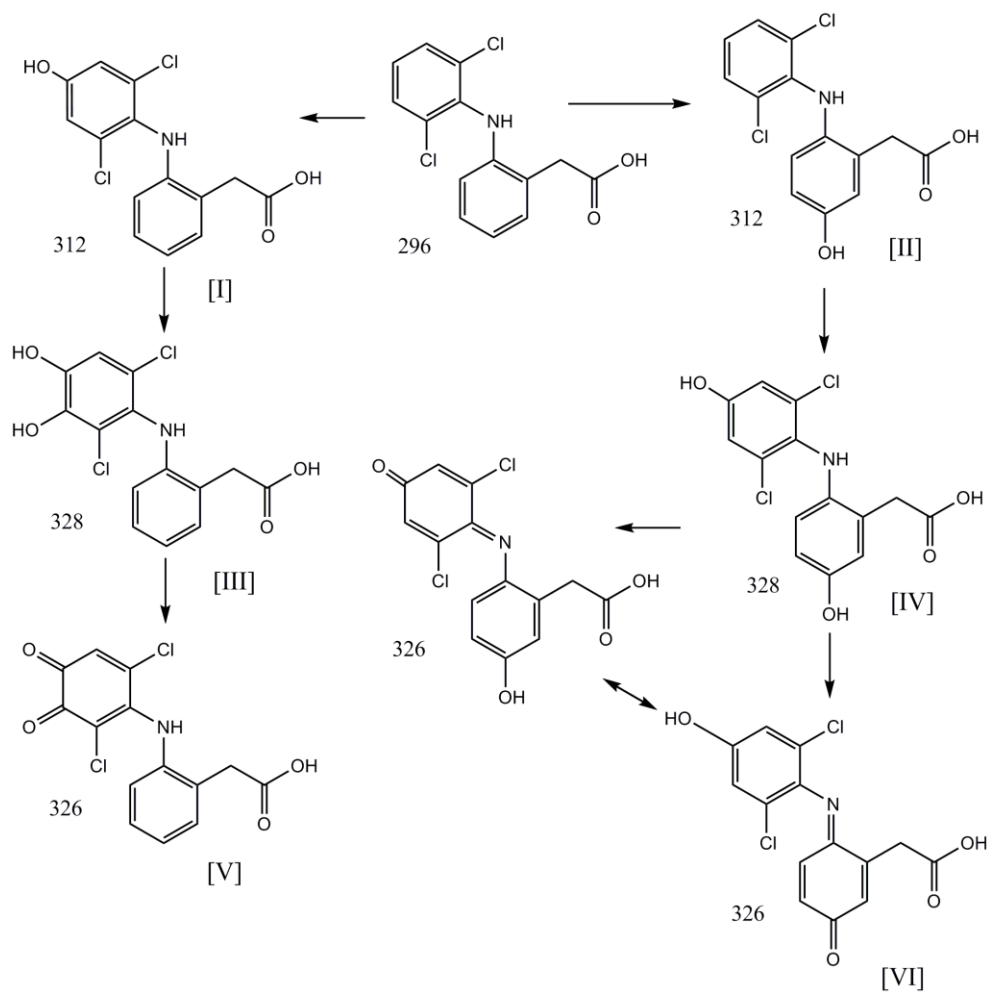


Fig. 4 Proposed degradation pathway of diclofenac during CPO-catalytic oxidative process.

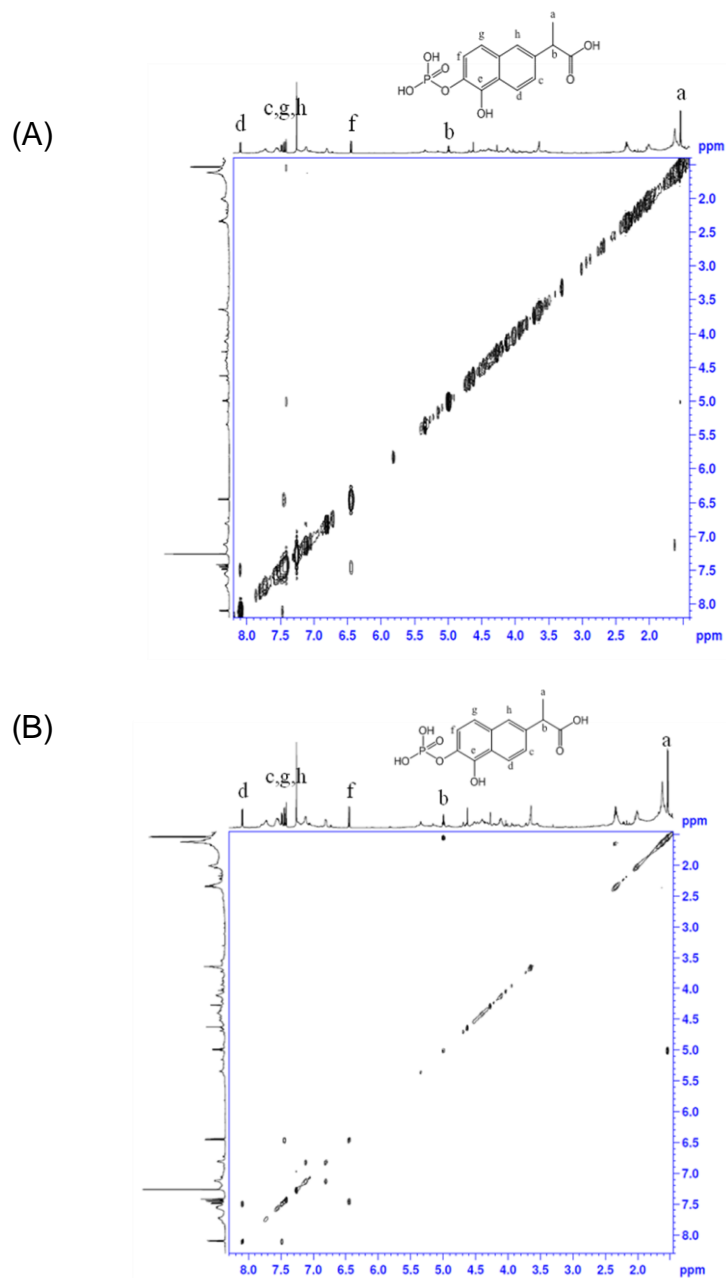


Fig. 5 Proton NMR (A) NOESY and (B) COSY spectra of naproxen product [1]. The weak NOEs between peaks “a” and “c” and between peaks “b” and “c” can only be observed at lower contour levels. The NOE and coupling patterns unequivocally define the structure of this degradation product.

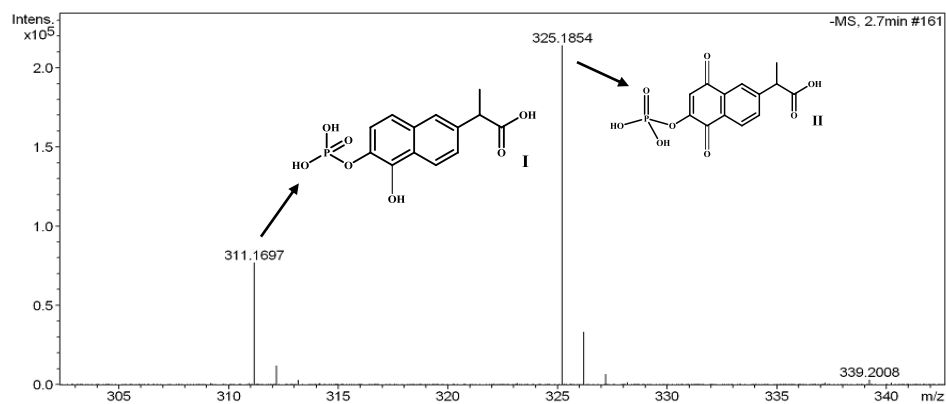


Fig. 6 ESI-ion trap mass spectra of the degradation products from CPO catalyzed oxidation of naproxen recorded in negative mode.

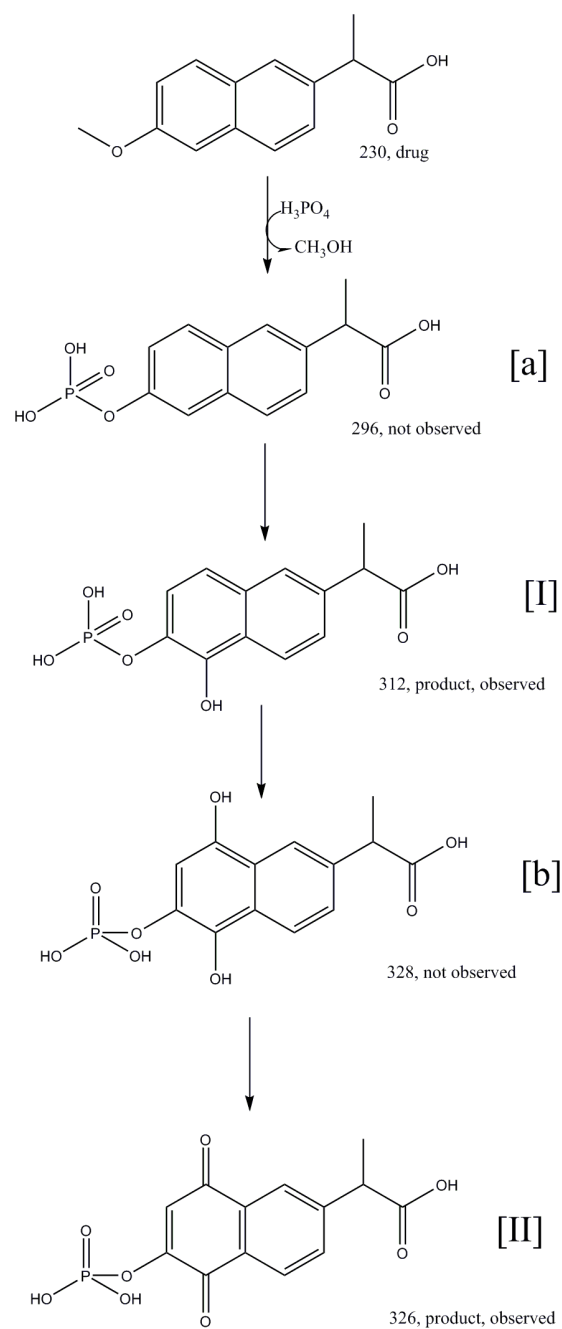


Fig. 7 Proposed degradation pathway of naproxen during CPO-catalytic oxidative process

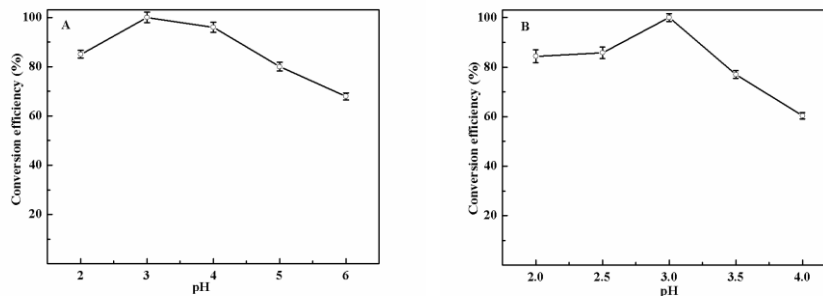
Table 1 Elimination of COD and TOC by CPO catalyzed oxidative degradation

substance	COD (mg · L ⁻¹)	COD removal (%)	TOC (mg · L ⁻¹)	TOC removal (%)
diclofenac	41→39	4.9	8.3→6.2	25
naproxen	22→20	9.1	158→146	7.6

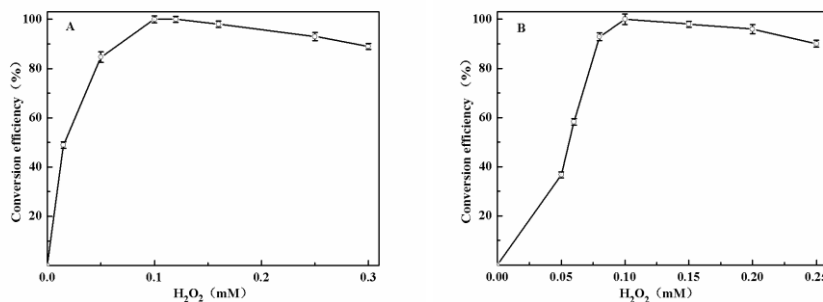
Supporting Information

Fig. S1 The relationship between degradation efficiency and reaction condition of CPO catalyzed degradation of diclofenac (left) and naproxen (right).

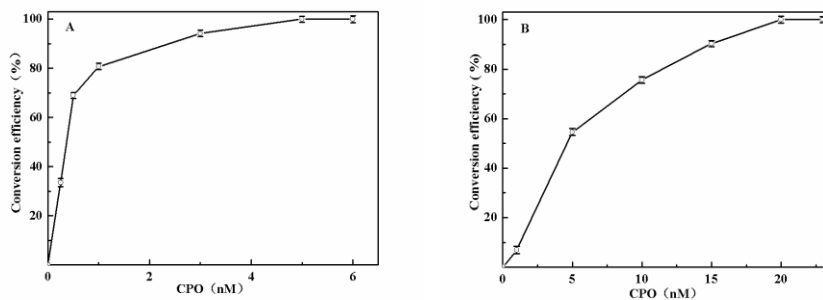
(A)



(B)



(C)



(D)

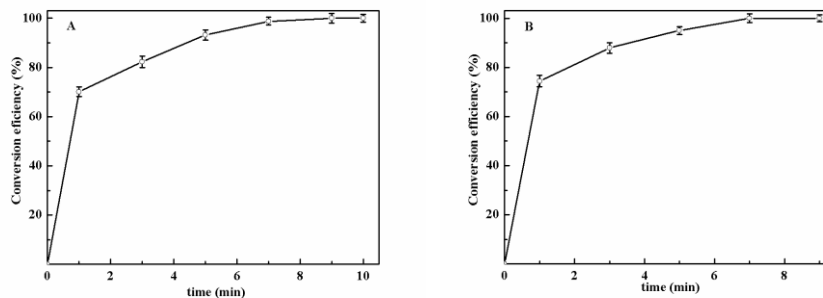


Fig. S2 The HPLC elution profile of degradation solution both of diclofenac and naproxen

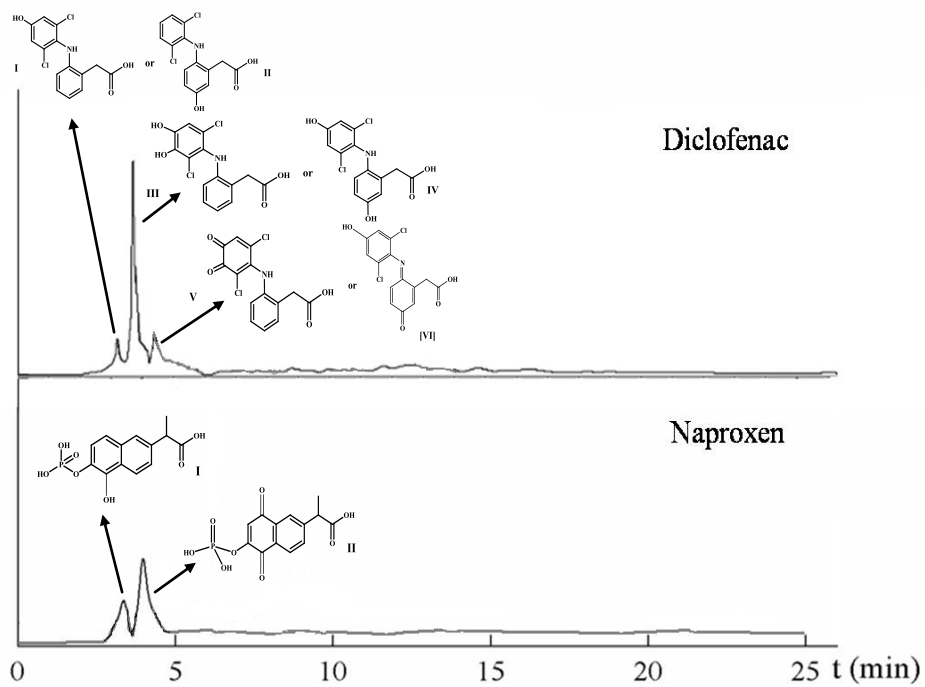


Fig. S3 NOESY of diclofenac product [II]

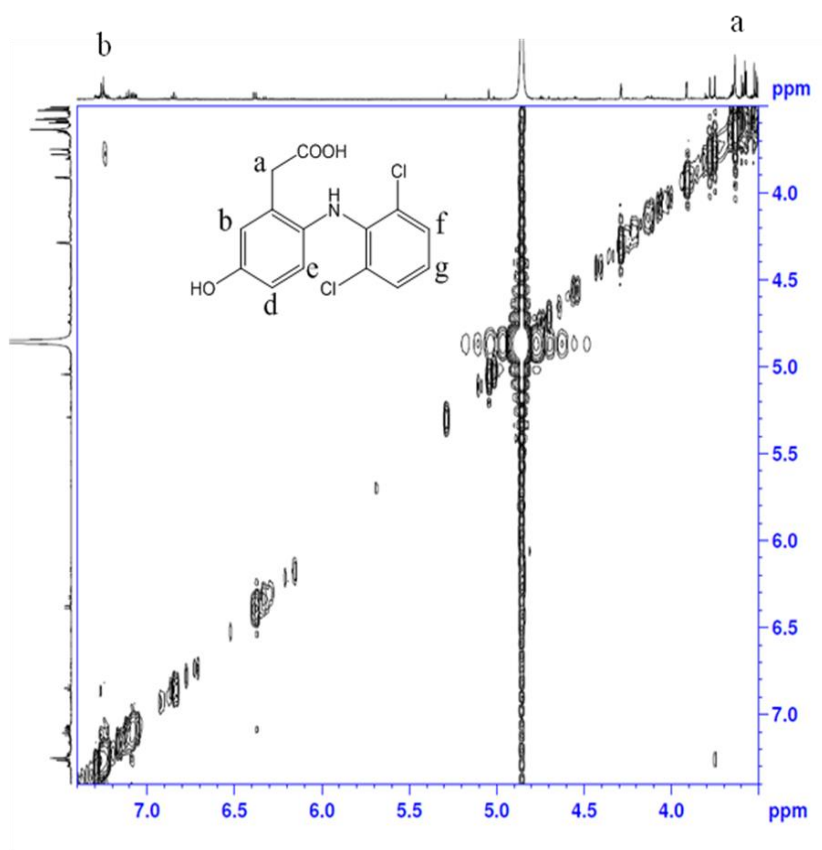


Fig. S4. COSY of authentic 4'-hydroxydiclofenac purchased from Sigma Aldrich

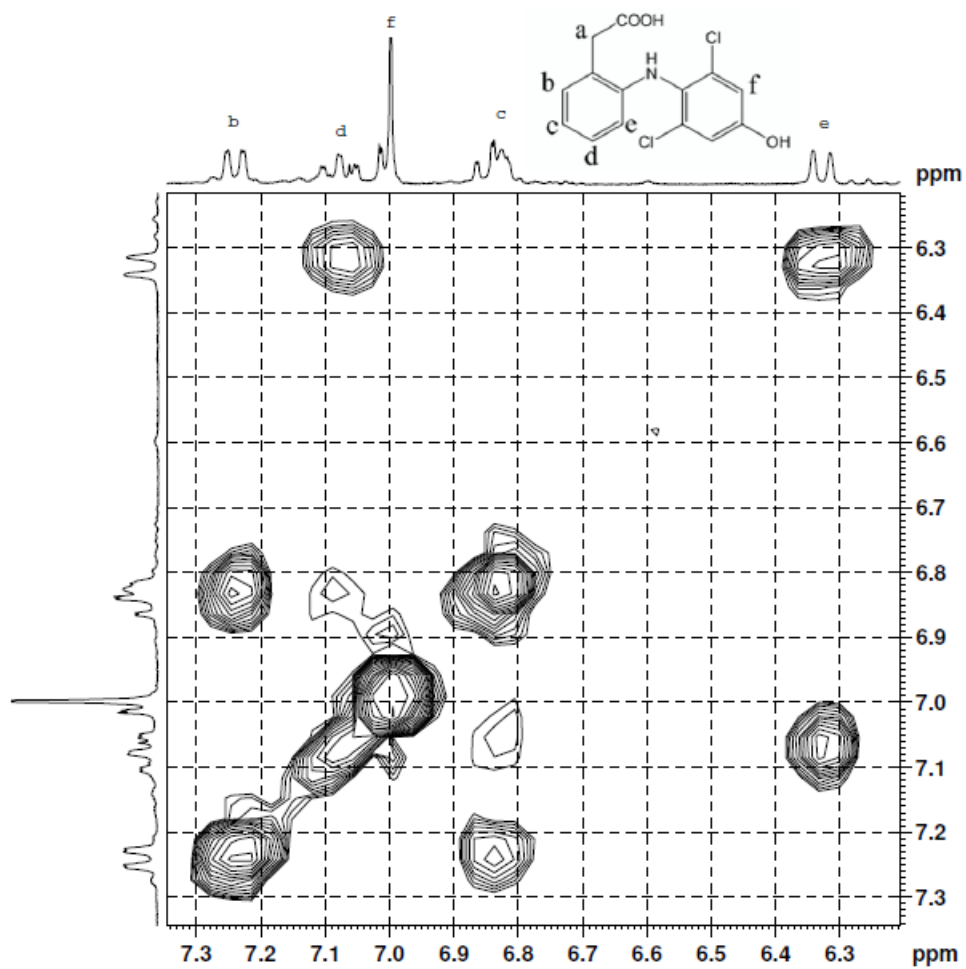


Fig. S5. NOESY of authentic 4'-hydroxydiclofenac purchased from Sigma Aldrich

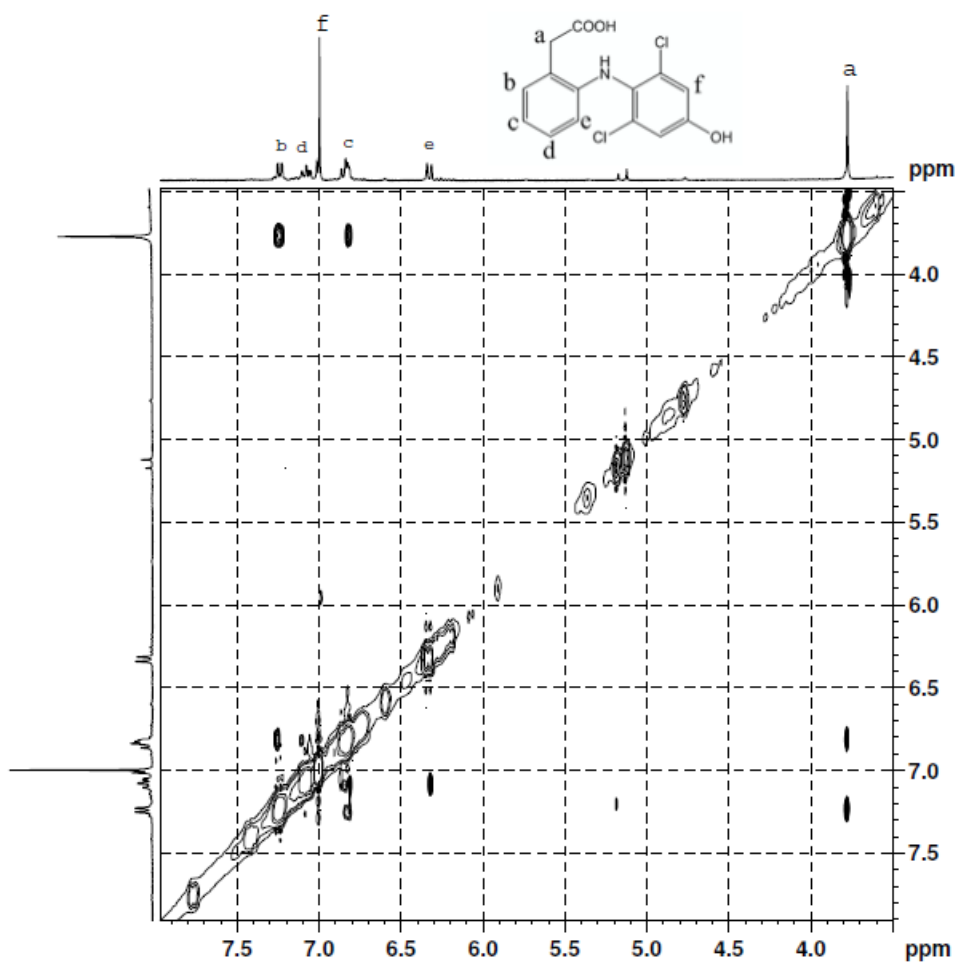


Fig. S6. MS of diclofenac

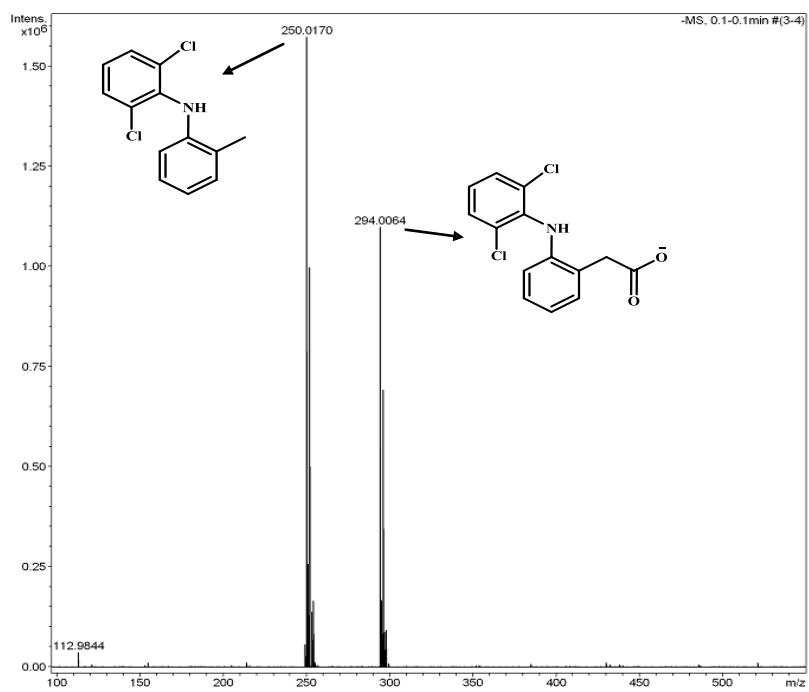


Fig. S7. COSY of diclofenac product [IV]

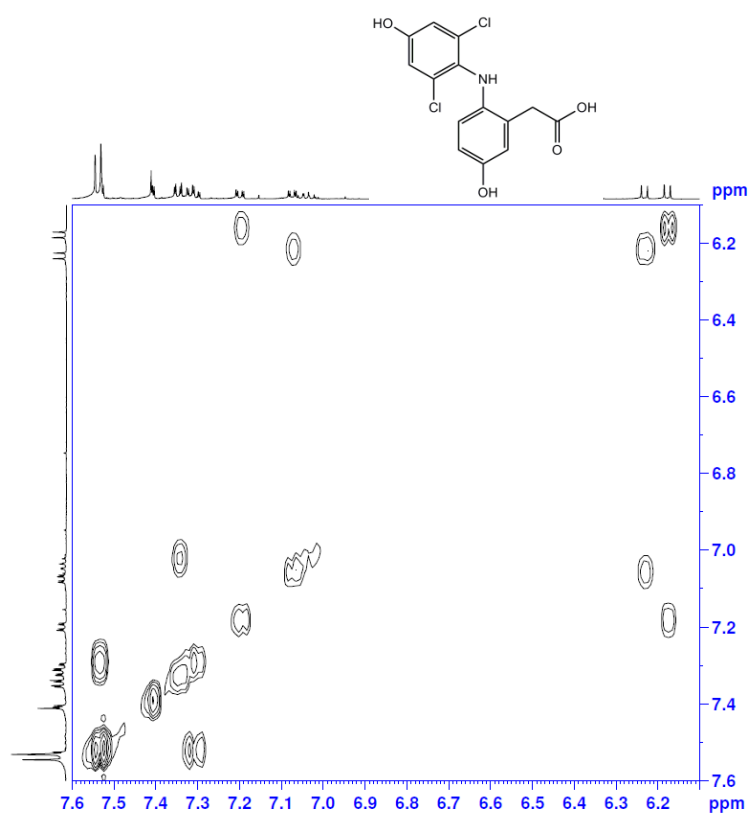


Fig. S8. COSY of naproxen

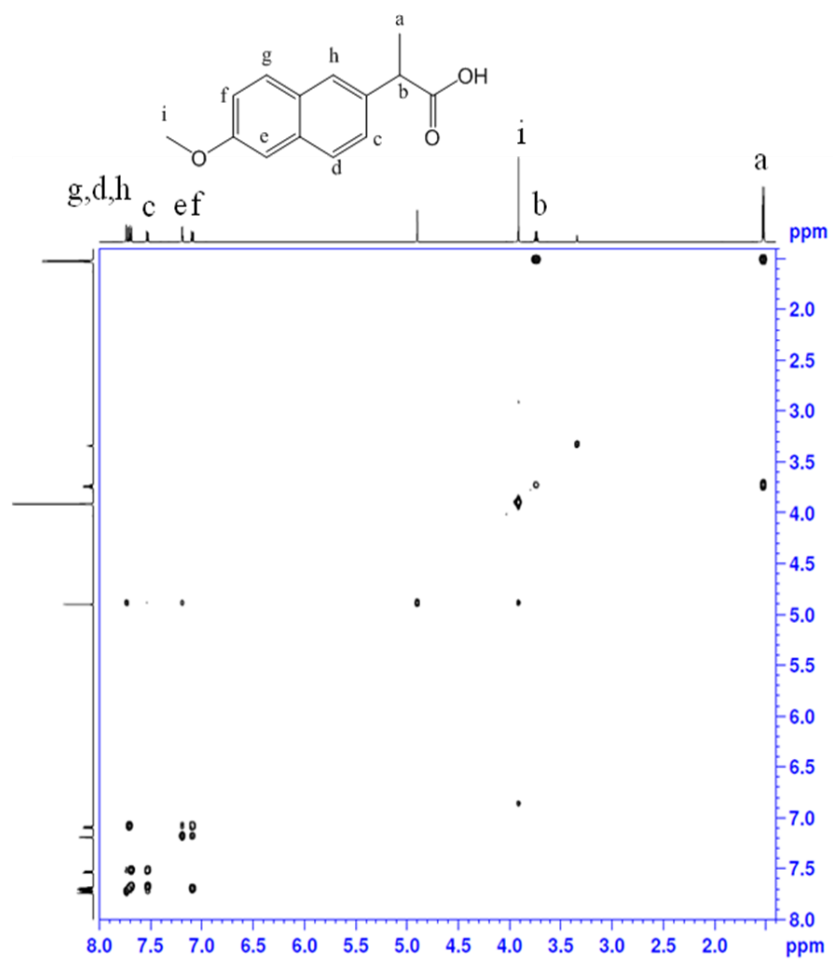


Fig. S9. NOESY of naproxen

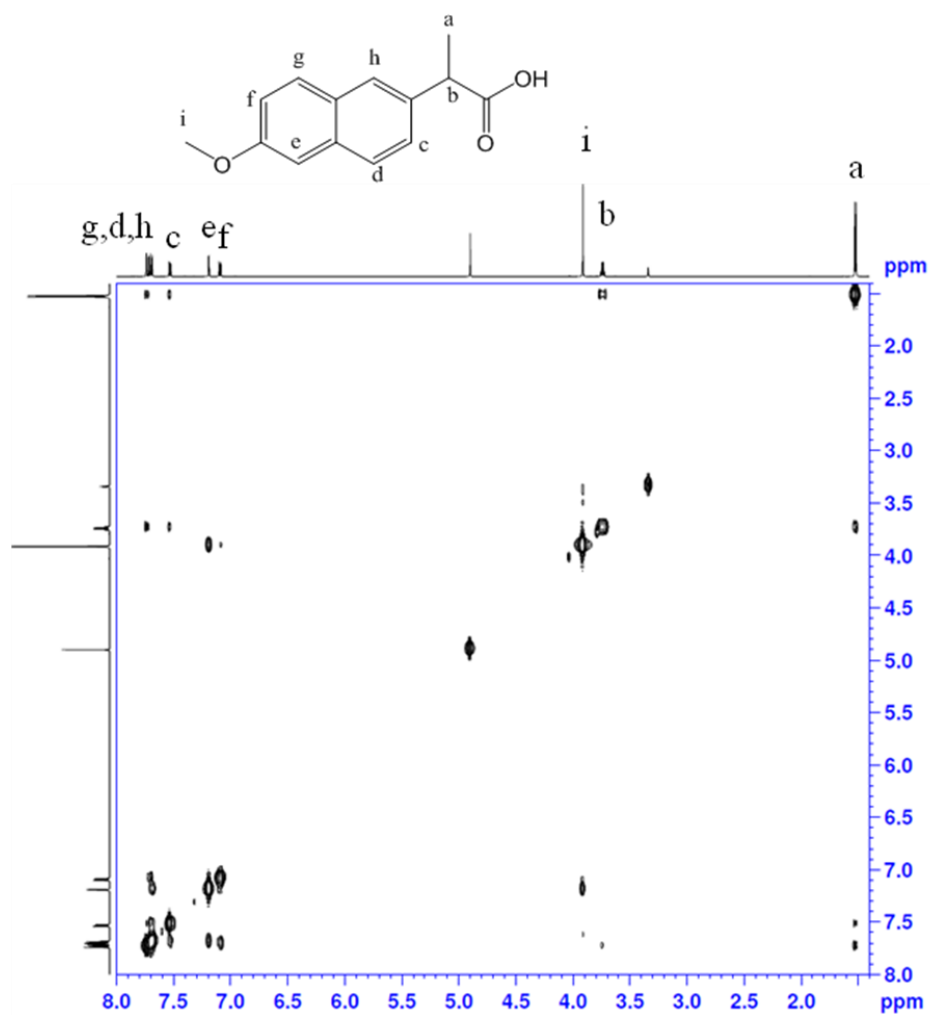


Fig. S10. COSY of authentic desmethylnaproxen purchased from Sigma Aldrich

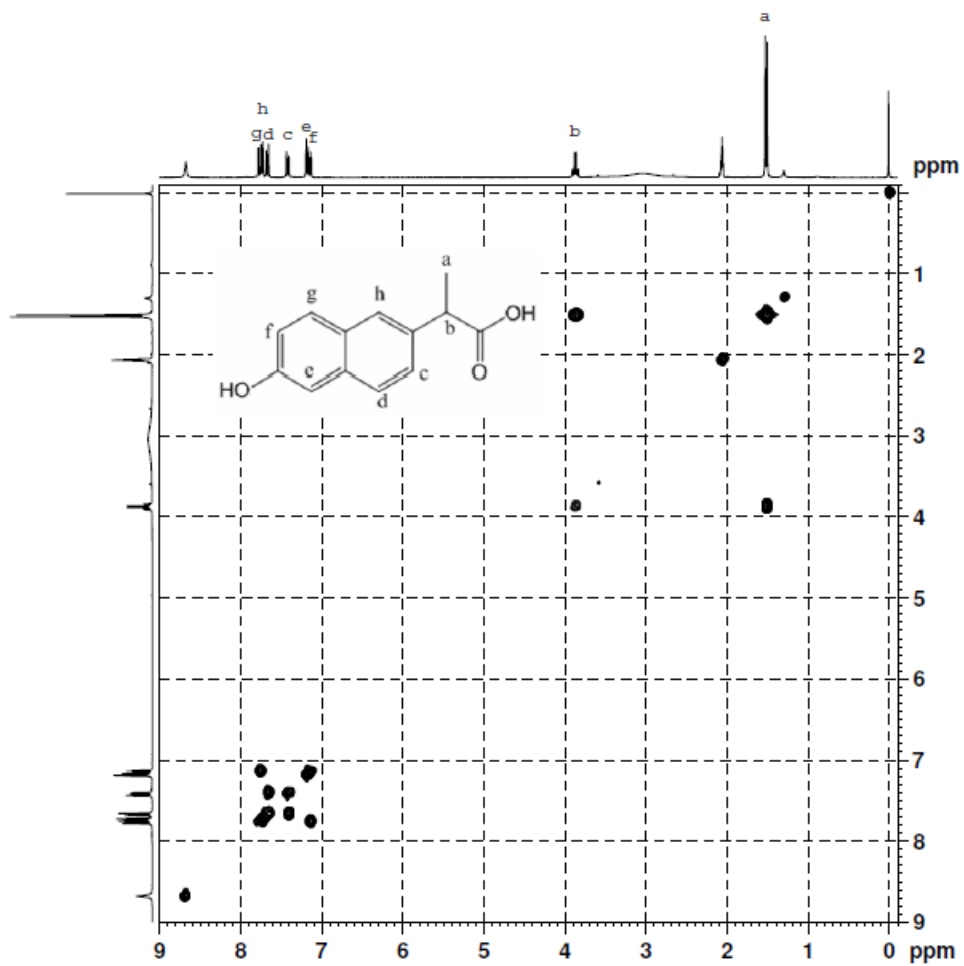


Fig. S11. NOESY of authentic desmethylnaproxen purchased from Sigma Aldrich

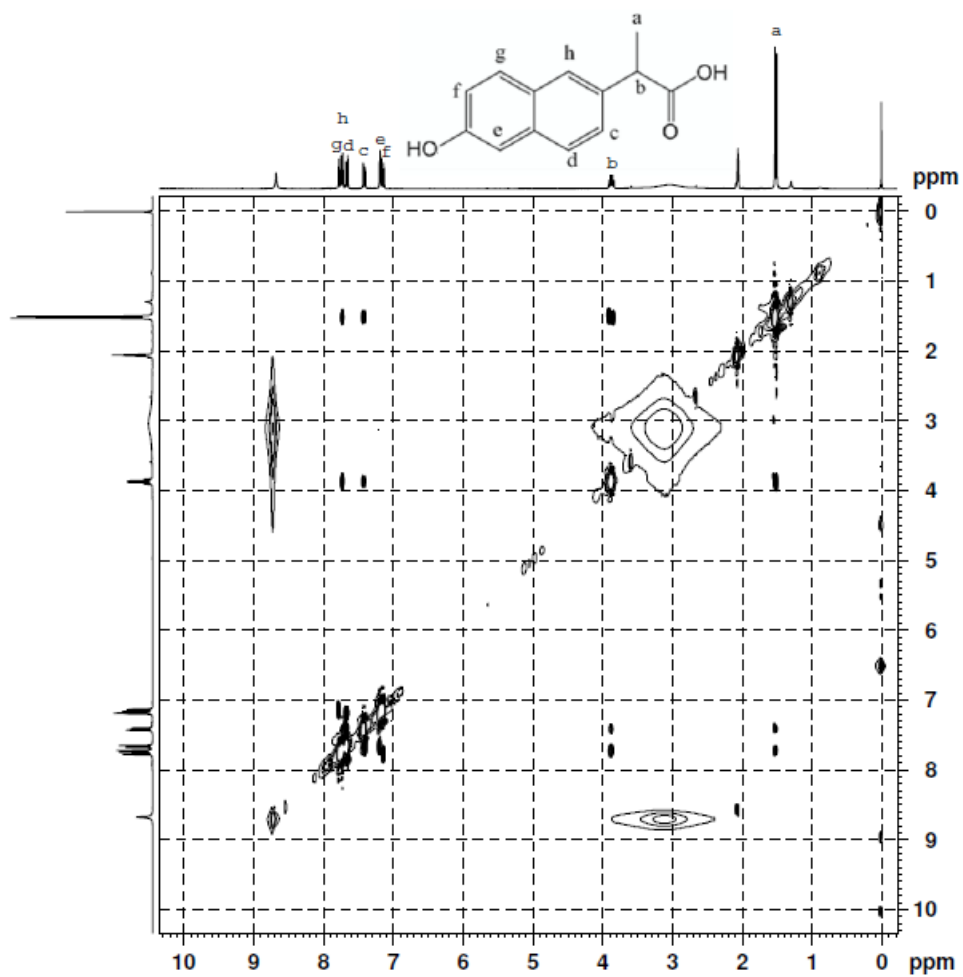
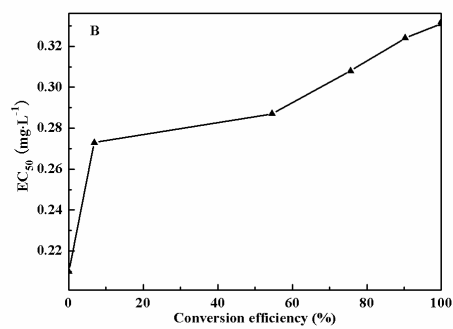
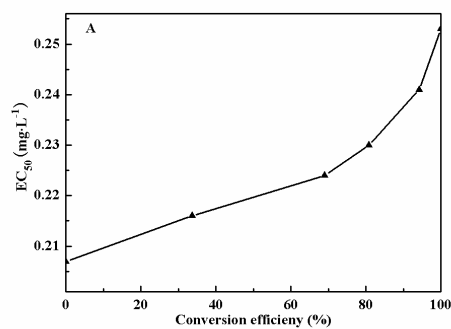


Fig. S12. Dependence of EC_{50} value on degradation efficiency of diclofenac (A) and naproxen (B). (Green algae ($OD_{10}=0.05$) and final substrate concentration range $0.15-0.36 \text{ mg}\cdot\text{L}^{-1}$)



REFERENCE

1. W.H.O, *Pharmaceuticals in drinking-water*, W.L.C.-i.-P. Data, Editor. 2012.
2. Conesa, A., et al., *Expression of the Caldariomyces fumago chloroperoxidase in Aspergillus niger and characterization of the recombinant enzyme*. Journal of Biological Chemistry, 2001. 276(21): p. 17635-17640.
3. Holm, J.V., et al., *Occurrence and distribution of pharmaceutical organic compounds in the groundwater downgradient of a landfill (Grindsted, Denmark)*. Environmental Science & Technology, 1995. 29(5): p. 1415.
4. Ternes, T.A., *Occurrence of drugs in German sewage treatment plants and rivers*. Water research (Oxford), 1998. 32(11): p. 3245-3260.
5. Triebkorna, R., et al., *Toxic effects of the non-steroidal anti-inflammatory drug diclofenac*. Aquatic Toxicology, 2004. 68(2): p. 151-166.
6. Parrott, J.L. and B.R. Blunt, *Life-cycle exposure of fathead minnows (Pimephales promelas) to an ethinylestradiol concentration below 1 ng/L reduces egg fertilization success and demasculinizes males*. Environmental Toxicology, 2004. 20(2): p. 131-141.
7. Fent, K., A.A. Weston, and D. Caminada, *Ecotoxicology of human pharmaceuticals*. Aquatic Toxicology, 2005. 76(2): p. 122-159.
8. Ou, D., et al., *Contamination of sulfonamide antibiotics and sulfamethazine-resistant bacteria in the downstream and estuarine areas of Jiulong River in Southeast China*. Environmental Science and Pollution Research International, 2015. 22(16): p. 12104-12113.
9. Baquero, F., J.L. Martinez, and R. Canton, *Antibiotics and antibiotic resistance in water environments*. Current Opinion in Biotechnology, 2008. 19(3): p. 260-265.

10. Jones, O.A., et al., *Pharmaceuticals: a threat to drinking water?* Trends in Biotechnology, 2005. 23(4): p. 163-167.
11. Benotti, M.J., et al., *Pharmaceuticals and endocrine disrupting compounds in U.S. drinking water.* Environmental Science & Technology, 2009. 43(3): p. 597-603.
12. Reddersena, K., T. Heberera, and U. Dünnebier, *Identification and significance of phenazone drugs and their metabolites in ground- and drinking water.* Chemosphere, 2002. 49(6): p. 539-544.
13. Vestel, J., et al., *Use of acute and chronic ecotoxicity data in environmental risk assessment of pharmaceuticals Ecotoxicity data and environmental risk assessment.* Environmental Toxicology and Chemistry, 2016. 35(5): p. 1201-1212.
14. Ziylan, A. and N.H. Ince, *The occurrence and fate of anti-inflammatory and analgesic pharmaceuticals in sewage and fresh water: Treatability by conventional and non-conventional processes.* Journal of Hazardous Materials, 2011. 187(1-3): p. 24-36.
15. Ternes, T.A., *Occurrence of drugs in German sewage treatment plants and rivers.* Water Research, 1998. 32(11): p. 3245-3260.
16. Kasprzyk-Hordern, B., *The removal of pharmaceuticals, personal care products, endocrine disruptors and illicit drugs during wastewater treatment and its impact on the quality of receiving waters.* Water Research 2008. 43(2): p. 363-380.
17. Lin, A.Y.-C., J.H.-F. Hsueh, and P.K.A. Hong, *Removal of antineoplastic drugs cyclophosphamide, ifosfamide, and 5-fluorouracil and a vasodilator drug pentoxifylline from wastewaters by ozonation.* Environmental Science and Pollution Research International, 2015. 22(1): p. 508-515.
18. Morris, D.R. and L.P. Hager, *Chloroperoxidase I. Isolation and properties of the crystalline glycoprotein.* The Journal of Biological Chemistry, 1966. 241(8).

19. Conesa, A., et al., *C-terminal propeptide of the Caldariomyces fumago chloroperoxidase: an intramolecular chaperone?* FEBS Lett., 2001. 503(2,3): p. 117-120.
20. Sundaramoorthy, M., J. Turner, and T.L. Poulos, *The crystal structure of chloroperoxidase: a heme peroxidase–cytochrome P450 functional hybrid.* Structure, 1995. 3(12): p. 1367-1378.
21. Wang, X., et al., *Two-dimensional NMR study of the heme active site structure of chloroperoxidase.* The Journal of Biological Chemistry, 2003. 278(10): p. 7765-74.
22. Kuhnel, K., et al., *Crystal structures of chloroperoxidase with its bound substrates and complexed with formate, acetate, and nitrate.* The Journal of Biological Chemistry, 2006. 281(33): p. 23990-8.
23. Yi, X., et al., *Examining the Role of Glutamic Acid 183 in Chloroperoxidase Catalysis.* Journal of Biological Chemistry, 2003. 278(16): p. 13855-13859.
24. Manoj, K.M. and L.P. Hager, *Chloroperoxidase, a Janus Enzyme.* Biochemistry, 2008. 47(9): p. 2997-3003.
25. Hager, L.P., et al., *Chloroperoxidase. IX. The structure of compound I.* Journal of the American Chemical Society, 1972. 94(12): p. 4364-4366.
26. Palcic, M.M., et al., *Spectrum of Chloroperoxidase Compound I.* Biochemical and biophysical research communications, 1980. 94(4): p. 1123-1127.
27. Nakajima, R., I. Yamazaki, and B.W. Griffin, *Spectra of chloroperoxidase Compounds II and III.* Biochemical and Biophysical Research Communications, 1985. 128(1): p. 1-6.
28. Zhang, R., et al., *Spectroscopic and QM/MM investigations of Chloroperoxidase catalyzed degradation of orange G.* Archives of Biochemistry and Biophysics, 2016. 596: p. 1-9.

29. Colonnaa, S., et al., *Recent biotechnological developments in the use of peroxidases*. Trends in Biotechnology 1999. 17(4): p. 163-168.
30. Hofrichter, M. and R. Ullrich, *Heme-thiolate haloperoxidases: versatile biocatalysts with biotechnological and environmental significance*. Applied Microbiology and Biotechnology, 2006. 71(3): p. 276-288.
31. Manoj, K.M., *Chlorinations catalyzed by chloroperoxidase occur via diffusible intermediate(s) and the reaction components play multiple roles in the overall process*. Biochimica et Biophysica Acta, 2006. 1764(8): p. 1325-1339.
32. Libby, R.D., et al., *Defining the involvement of HOCl or Cl₂ as enzyme-generated intermediates in chloroperoxidase-catalyzed reactions*. Journal of Biological Chemistry, 1992. 267(3): p. 1769-75.
33. Osborne, R.L., et al., *Caldariomyces fumago chloroperoxidase catalyzes the oxidative dehalogenation of chlorophenols by a mechanism involving two one-electron steps*. Journal of the American Chemical Society, 2007. 129(48): p. 14838-14839.
34. Murphy, C.D., *Fluorophenol oxidation by a fungal chloroperoxidase*. Biotechnology letters, 2007. 29(1): p. 45-49.
35. Potter, D.W., D.W. Miller, and J.A. Hinson, *Identification of acetaminophen polymerization products catalyzed by horseradish peroxidase*. The Journal of Biological Chemistry, 1985. 260(22): p. 12174-80.
36. Gallati, H., *Horseradish peroxidase: a study of the kinetics and the determination of optimal reaction conditions, using hydrogen peroxide and 2,2'-azinobis 3-ethylbenzthiazoline-6-sulfonic acid (ABTS) as substrates (author's transl)*. Journal of Clinical Chemistry and Clinical Biochemistry, 1979. 17(1): p. 1-7.
37. Hager, L.P., et al., *Chloroperoxidase. II. Utilization of halogen anions*. The Journal of Biological Chemistry, 1965. 241(8): p. 1769-1777.

38. Libby, R.D., et al., *Chloroperoxidase halogenation reactions. Chemical versus enzymic halogenating intermediates*. The Journal of Biological Chemistry, 1982. 257(9): p. 5030.
39. Vázquez-Duhalta, R., et al., *Biocatalytic chlorination of aromatic hydrocarbons by chloroperoxidase of Caldariomyces fumago*. Phytochemistry, 2001. 58(6): p. 929-933.
40. Zaks, A. and D.R. Dodds, *Chloroperoxidase-catalyzed asymmetric oxidations: substrate specificity and mechanistic study*. Journal of the American Chemical Society, 1995. 117(42): p. 10419.
41. Kiljunen, E. and L.T. Kanerva, *Novel applications of chloroperoxidase: enantioselective oxidation of racemic epoxyalcohols*. Tetrahedron: Asymmetry, 1999. 10(18): p. 3529-3535.
42. Zhang, J., et al., *Efficient decolorization/degradation of aqueous azo dyes using buffered H₂O₂ oxidation catalyzed by a dosage below ppm level of chloroperoxidase*. Chemical Engineering Journal, 2012. 191: p. 236.
43. Zhang, X., et al., *Combination of enzymatic degradation by chloroperoxidase with activated sludge treatment to remove sulfamethoxazole: performance, and eco-toxicity assessment*. Journal of Chemical Technology & Biotechnology, 2016: p. n/a-n/a.
44. Wu, S., L. Zhang, and J. Chen, *Paracetamol in the environment and its degradation by microorganisms*. Applied microbiology and biotechnology, 2012. 96(4): p. 875-884.
45. Larsen, F.S. and J. Wendon, *Understanding paracetamol-induced liver failure*. Intensive care medicine, 2014. 40(6): p. 888-890.
46. Framma, M.S. and K. Belitzb, *Occurrence and concentrations of pharmaceutical compounds in groundwater used for public drinking-water supply in California*. The Science of the total environment, 2011. 409(18): p. 3409-3417.

47. Al Qarni, H., et al., *Investigating the removal of some pharmaceutical compounds in hospital wastewater treatment plants operating in Saudi Arabia*. Environmental science and pollution research international, 2016: p. 1-12.
48. Karaman, R., et al., *Paracetamol biodegradation by activated sludge and photocatalysis and its removal by a micelle–clay complex, activated charcoal, and reverse osmosis membranes*. Environmental technology, 2016: p. 1-14.
49. Bessems, J.G., et al., *3,5-Disubstituted analogues of paracetamol. Synthesis, analgesic activity and cytotoxicity*. Chemico-Biological Interactions, 1995. 98(3): p. 237-50.
50. Xianwen Yi, M.M., Kelath M. Manoj, Xiaotang Wang, and Lowell P. Hager, *Replacement of the proximal heme thiolate ligand in chloroperoxidase with a histidine residue*. Proceedings of the National Academy of Sciences - PNAS, 1999. 96(22).
51. Chiron, S., E. Gomez, and H. Fenet, *Nitration processes of acetaminophen in nitrifying activated sludge*. Environmental Science & Technology, 2010. 44(1): p. 284.
52. Tudur Smith, C., *Carbamazepine versus phenytoin monotherapy for epilepsy*. Cochrane database of systematic reviews, 2002(2): p. CD001911.
53. Donner, E., et al., *Ecotoxicity of carbamazepine and its UV photolysis transformation products*. The Science of the total environment, 2013. 443: p. 870-876.
54. Parolini, M., et al., *Cytotoxicity assessment of four pharmaceutical compounds on the zebra mussel (*Dreissena polymorpha*) haemocytes, gill and digestive gland primary cell cultures*. Chemosphere (Oxford), 2011. 84(1): p. 91-100.
55. Andrade-Mena, C.E. and C.E. Andrade - mena, *Effects of Carbamazepine on Murine Humoral and Cellular Immune Responses*. Epilepsia (Copenhagen). 35(1): p. 205-208.

56. Singh, G., P.H.i. Driever, and J.W. Sander¹, *Cancer risk in people with epilepsy: the role of antiepileptic drugs*. *Brain* (London, England : 1878), 2005. 128(1): p. 7-17.
57. Xiong, J.-Q., *Biodegradation of carbamazepine using freshwater microalgae Chlamydomonas mexicana and Scenedesmus obliquus and the determination of its metabolic fate*. *Bioresource technology*, 2016. 205: p. 183-190.
58. Ernest Marco-Urreaa, et al., *Ability of white-rot fungi to remove selected pharmaceuticals and identification of degradation products of ibuprofen by Trametes versicolor*. *Chemosphere* (Oxford), 2008. 74(6): p. 765-772.
59. Achilleos, A., et al., *UV-A and solar photodegradation of ibuprofen and carbamazepine catalyzed by TiO₂*. *Separation science and technology*, 2010. 45(11): p. 1564-1570.
60. Thomas, J.A., D.R. Morris, and L.P. Hager, *Chloroperoxidase. VII. Classical peroxidatic, catalatic, and halogenating forms of the enzyme*. *J Biol Chem*, 1970. 245(12): p. 3129-34.
61. Manoj, K.M., et al., *Explaining the atypical reaction profiles of heme enzymes with a novel mechanistic hypothesis and kinetic treatment*. *PLoS one*, 2010. 5(5): p. e10601.
62. Kosjek, T., et al., *Fate of carbamazepine during water treatment*. *Environmental science & technology*, 2009. 43(16): p. 6256-6261.
63. Kruglova, a., et al., *Biodegradation of ibuprofen, diclofenac and carbamazepine in nitrifying activated sludge under 12°C temperature conditions*. *The Science of the total environment*, 2014. 499: p. 394-401.
64. Monsalvo, V.M., et al., *Application of Fenton-like oxidation as pre-treatment for carbamazepine biodegradation*. *Chemical engineering journal* (Lausanne, Switzerland : 1996), 2014. 264: p. 856-862.

65. Mcdoqell, D., et al., *Ozonation of Carbamazepine in Drinking Water: Identification and Kinetic Study of Major Oxidation Products*. Environmental science & technology, 2005. 39(20): p. 8014-8022.
66. Golan-Rozen, et al., *Transformation Pathways of the Recalcitrant Pharmaceutical Compound Carbamazepine by the White-Rot Fungus : Effects of Growth Conditions*. Environmental science & technology, 2015. 49(20): p. 12351-12362.
67. Ferguson, L.R. and W.A. Denny, *The genetic toxicology of acridines*. Mutation research, 1991. 258(2): p. 123-160.
68. Alastuey, A., D. Barceló, and SpringerLink, *Emerging organic contaminants and human health*. Handbook of environmental chemistry ; v. 20. 2012, Heidelberg ; New York: Springer.
69. Verlicchia, P., et al., *Hospital effluents as a source of emerging pollutants: An overview of micropollutants and sustainable treatment options*. Journal of hydrology (Amsterdam), 2010. 389(3-4): p. 416-428.
70. Haller, M.Y., et al., *Quantification of veterinary antibiotics (sulfonamides and trimethoprim) in animal manure by liquid chromatography–mass spectrometry*. Journal of chromatography. A, 2002. 952(1-2): p. 111-120.
71. Lee, T.A., *A beginner's guide to mass spectral interpretation*. 1998, Chichester ; New York: Wiley.
72. García-Galán, M.J., et al., *Biodegradation of sulfamethazine by Trametes versicolor: Removal from sewage sludge and identification of intermediate products by UPLC–QqTOF-MS*. The Science of the total environment, 2010. 409(24): p. 5505-5512.
73. Neafsey, K., X. Zeng, and A.T. Lemley, *Degradation of sulfonamides in aqueous solution by membrane anodic fenton treatment*. Journal of agricultural and food chemistry, 2010. 58(2): p. 1068-1076.
74. Saidi, I., et al., *Flow electrolysis on high surface electrode for biodegradability enhancement of sulfamethazine solutions*. Journal of

- electroanalytical chemistry (Lausanne, Switzerland), 2013. 707: p. 122-128.
75. Carstens, K.L., et al., *Sorption and photodegradation processes govern distribution and fate of sulfamethazine in freshwater–sediment microcosms*. Environmental science & technology, 2013. 47(19): p. 10877-10883.
 76. Unold, M., et al., *Transport and transformation of sulfadiazine in soil columns packed with a silty loam and a loamy sand*. Journal of contaminant hydrology, 2009. 103(1-2): p. 38-47.
 77. Schwarz, J., M.-O. Austc, and S. Thiele-Bruhnc, *Metabolites from fungal laccase-catalysed transformation of sulfonamides*. Chemosphere (Oxford), 2010. 81(11): p. 1469-1476.
 78. Gao, J., et al., *Transformation of sulfamethazine by manganese oxide in aqueous solution*. Environmental science & technology, 2012. 46(5): p. 2642-2651.
 79. Gaoa, Y.-q., et al., *Ultraviolet (UV) light-activated persulfate oxidation of sulfamethazine in water*. Chemical engineering journal (Lausanne, Switzerland : 1996), 2012. 195-196: p. 248-253.
 80. Fana, Y., et al., *Kinetic and mechanistic investigations of the degradation of sulfamethazine in heat-activated persulfate oxidation process*. Journal of hazardous materials, 2015. 300: p. 39-47.
 81. Fukahori, S. and T. Fujiwara, *Photocatalytic decomposition behavior and reaction pathway of sulfamethazine antibiotic using TiO₂*. Journal of environmental management, 2015. 157: p. 103-110.
 82. Ramakrishnan, K., et al., *Stereoselectivity of chloroperoxidase-dependent halogenation*. Biochemistry (Easton), 1983. 22(13): p. 3271-3277.
 83. Melton, T.C. and S.D. Brown, *The Fate of Sulfamethazine in Sodium-Hypochlorite-Treated Drinking Water: Monitoring by LC-MS*. International Journal of Medicinal Chemistry (Online), 2012. 68(8): p. 1-6.

84. Hutner, S.H., et al., *Some Approaches to the Study of the Role of Metals in the Metabolism of Microorganisms*. Proceedings of the American Philosophical Society, 1950. 94(2): p. 152-170.

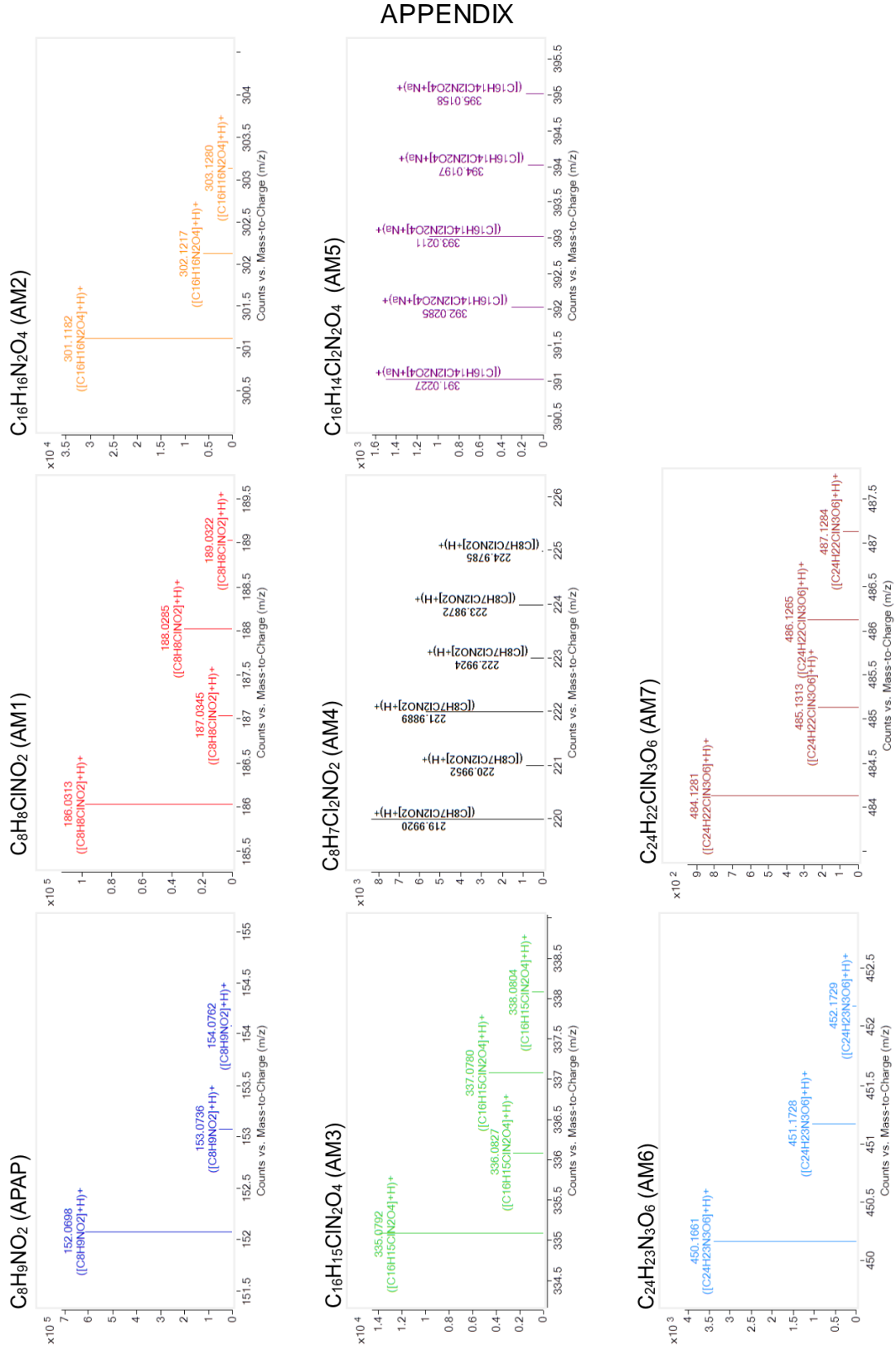


Figure A.1.1 Mass Spectrums of APAP and its metabolites

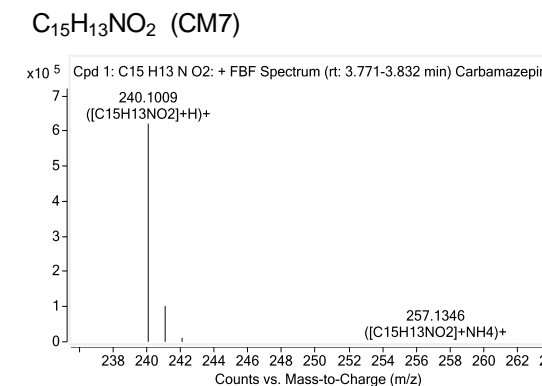
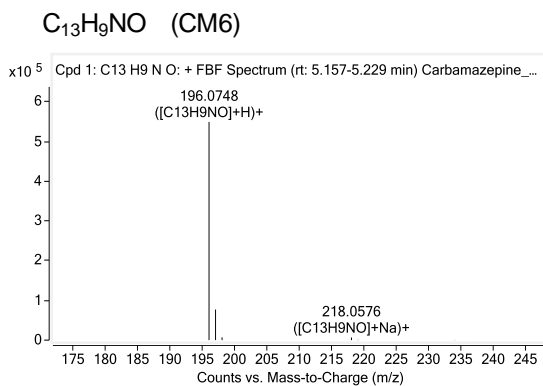
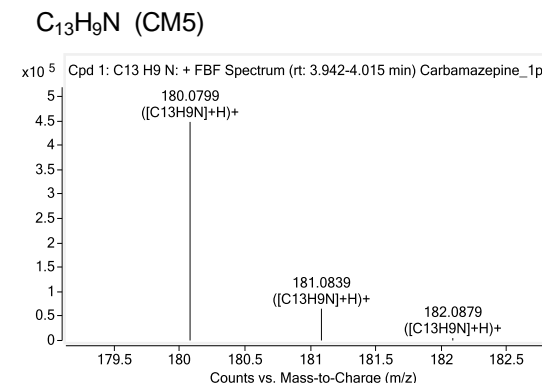
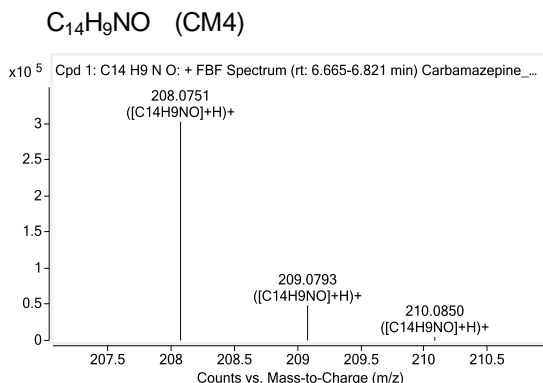
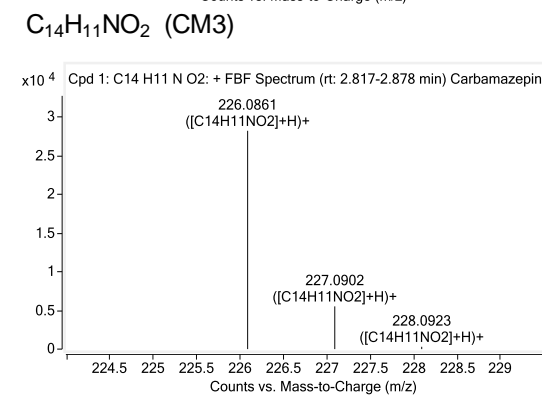
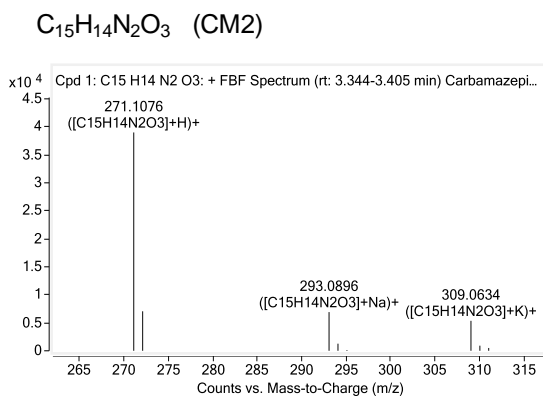
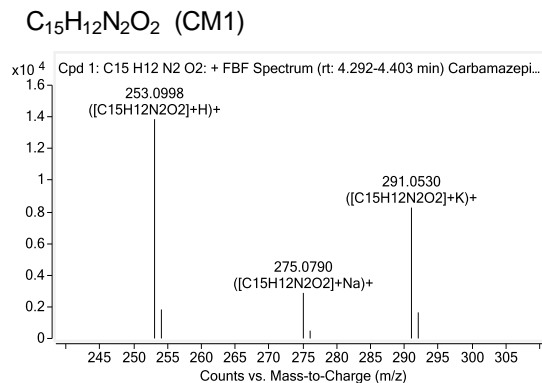
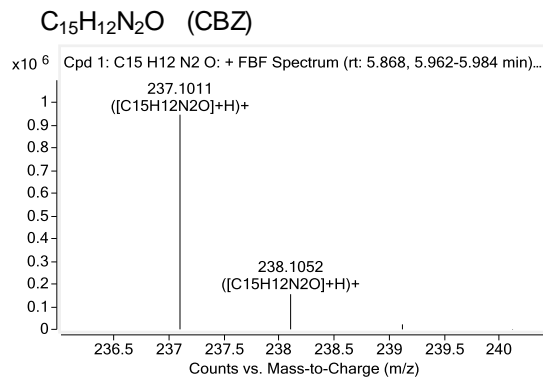


Figure A1.2 The mass spectra of CBZ and its metabolites.

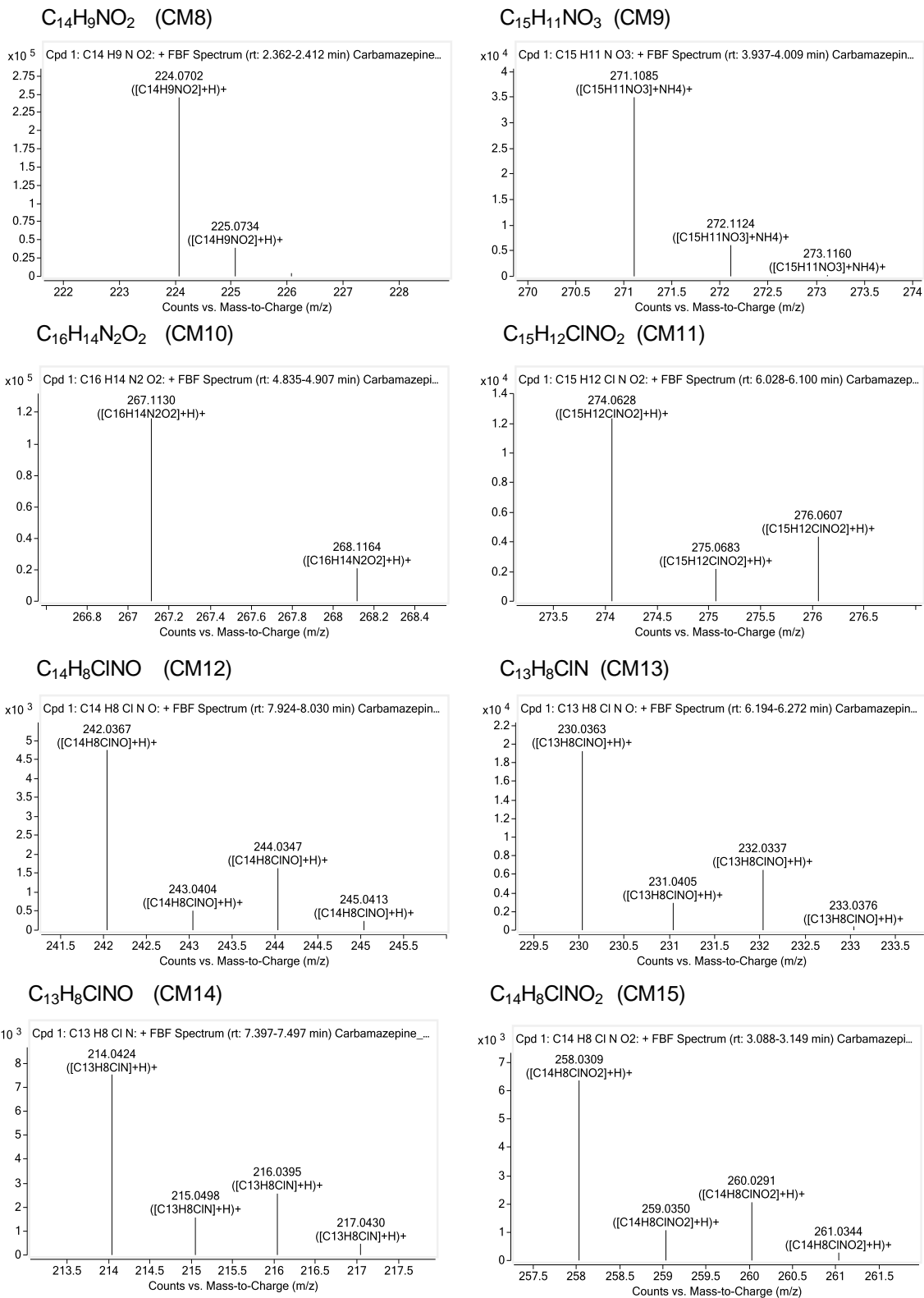


Figure A1.2 (cont.) The mass spectra of CBZ and its metabolites.

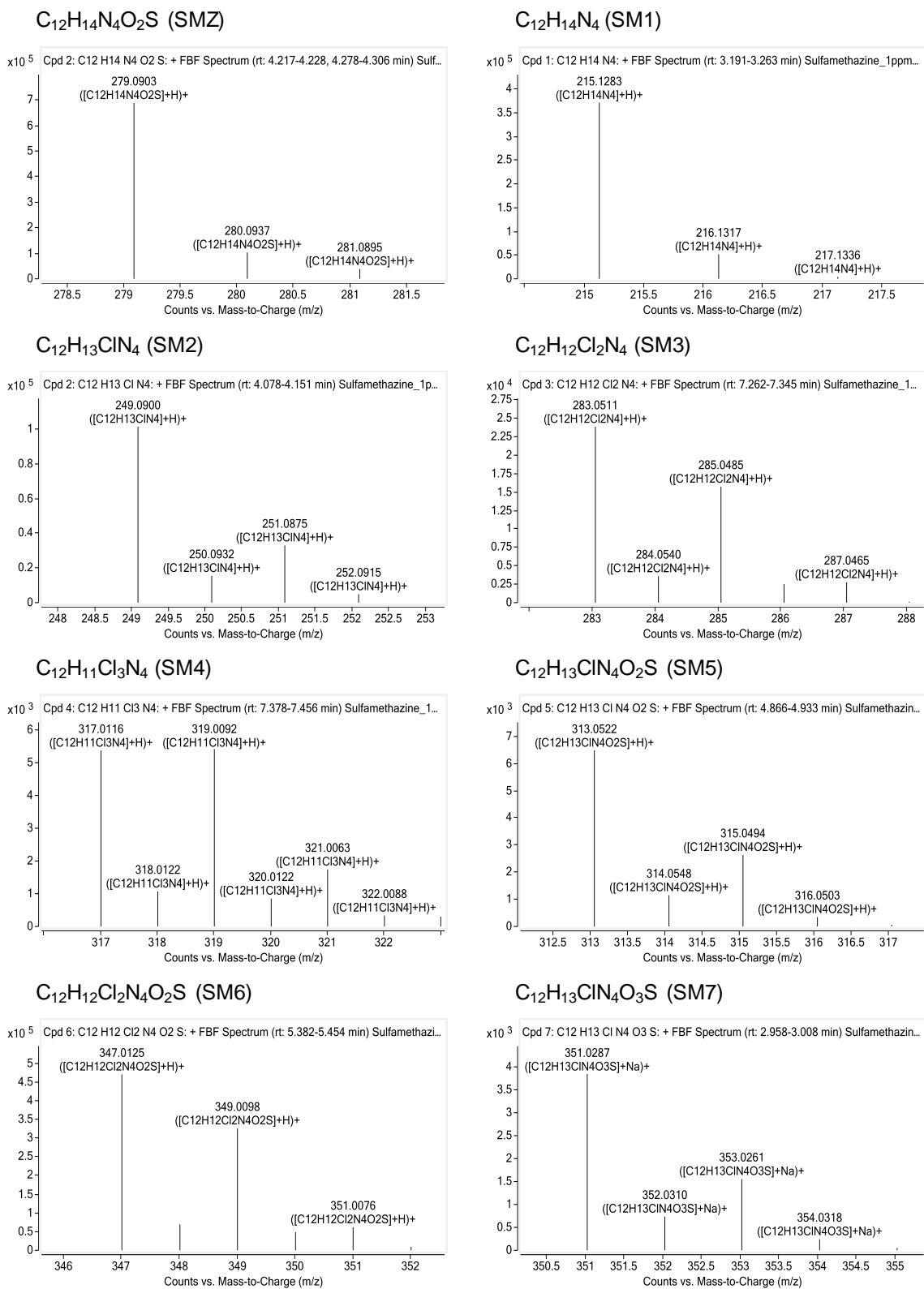


Figure A1.3 The mass spectra of SMZ and its metabolites.

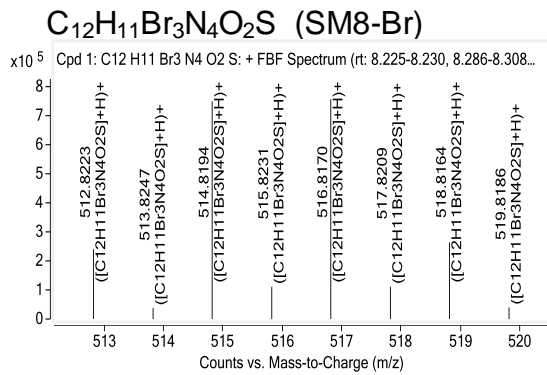
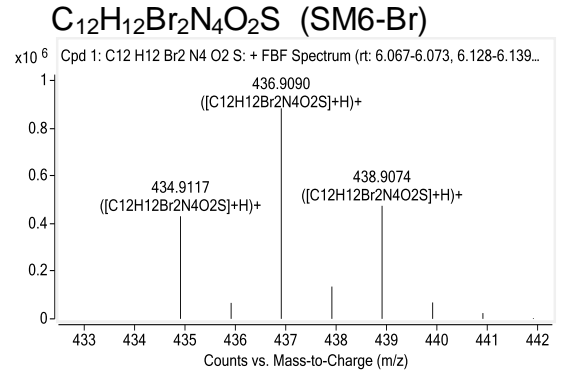
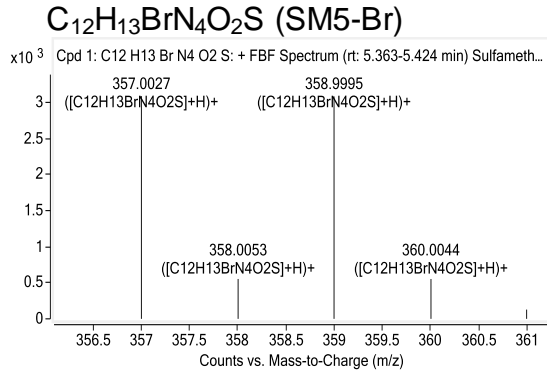
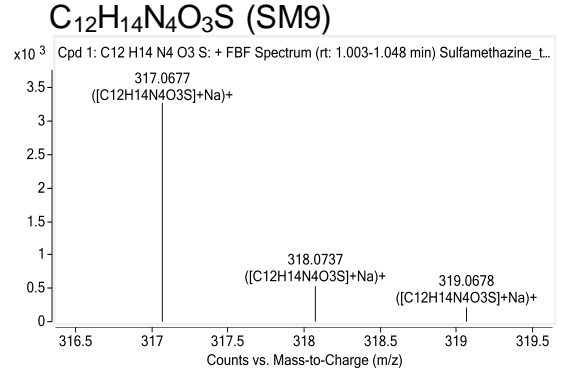
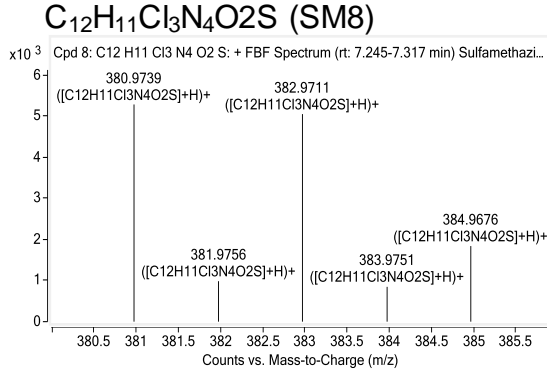


Figure A1.3 (cont.) The mass spectra of SMZ and its metabolites.

Instrument Information

Project Name Amphetamines
Instrument Name Instrument 1
Instrument Model G6460A

Compound Name	Formula	Mass	Sample Position
Acetaminophen	C8H9NO2	151.06	P1-A1

Method Name

D:\MassHunter\Methods\OnLine SPE\FlexCube\FlexCube_Flow_Injection_analysis.m

Polarity Positive **Ion Source** AJS ESI

Precursor Ion	Fragmentor
152.1	108

Product Ion	Collision Energy	Abundance
110	16	1271629
65.1	36	522812
43.1	40	221110
93	24	316142
39.1	60	174190
92	24	136673
80.1	56	29381
82.1	24	44093
67.1	36	22965
134	12	28124

Compound Name	Formula	Mass	Sample Position
AcetaminophenM1	C8H8ClNO2	185.02	P1-A1

Method Name

D:\MassHunter\Methods\OnLine SPE\FlexCube\FlexCube_Flow_Injection_analysis.m

Polarity Positive **Ion Source** AJS ESI

Precursor Ion	Fragmentor
186.03	96

Product Ion	Collision Energy	Abundance
109	28	156551
80.1	52	83677
43.1	44	39417
144	12	107318
53.1	60	15715
81.1	44	9643
82.1	56	2741
54.2	60	3453
73	60	1922
168.2	16	2420

Compound Name	Formula	Mass	Sample Position
AcetaminophenM2	C16H16N2O4	300.11	P1-A1

Method Name

D:\MassHunter\Methods\OnLine SPE\FlexCube\FlexCube_Flow_Injection_analysis.m

Polarity	Ion Source
Positive	AJS ESI

Precursor Ion	Fragmentor
301.12	120

Product Ion	Collision Energy	Abundance
259.1	12	31228
200	28	21422
172	44	10009
217.1	20	11971
283.1	16	9848
108	44	6571
182.1	40	7265
43.1	60	4689
154.1	52	6724
127	56	7242

Compound Name	Formula	Mass	Sample Position
AcetaminophenM3	C16H15ClN2O4	334.07	P1-A1

Method Name

D:\MassHunter\Methods\OnLine SPE\FlexCube\FlexCube_Flow_Injection_analysis.m

Polarity	Ion Source
Positive	AJS ESI

Precursor Ion	Fragmentor
335.08	120

Product Ion	Collision Energy	Abundance
293	16	22562
198.4	40	11060
199.1	36	7639
170	56	8854
215.1	28	9290
43.1	56	5123
142.1	48	2684
257.1	20	8823
317.1	16	8000
124	24	3382

Compound Name	Formula	Mass	Sample Position
AcetaminophenM4	C16H14Cl2N2O4	368.03	P1-A1

Method Name

D:\MassHunter\Methods\OnLine SPE\FlexCube\FlexCube_Flow_Injection_analysis.m

Polarity Positive **Ion Source** AJS ESI

Precursor Ion	Fragmentor
369.04	120

Product Ion	Collision Energy	Abundance
326.9	12	4881
218.1	12	130

Compound Name	Formula	Mass	Sample Position
AcetaminophenM5	C24H23N3O6	449.16	P1-A1

Method Name

D:\MassHunter\Methods\OnLine SPE\FlexCube\FlexCube_Flow_Injection_analysis.m

Polarity Positive **Ion Source** AJS ESI

Precursor Ion	Fragmentor
450.17	120

Product Ion	Collision Energy	Abundance
57	40	1944
71.1	32	1683
191.1	16	2118
433.4	4	4704
253.1	20	127

Compound Name	Formula	Mass	Sample Position
AcetaminophenM6	C24C22ClN3O6	724.95	P1-A1

Method Name

D:\MassHunter\Methods\OnLine SPE\FlexCube\FlexCube_Flow_Injection_analysis.m

Polarity Positive **Ion Source** AJS ESI

Precursor Ion	Fragmentor
725.96	120

Product Ion	Collision Energy	Abundance
129	44	4801
111	56	6701
215.2	40	5935
101	56	4402
69.1	60	4178
83.1	60	2064
429.4	36	2173
55.1	56	1718
327.2	20	2241
57.2	52	1104

Compound Name	Formula	Mass	Sample Position
AcetaminophenM7	C8H7Cl2NO2	218.99	P1-A1

Method Name

D:\MassHunter\Methods\OnLine SPE\FlexCube\FlexCube_Flow_Injection_analysis.m

Polarity Positive Ion Source AJS ESI

Precursor Ion	Fragmentor
220	108

Product Ion	Collision Energy	Abundance
143	20	4676
177.9	12	2243
79.1	48	1531
43.1	36	1086
52.1	60	1106

Instrument Information

Project Name Amphetamines
Instrument Name Instrument 1
Instrument Model G6460A

Compound Name	Formula	Mass	Sample Position
Carbamazepine drug	C15H12N2O	236.09	P1-A1

Method Name

D:\MassHunter\Methods\OnLine SPE\FlexCube\FlexCube_Flow_Injection_analysis.m

Polarity Positive **Ion Source** AJS ESI

Precursor Ion	Fragmentor
237.1	120

Product Ion	Collision Energy	Abundance
194.1	16	702396
193.5	20	111989
165	52	80398
179	40	100756
167.1	52	35826
152	56	34123
151.6	60	29833
89	60	25625
181	16	9979

Compound Name	Formula	Mass	Sample Position
Carbamazepine M1	C15H14N2O3	270.1	P1-A1

Method Name

D:\MassHunter\Methods\OnLine SPE\FlexCube\FlexCube_Flow_Injection_analysis.m

Polarity Positive **Ion Source** AJS ESI

Precursor Ion	Fragmentor
271.11	120

Product Ion	Collision Energy	Abundance
193.1	28	56095
180.1	32	44419
228	12	34033
253.1	4	29021
167.1	44	11376
210.1	12	19729
165	56	8218
236.1	8	26397
226	20	6669
182.1	24	10653

Compound Name	Formula	Mass	Sample Position
Carbamazepine M2	C15H13NO2	239.09	P1-A1

Method Name

D:\MassHunter\Methods\OnLine SPE\FlexCube\FlexCube_Flow_Injection_analysis.m

Polarity Positive **Ion Source** AJS ESI

Precursor Ion	Fragmentor
240.1	120

Product Ion	Collision Energy	Abundance
180	24	2478224
152	60	405603
208	16	354604
128	60	79867
153.1	60	46695
127	60	63507
77.1	60	54522
101	60	33435
154.1	56	20671
51.1	60	16133

Compound Name	Formula	Mass	Sample Position
Carbamazepine M3	C13H9N	179.07	P1-A1

Method Name

D:\MassHunter\Methods\OnLine SPE\FlexCube\FlexCube_Flow_Injection_analysis.m

Polarity Positive **Ion Source** AJS ESI

Precursor Ion	Fragmentor
180.08	120

Product Ion	Collision Energy	Abundance
152	40	224584
77.1	60	90327
127	48	47794
128	44	40418
101	52	36077
51.1	60	45047
153.1	48	25083
75	60	38516
102.1	60	17325
140	56	9300

Compound Name	Formula	Mass	Sample Position
Carbamazepine M4	C13H9NO	195.07	P1-A1

Method Name

D:\MassHunter\Methods\OnLine SPE\FlexCube\FlexCube_Flow_Injection_analysis.m

Polarity Positive **Ion Source** AJS ESI

Precursor Ion	Fragmentor
196.08	120

Product Ion	Collision Energy	Abundance
167	40	44065
139.1	60	10838
140	60	6725
115	56	3799
77.1	60	2468
168.1	32	2372
178.1	28	1859
128.1	48	1491
151	44	1649
51.2	60	1238

Compound Name	Formula	Mass	Sample Position
Carbamazepine M5	C14H9NO2	223.06	P1-A1

Method Name

D:\MassHunter\Methods\OnLine SPE\FlexCube\FlexCube_Flow_Injection_analysis.m

Polarity Positive **Ion Source** AJS ESI

Precursor Ion	Fragmentor
224.07	120

Product Ion	Collision Energy	Abundance
193.1	24	112675
180.1	28	62916
196	24	35071
167.1	44	30631
152	60	15597
166.5	52	8105
139.4	60	6418
77	60	4564
140.1	60	5174
128	60	2364

Compound Name	Formula	Mass	Sample Position
Carbamazepine M6	C15H11NO3	253.07	P1-A1

Method Name

D:\MassHunter\Methods\OnLine SPE\FlexCube\FlexCube_Flow_Injection_analysis.m

Polarity Positive **Ion Source** AJS ESI

Precursor Ion	Fragmentor
254.08	84

Product Ion	Collision Energy	Abundance
181.1	36	103302
211	12	50698
237	8	64186
183.1	20	26258
168	44	12561
152.6	60	14691
152.1	60	7638
128	60	3362
77.1	60	1563

Compound Name	Formula	Mass	Sample Position
Carbamazepine M7	C14H9NO	207.07	P1-A1

Method Name

D:\MassHunter\Methods\OnLine SPE\FlexCube\FlexCube_Flow_Injection_analysis.m

Polarity Positive **Ion Source** AJS ESI

Precursor Ion	Fragmentor
208.08	120

Product Ion	Collision Energy	Abundance
180	24	724769
152	48	142701
77.1	60	41377
128	52	26096
127	56	25774
101	60	23443
51.1	60	16857
75	60	12887
154.1	40	7490
102.1	60	7900

Compound Name	Formula	Mass	Sample Position
Carbamazepine M8	C15H12N2O2	252.09	P1-A1

Method Name

D:\MassHunter\Methods\OnLine SPE\FlexCube\FlexCube_Flow_Injection_analysis.m

Polarity Positive **Ion Source** AJS ESI

Precursor Ion	Fragmentor
253.1	108

Product Ion	Collision Energy	Abundance
180.1	32	741709
210.1	12	287992
236	8	368575
182.1	24	185407
167	44	104330
152	60	92198
208	12	26569
128	60	12392
153.1	60	12086
77.1	60	12527

Compound Name	Formula	Mass	Sample Position
Carbamazepine M9	C16H14N2O2	266.11	P1-A1

Method Name

D:\MassHunter\Methods\OnLine SPE\FlexCube\FlexCube_Flow_Injection_analysis.m

Polarity Positive **Ion Source** AJS ESI

Precursor Ion	Fragmentor
267.12	108

Product Ion	Collision Energy	Abundance
224.1	12	766679
193.1	32	430735
180.1	40	274087
165.1	60	61264
208.1	36	31319
194.2	28	32976
167	56	28610
208.7	24	31300
152	60	35539
222.1	20	26660

Compound Name	Formula	Mass	Sample Position
Carbamazepine M10	C14H11NO2	225.08	P1-A1

Method Name

D:\MassHunter\Methods\OnLine SPE\FlexCube\FlexCube_Flow_Injection_analysis.m

Polarity Positive **Ion Source** AJS ESI

Precursor Ion	Fragmentor
226.09	120

Product Ion	Collision Energy	Abundance
180	28	6250
152	56	1477
150.1	60	243

Compound Name	Formula	Mass	Sample Position
Carbamazepine M18	C15H12ClNO2	273.06	P1-A1

Method Name

D:\MassHunter\Methods\OnLine SPE\FlexCube\FlexCube_Flow_Injection_analysis.m

Polarity Positive **Ion Source** AJS ESI

Precursor Ion	Fragmentor
274.07	120

Product Ion	Collision Energy	Abundance
214.1	20	2694
194.1	28	2883
179.1	48	1645
193.6	44	1497
167	48	364

Compound Name	Formula	Mass	Sample Position
Carbamazepine M19	C13H8ClN	213.03	P1-A1

Method Name

D:\MassHunter\Methods\OnLine SPE\FlexCube\FlexCube_Flow_Injection_analysis.m

Polarity Positive **Ion Source** AJS ESI

Precursor Ion	Fragmentor
214.04	120

Product Ion	Collision Energy	Abundance
-------------	------------------	-----------

Compound Name	Formula	Mass	Sample Position
Carbamazepine M20	C13H8CINO	229.03	P1-A1

Method Name

D:\MassHunter\Methods\OnLine SPE\FlexCube\FlexCube_Flow_Injection_analysis.m

Polarity Positive **Ion Source** AJS ESI

Precursor Ion	Fragmentor
230.04	120

Product Ion	Collision Energy	Abundance
193	20	3703
115	52	165

Compound Name	Formula	Mass	Sample Position
Carbamazepine M21	C14H8CIN	225.03	P1-A1

Method Name

D:\MassHunter\Methods\OnLine SPE\FlexCube\FlexCube_Flow_Injection_analysis.m

Polarity Positive **Ion Source** AJS ESI

Precursor Ion	Fragmentor
226.04	120

Product Ion	Collision Energy	Abundance
180.1	24	4377

Compound Name	Formula	Mass	Sample Position
Carbamazepine M22	C14H8CINO	241.03	P1-A1

Method Name

D:\MassHunter\Methods\OnLine SPE\FlexCube\FlexCube_Flow_Injection_analysis.m

Polarity Positive **Ion Source** AJS ESI

Precursor Ion	Fragmentor
242.04	108

Product Ion	Collision Energy	Abundance
182.1	24	23197
181.2	20	6678
58.1	20	977
210	16	5012
154.5	60	584

Figure A3.1 DNA sequence of full-length wide type CPO gene.

ATGTTCTCCAAGGTCCTTCCCTTCGTGGGAGCGGTTGCCGCCCTCCCTCACTC
CGTCCGTCAGGAGCCTGGCTCCGGCATTGGCTACCCATACGACAACAACACC
CTGCCATATGTCGCCCCAGGTCTACCGACTCTCGTGCTCCTTGCCCAGCTCT
GAACGCTCTTGCCAACCACGGTTACATTCCTCACGATGGCCGTGCCATCAGC
AGGGAGACCCTCCAGAACGCTTTCCTCAACCACATGGGTATTGCCAACTCCG
TCATTGAGCTTGCTCTGACCAACGCCTTCGTCTGCTGCGAGTACGTTACTGGC
TCCGACTGTGGTGACAGCCTTGTC AACCTGACTCTGCTCGCCGAGCCCCACGC
TTTCGAGCACGACCACTCCTTCTCCCGCAAGGATTACAAGCAGGGTGTGCC
AACTCCAACGACTTCATCGACAACAGGAACTTCGATGCCGAGACCTTCCAGA
CCTCTCTGGATGTCGTTGCAGGCAAGACCCACTTCGACTATGCCGACATGAA
CGAGATCCGCCTTCAGCGCGAGTCCCTCTCCAACGAGCTTGACTTCCCCGGTT
GGTTCACCGAGTCCAAGCCAATCCAGAACGTGAGTCTGGCTTCATCTTCGCC
CTTGTCTCTGACTTCAACCTGCCCGACAACGATGAGAACCCTCTGGTTTCGCAT
TGACTGGTGGAAGTACTGGTTCACCAACGAGTCCTTCCCATAACCACCTCGGCT
GGCACCCCCGTCTCCAGCCAGGGAGATCGAGTTCGTACCTCCGCCTCCTCC
GCTGTCTGGCTGCCCTCTGTCACCTCTACTCCATCTTCCCTTCCATCCGGTGCC
ATCGGCCAGGTGCCGAGGCTGTCCCTCTCTCCTTCGCCTCCACCATGACCCC
ATTCTCTCGCCACCAATGCTCCTTACTACGCCAGGACCCAACCTCTCGGCC
CCAACGACAAGCGTGAGGCTGCCCCAGCTGCCACCACCTCCATGGCCGTCTT
CAAGAACCCATACCTCGAGGCCATTGGCACCCAGGACATCAAGAACCAGCA
GGCTTACGTCAGCTCCAAGGCTGCTGCCATGGCCTCTGCCATGGCCGCCAAC
AAGGCCCGCAACCTTTAA

Figure A3.2 Amino acid sequence of full-length of wide type CPO.

1 XEPGSGIGYP YDNNTLPYVA PGPTDSRAPC PALNALANHG YIPHDGRAIS
51 RETLQNAFLN HMGIANSVIE LALTNAFVVC EYVTGSDCGD SLVNLTLLAE
101 PHAFEHDHSF SRKDYKQGVA NSNDFIDNRN FDAETFQTSL DVVAGKTHFD
151 YADMNEIRLQ RESLSNELDF PGWFTESKPI QNVESGFIFA LVSDFNLPDN
201 DENPLVRIDW WKYWFTNESF PYHLGWHPPS PAREIEFVTS ASSAVLAASV
251 TSTPSSLPSG AIGPGAEAVP LSFASMTMPF LLATNAPYYA QDPTLGPND

VITA

QINGHAO HE

Dec 07, 1988	Born, Nanjing, China
2007-2011	Bachelor of Management, Nanjing University of Chinese Medicine
2011-	Doctoral Candidate in Chemistry Florida international University

PUBILICATIONS

Rui Zhang, Qinghao He, David Chatfield, and Xiaotang Wang “Paramagnetic nuclear magnetic resonance relaxation and molecular mechanics studies of the chloroperoxidase–indole complex: insights into the mechanism of chloroperoxidase-catalyzed regioselective oxidation of indole”. *Biochemistry*, 2013. 52(21): p. 3688-3701.

Rui Zhang , Qinghao He, Yi Huang and Xiaotang Wang “Spectroscopic and QM/MM investigations of Chloroperoxidase catalyzed degradation of orange G” *Archives of Biochemistry and Biophysics*, 2016. 596 P. 1-9